Advances in 3D Geologic Modeling of Alluvial Basins with a Focus on Facies and Property Modeling

Spent Fuel and Waste Disposition

Los Alamos National Laboratory
Michael Gross, Eric Guiltinan, Damien Milazzo, Terry A. Miller, Erika Swanson, Elizabeth Miller, Anita Lavadie-Bulnes and Philip Stauffer

Sandia National Laboratories
Tara LaForce

September 30, 2021
LA-UR-21-29521

Los Alamos National Laboratory Document

APPENDIX E

NFCSC DOCUMENT COVER SHEET[1]

Name/Title of Deliverable/Milestone/Revision No.	Advances in 3D geologic modeling of alluvial basins with a focus on facies and property modeling Milestone No. M3SF-21LA010304022
Work Package Title and Number	GDSA - Geologic Modeling – LANL, SF-21LA01030402
Work Package WBS Number	1.08.01.03.04
Responsible Work Package Manager	Michael Gross (signature on file) (Name/Signature)
Date Submitted	

Quality Rigor Level for Deliverable/Milestone[2]	☐ QRL-1 ☐ Nuclear Data	☐ QRL-2	☒ QRL-3	☐ QRL-4 Lab QA Program[3]

This deliverable was prepared in accordance with   <u>Los Alamos National Laboratory</u>

(Participant/National Laboratory Name)

QA program which meets the requirements of

    ☒ DOE Order 414.1   ☐ NQA-1   ☐ Other

This Deliverable was subjected to:

☒ Technical Review   ☐ Peer Review

Technical Review (TR)   **Peer Review (PR)**

Review Documentation Provided   **Review Documentation Provided**

☐ Signed TR Report or,   ☐ Signed PR Report or,

☐ Signed TR Concurrence Sheet or,   ☐ Signed PR Concurrence Sheet or,

☒ Signature of TR Reviewer(s) below   ☐ Signature of PR Reviewer(s) below

Name and Signature of Reviewers

<u>   Michelle Bourret (signature on file)   </u>   <u>   </u>

<u>   Nathan Welch (signature on file   </u>   <u>   </u>

NOTE 1: *Appendix E should be filled out and submitted with the deliverable. Or, if the PICS:NE system permits, completely enter all applicable information in the PICS:NE Deliverable Form. The requirement is to ensure that all applicable information is entered either in the PICS:NE system or by using the NFCSC Document Cover Sheet.*

- *In some cases there may be a milestone where an item is being fabricated, maintenance is being performed on a facility, or a document is being issued through a formal document control process where it specifically calls out a formal review of the document. In these cases, documentation (e.g., inspection report, maintenance request, work planning package documentation or the documented review of the issued document through the document control process) of the completion of the activity, along with the Document Cover Sheet, is sufficient to demonstrate achieving the milestone.*

NOTE 2: *If QRL 1, 2, or 3 is not assigned, then the QRL 4 box must be checked, and the work is understood to be performed using laboratory QA requirements. This includes any deliverable developed in conformance with the respective National Laboratory / Participant, DOE or NNSA-approved QA Program.*

NOTE 3: *If the lab has an NQA-1 program and the work to be conducted requires an NQA-1 program, then the QRL-1 box must be checked in the work Package and on the Appendix E cover sheet and the work must be performed in accordance with the Lab's NQA-1 program. The QRL-4 box should not be checked.*

CONTENTS

LIST OF FIGURES

LIST OF TABLES

ACRONYMS

AoI	area of interest
DEM	digital elevation model
DOE	Department of Energy
DOE-EM	DOE Office of Environmental Management
DOE-NE	DOE Office of Nuclear Energy
EBS	engineered barrier system
ESRI	Environmental Systems Research Institute
FEHM	Finite Element Heat and Mass Transfer (simulation code)
FY	fiscal year (October-September)
GDACC	Geospatial Data Acquisition Coordination Committee
GDSA	geologic disposal safety assessment
GFM	geologic framework model
HLW	high level nuclear waste
HSU	hydrostratigraphic units
JS	JewelSuite™
LaGriT	Los Alamos Grid Toolbox
LANL	Los Alamos National Laboratory
Ma	millions of years ago
MD	measured depth
MSL	mean sea level (amsl = above mean sea level; bmsl = below mean sea level)
PA	performance assessment
PFLOTRAN	Parallel Flow and Transport (simulation code)
R&D	research and development
SFWD	Spent Fuel & Waste Disposition (DOE-NE program)
SFWST	Spent Fuel and Waste Science and Technology (DOE-NE program)
SGS	sequential gaussian simulation
SIS	sequential indicator simulation
SNF	spent nuclear fuel
SNL	Sandia National Laboratories
TGS	truncated gaussian simulation
TOUGH	Transport of Unsaturated Groundwater and Heat (simulation code)
TVDSS	true vertical depth sub-sea
US	United States
USGS	United States Geological Survey
UWI	unique well identifier
UZ	unsaturated zone
VoI	volume of interest

This page is intentionally left blank.

ADVANCES IN 3D GEOLOGIC MODELING OF ALLUVIAL BASINS WITH A FOCUS ON FACIES AND PROPERTY MODELING

1. Introduction

The unsaturated zone alluvium reference case is one of several geologic systems under consideration by the U.S. Department of Energy Office of Nuclear Energy for hosting repositories for spent nuclear fuel and associated waste (Sevougian et al., 2019). As noted by Mariner et al. (2018), the generic alluvial basin offers positive attributes that merit its consideration as a reference case by the Spent Fuel and Waste Science and Technology (SFWST) campaign. There are hundreds of alluvial basins and sub-basins scattered across the arid western United States (Figure 1-1). Precipitation and infiltration rates are relatively low with high evapotranspiration, resulting in vertical separation between repository and water table and thus longer transport paths to an aquifer. Accumulations of alluvial sediments within these basins are typically on the order of hundreds of meters, and locally may exceed 1,000 m in thickness, as is the case for the Deming sub-basin in southern New Mexico. A thick geologic host medium, which serves as the natural barrier system (NBS) in the conceptual model framework of a geologic disposal system, isolates the waste packages from receptors in the biosphere. Further, alluvial basin fill is typically comprised of stacked playa and lacustrine deposits along the basin axis (Perry et al., 2018). Characterized by low permeability, these layers protect the biosphere above the repository and the groundwater resources below the repository.

This marks the third year of LANL's Geologic Disposal Safety Assessment (GDSA) of generic alluvial basins, using the Mimbres Basin of southwestern New Mexico as a case study (Figure 1-2). The first year was an exploration phase, consisting of regional reconnaissance and basin-scale integration of tectonics, hydrology, geophysics and sedimentology (Gross et al., 2019). A rudimentary geologic framework model (GFM) was constructed that defines basin-bounding faults, the top surface of bedrock and the thickness of alluvial sediments. In essence, this phase focused on describing the three-dimensional geometry of the "container" that hosts the alluvium.

In the second year we defined the ~30 km x 20 km Deming sub-basin as the area of interest (Figure 1-3) and focused on the alluvial sediments that accumulated in this structurally-controlled sub-basin (Gross et al., 2000). The 3D grid model of alluvium in the refined FY20 GFM contains ~430,000 cells, each with horizontal dimensions of 200 m x 200 m and a vertical dimension of 50 m. We subdivided the alluvium into seven lithofacies according to the classification of Kennedy et al. (2000). We then developed a conceptual model of facies distribution along a cross section perpendicular to the axis of the Deming sub-basin (Figure 1-4a) with constraints provided by geologic maps, well data, tectonic history and paleoclimate considerations. Using subsurface formation (i.e., lithofacies) tops from synthetic vertical wells, we modeled the facies distribution in JewelSuite™ (JS) (Baker Hughes, 2020) using various geostatistical parameters (Figure 1-4b). This technique proved its value in the repository-scale facies modeling of FY21, as described in Chapter 2 of this report. As an independent exercise,

we generated 3D models of physical properties (porosity and permeability) for the alluvium grid for homogeneous, layered and anisotropic scenarios (Figure 1-5).
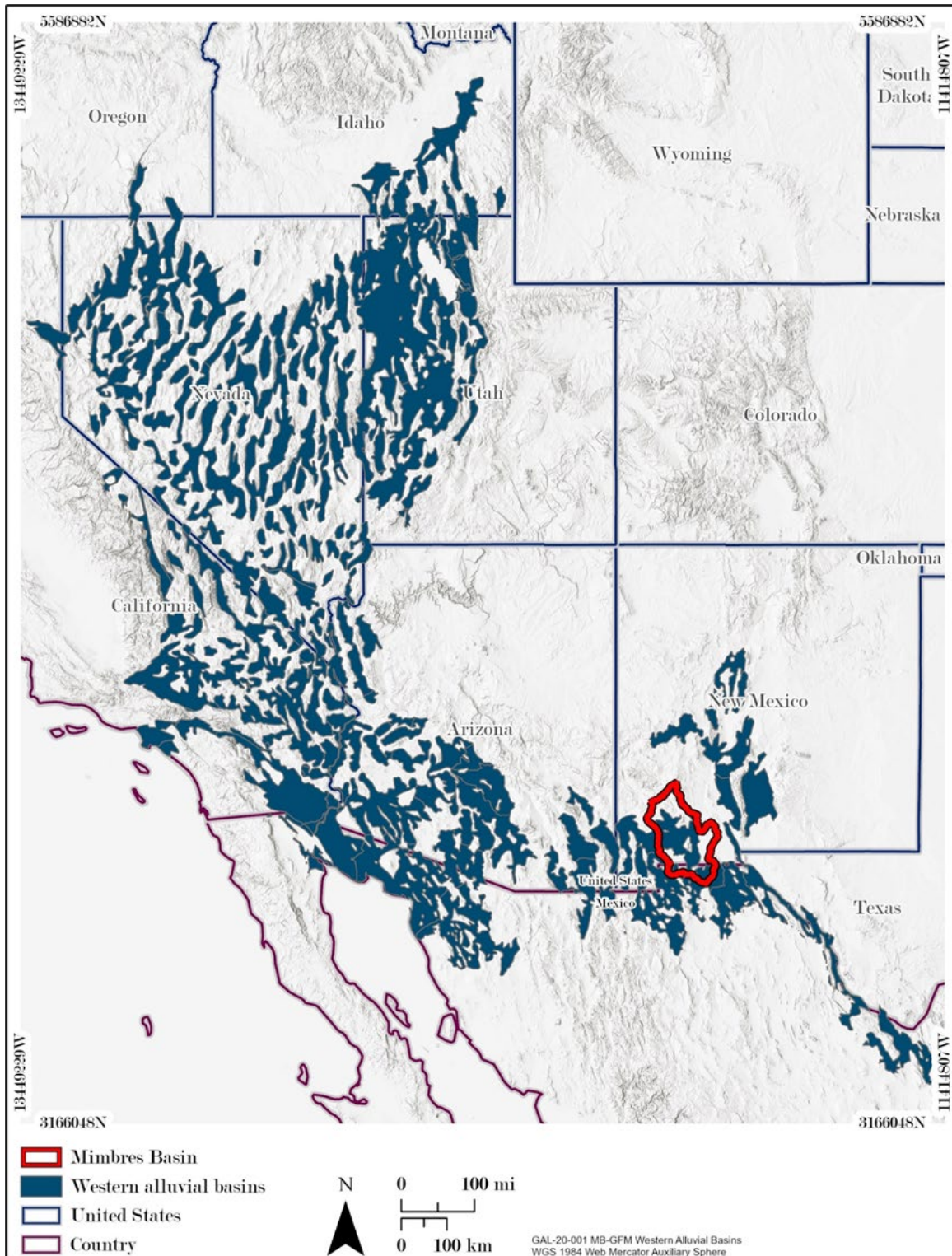
Figure 1-1. Alluvial basins of the Basin and Range province in western North America, with the outline of the Mimbres Basin in southwestern New Mexico.
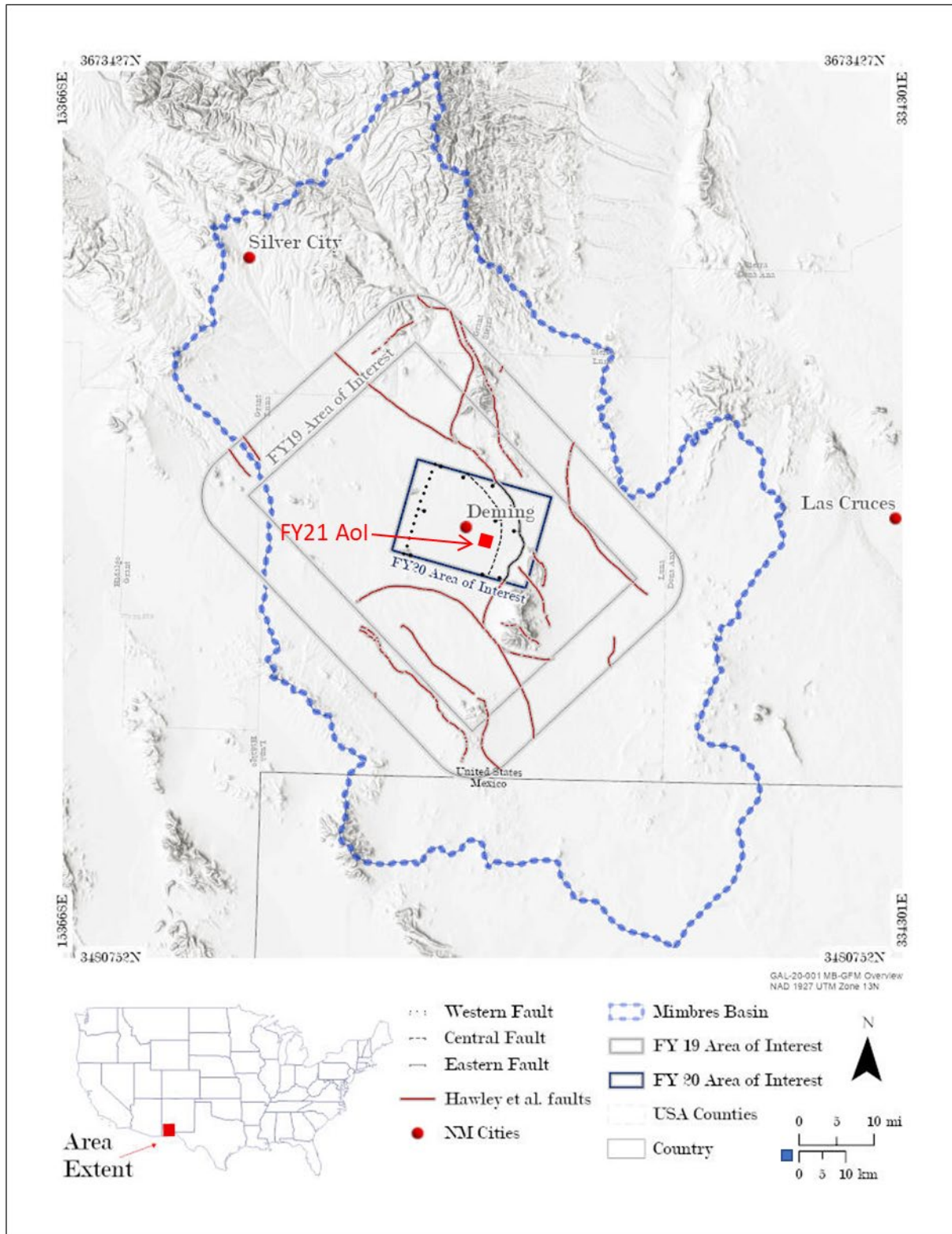
Figure 1-2. Shaded relief map of the Mimbres Basin showing FY19, FY20 and FY21 areas of interest (AoI), regional faults from Hawley et al. (2000) and the three normal faults incorporated into the geologic framework model (GFM).
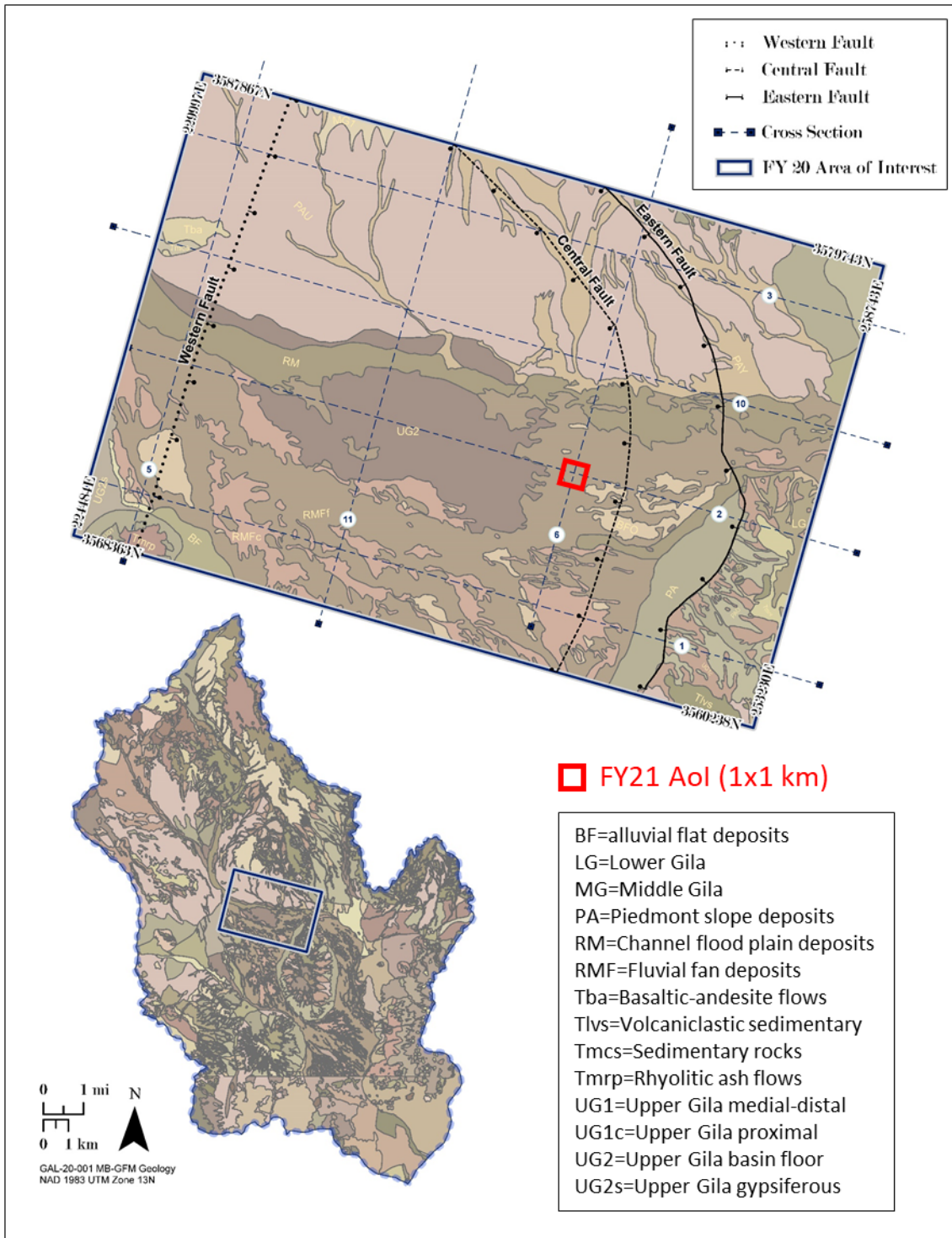
Figure 1-3. Surface geologic map adapted from Hawley et al. (2000) for the FY20 AoI including main normal faults and numbered cross section lines used to build the GFM. The FY21 area of interest (AoI) is the red square.
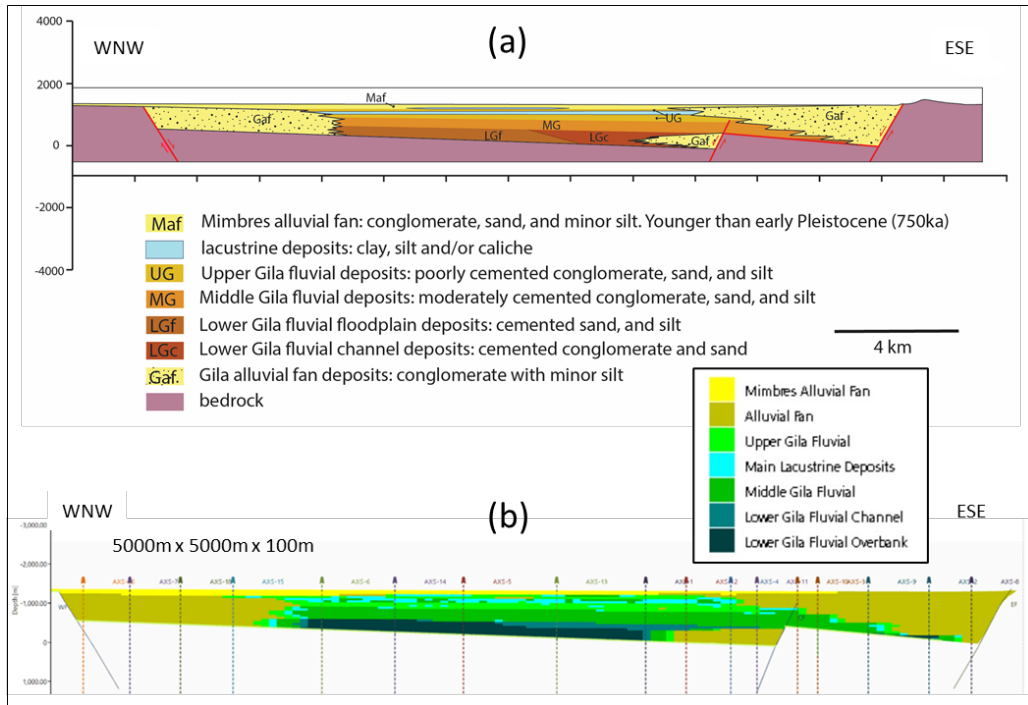
Figure 1-4. (a) Cross-section showing the conceptual distribution of alluvial lithofacies in the basin-fill sediments along section line #2 (Figure 1-3) of the Deming sub-basin. Elevation in meters above mean sea level; (b) Geostatistical model of lithofacies distribution based on vertical synthetic wells from FY20 report (Gross et al., 2020).
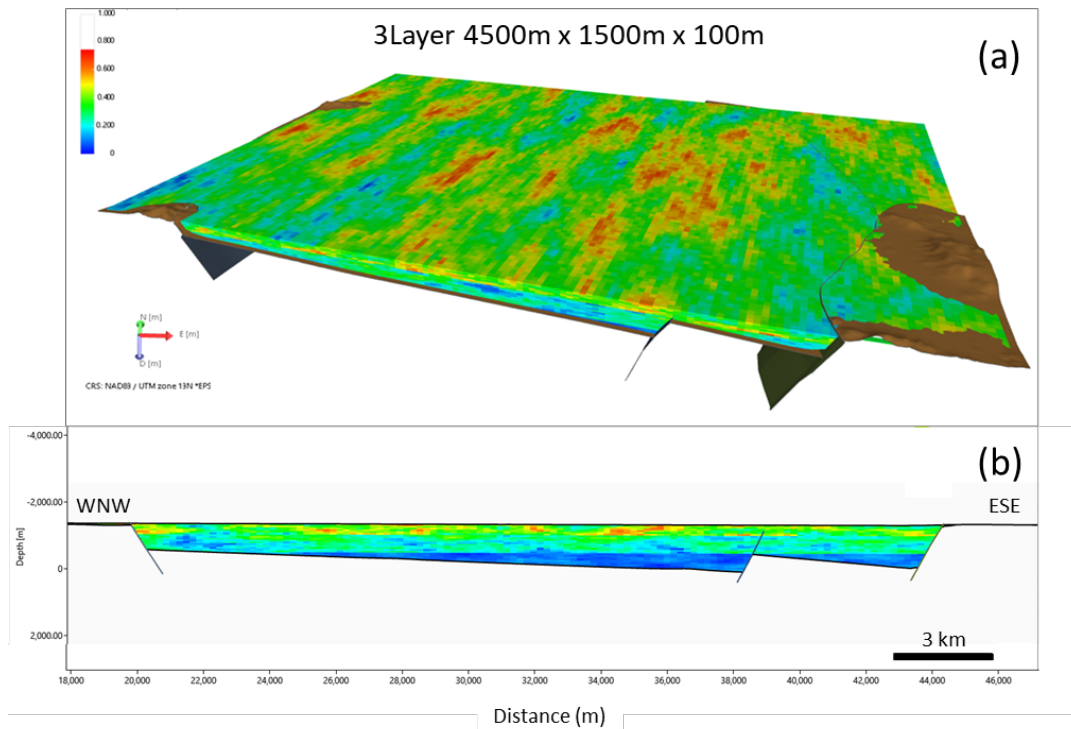
Figure 1-5. Three-dimensional perspective (a) and cross-sectional view (b) of a sub-basin scale porosity model from the FY20 report (Gross et al., 2020).

In FY21 we focused our modeling efforts on the repository scale ("near field" volume) with horizontal dimensions of 1 x 1 km and a vertical dimension of 1.5 km. The volume of interest (VOI) is located within the basin depocenter, west of the buried central fault, where alluvial sediments are thickest (Figure 1-6a, b). It is also strategically located along structural cross section #2, corresponding to the interpreted alluvial lithofacies section. The JS 3D model consists of cells with horizontal dimensions of 15 m x 15 m and a vertical dimension of 5 m, corresponding to ~1.9 million cells within the VOI (Figure 1-6c).

Alluvial sediments are notoriously heterogeneous, both laterally and vertically, in terms of their distribution and physical properties (Sun et al., 2008; Phelps et al., 2010). The main goal of this year's project is to evaluate the impact of this heterogeneity on the movement of radionuclides released from a hypothetical nuclear waste repository in the unsaturated zone (alluvium) reference case. We explore different scenarios for the geostatistical distributions of lithofacies and their corresponding physical properties to establish a baseline characterization of radionuclide transport in laterally continuous layered facies versus discontinuous facies.
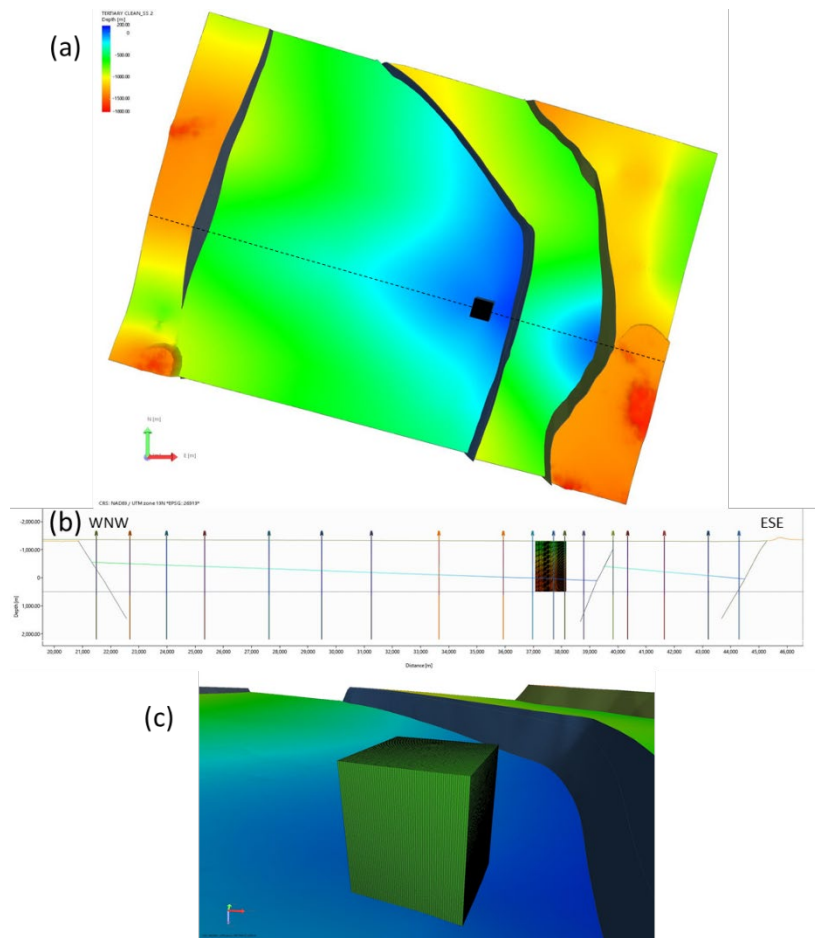
Figure 1-6. (a) Location of the FY21 volume of interest (black square) in the geologic framework model, showing base of alluvium surface (contours in subsea elevation), main normal faults and cross section (dashed line); (b) Cross section profile showing base of alluvium, normal faults, synthetic wells from FY20 and volume of interest; (c) 3D perspective of the grid volume for FY21 models.

2.   Lithofacies Modeling

2.1   Overview

Two main lithofacies models were constructed for the near-field volume. The first is a tabular model consisting of continuous, horizontally layered units of alluvial sediments. In this model each lithofacies unit has a constant thickness across the volume. The second is a discontinuous facies model, where facies thickness and connectivity vary both laterally and vertically throughout the volume. The method for building the 3D geocellular models is based on placing synthetic vertical wells at strategic locations in the conceptual lithofacies model (Figure 2-1). This reflects the scenario for a "frontier basin" at the exploratory phase, where subsurface data are limited. In contrast, a data-rich basin at an advanced stage of analysis would have available numerous wellbores drilled through the alluvium with recovered core and sample cuttings, suites of modern geophysical logs and measurements of petrophysical properties.
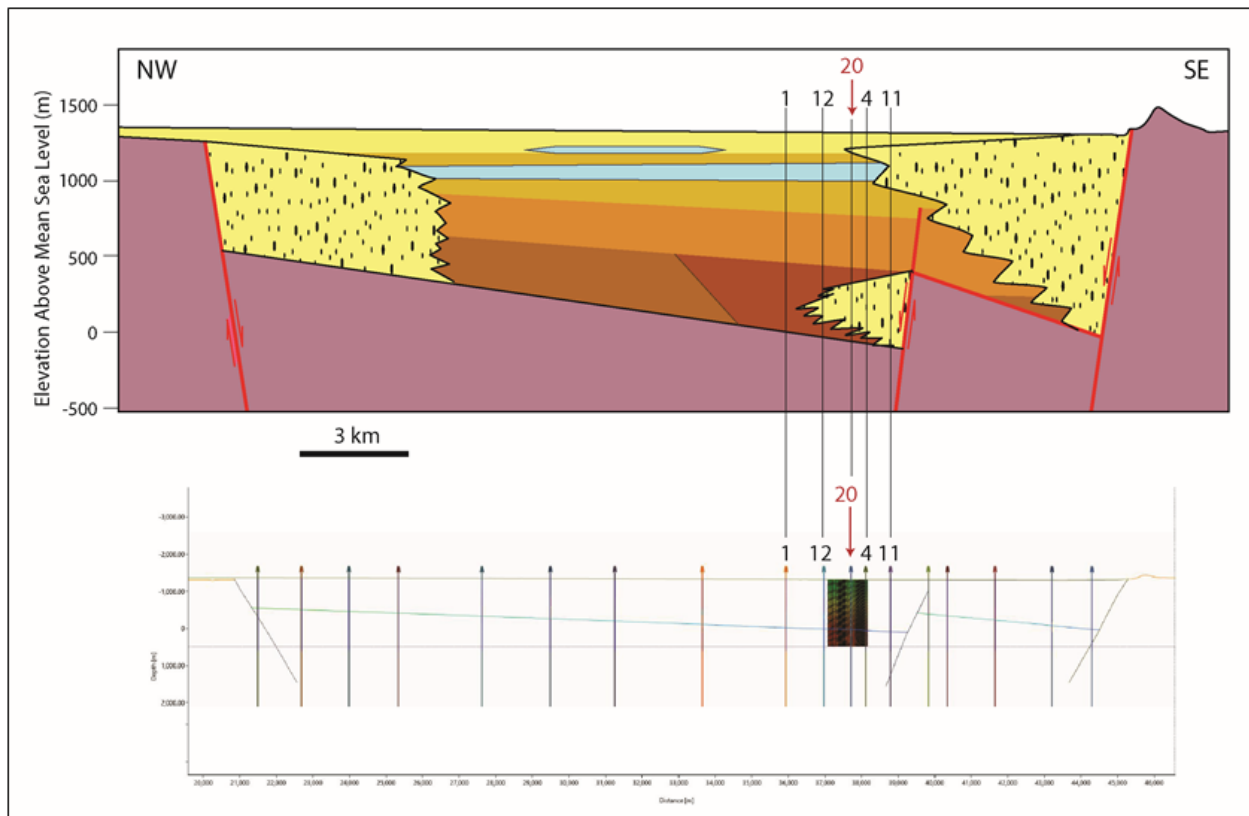
Figure 2-1. Vertical synthetic wells used to extract lithofacies tops for modeling facies and physical properties in JewelSuite[TM] for the near field volume. Refer to Figure 1-4 for facies legend. Conceptual facies model has 4x vertical exaggeration.

For FY21 one new synthetic well (Well No. 20) was added near the center of the near-field volume of interest and the four adjacent wells from FY20 were resampled. Moving from

southeast (Well No. 11) to northwest (Well No. 1), note how the facies interfinger, change thickness and may be repeated or missing in some wells (Figure 2-1). Lithofacies tops were measured for each synthetic well from the vertically exaggerated (4x) facies model (Table 2-1). A well log was then created for each synthetic well with the corresponding numeric facies values assigned at 10 m intervals. The well logs were upscaled to the grid through the k-layer averaging strategy (Baker Hughes, 2020).

Table 2-1. Tops of lithofacies units encountered in the five synthetic wells used for modeling the near field volume. Elevation in meters above mean sea level.

Lithofacies	JS Facies	Well 1 Elevation (m)	Well 4 Elevation (m)	Well 11 Elevation (m)	Well 12 Elevation (m)	Well 20 Elevation (m)
Top Mimbres alluvial fan	1	1324	1324	1324	1323	1323
Top Minor Lacustrine deposits	2	none	none	none	none	none
Top Alluvial Fan deposits	3	none	1224	1237	none	1219
Top Upper Gila fluvial	4	1182	1163	953	1182	1182
Top Main Lacustrine deposits	5	1118	1123	none	1119	1122
Top Upper Gila fluvial (repeated)	4	1001	1004	none	1003	999
Top Middle Gila fluvial	6	796	768	761	781	772
Top Lower Gila fluvial channel	7	463	420	407	441	425
Top Lower Gila fluvial overbank	8	none	none	none	none	none
Top Alluvial Fan deposits (repeated)	3	none	337	377	283	323
Top Lower Gila fluvial channel (repeated)	7	none	-47	none	64	27
Top Bedrock Volcanics	9	8	-75	-100	-38	-60

2.2 Tabular (single well) model

Lithofacies tops from a single well (Well No. 20) were used to construct the tabular facies model. For each interval (i.e., vertical distance between lithofacies tops in Table 2-1) encountered by Well No. 20, constant facies values were assigned to those k-layer grids throughout the volume. The result is a model of stacked horizontal layers, each having constant thickness across the volume (Figure 2-2). The lithofacies layers can thus be described as continuous (i.e., connected).
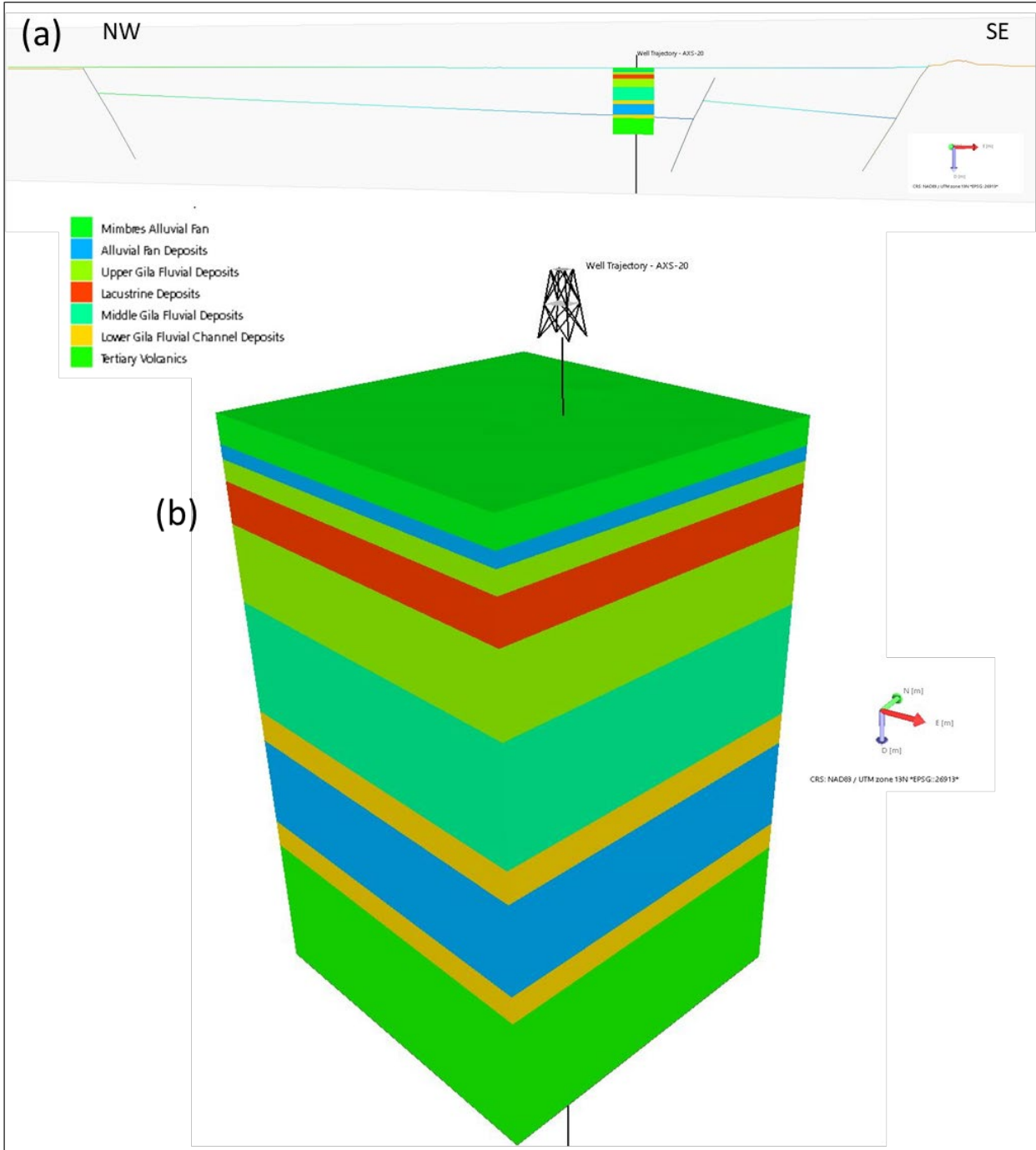
Figure 2-2. The tabular lithofacies model in cross section (a) and 3D perspective (b). Horizontal dimensions are 1 km x 1 km. Vertical dimension is approximately 1.5 km.

2.3 Discontinuous (multi-well) model

Five synthetic wells were used to model facies distributions across the model domain (Figure 2-1; Table 2-1). This required extending the model volume along the strike of the cross section to avoid edge effects and to evaluate the degree of facies connectivity. The sequential indicator simulation (SIS) was employed as the variogram-based geostatistical method for modeling facies as it is best suited for integer-coded discrete variables (Shepherd, 2009). Models were run for horizontal ranges of 2000m, 1000m, 750m and 500m to evaluate the impact of correlation distance on lateral facies continuity. For all cases the vertical range was set at 100 m and a spherical variogram type was employed.

The facies were conditioned to the wellbore data, as seen in the cross-sectional profiles in Figure 2-3 where the wells are projected in front of the grid. The 3D perspectives show how the facies distribution changes systematically from relatively continuous and layered at 1000 m range to isolated patches at 500 m range (Figure 2-4 and Figure 2-5). We selected two discontinuous facies models for property modeling, the 1000m and 750 m horizontal ranges. These were clipped to the near-field volume as shown in Figure 2-6 for export to LaGriT and computational meshing (refer to section 4).
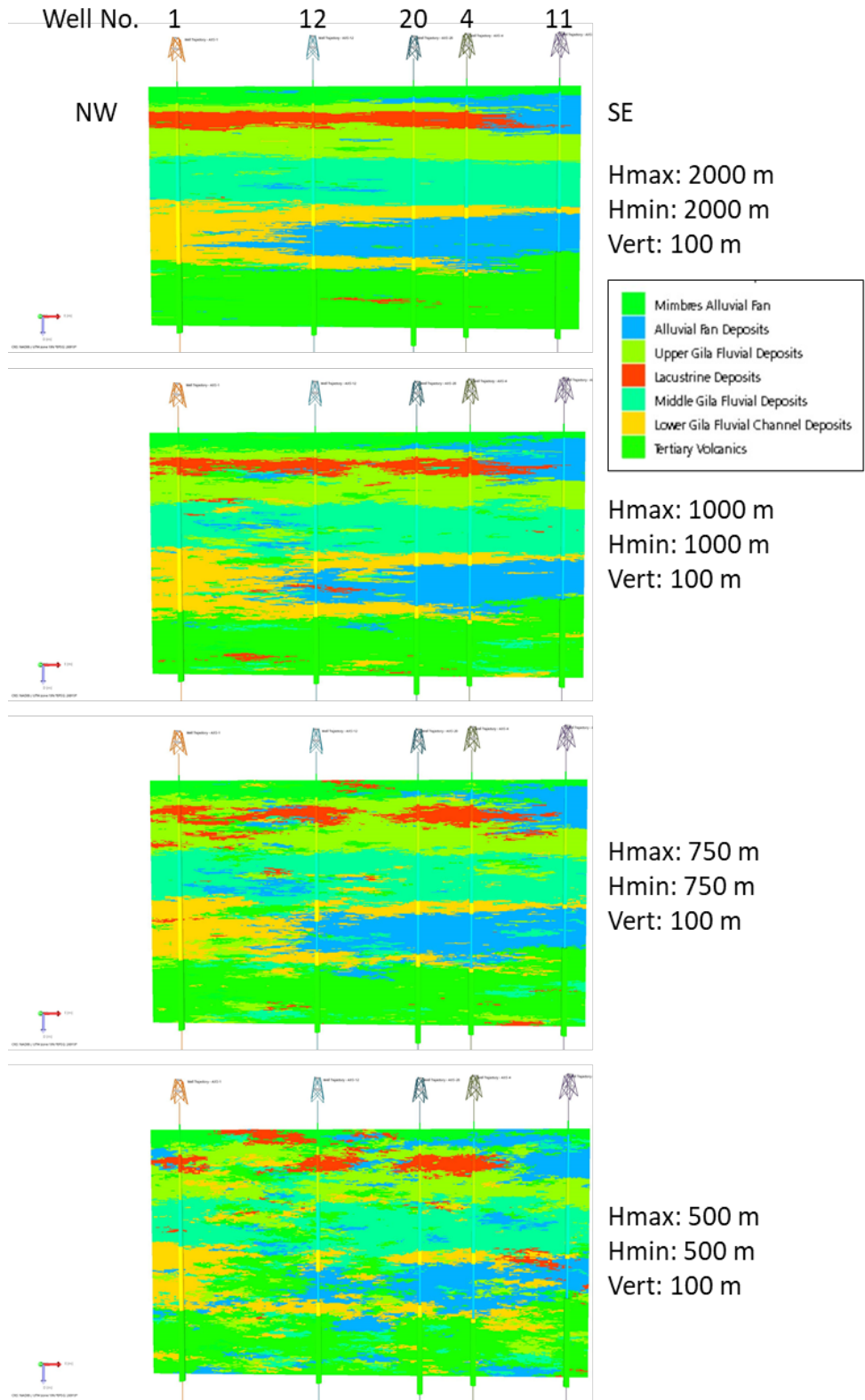
Figure 2-3. Model results for discontinuous facies using different horizontal variogram ranges. Synthetic wells are projected in front of the cross sections to show conditioning of facies.
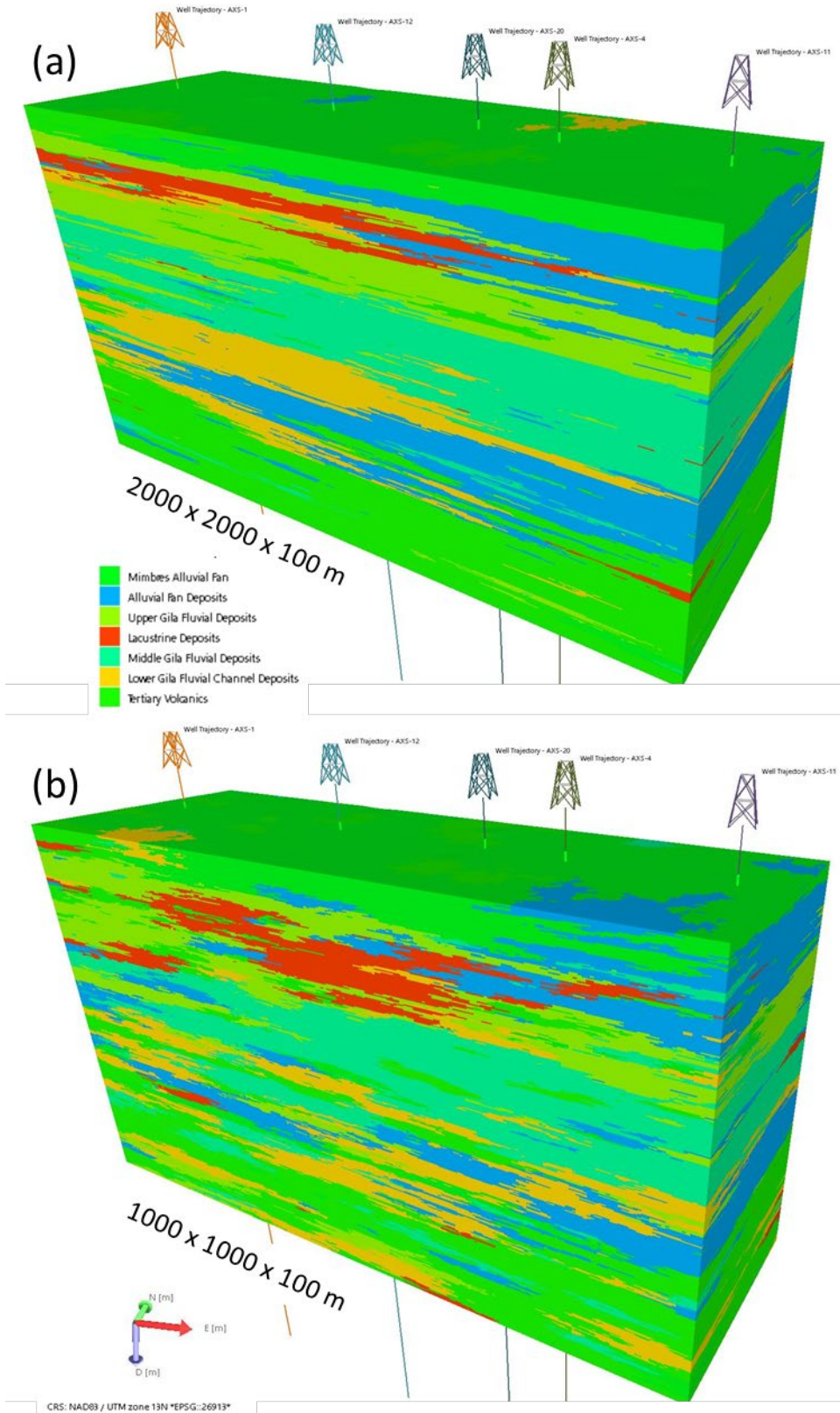
Figure 2-4. Three-dimensional perspectives of discontinuous facies models for (a) isotropic horizontal range of 2000 m, and (b) isotropic horizontal range of 1000 m.
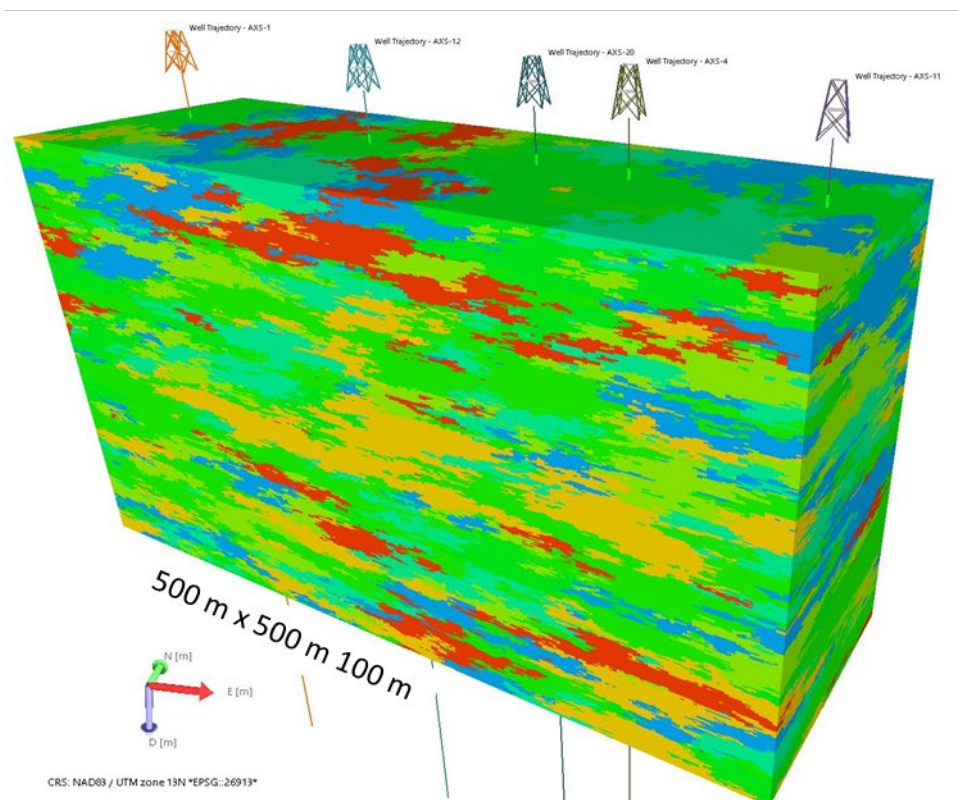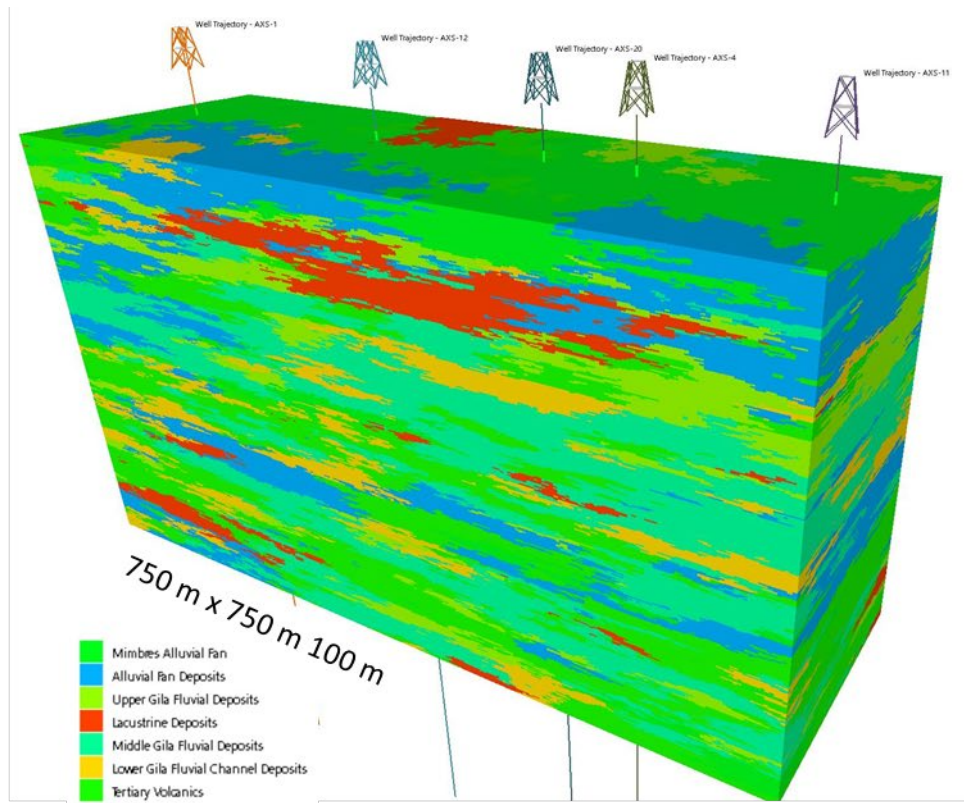
Figure 2-5. Three-dimensional perspectives of discontinuous facies models for (a) isotropic horizontal range of 750 m, and (b) isotropic horizontal range of 500 m.
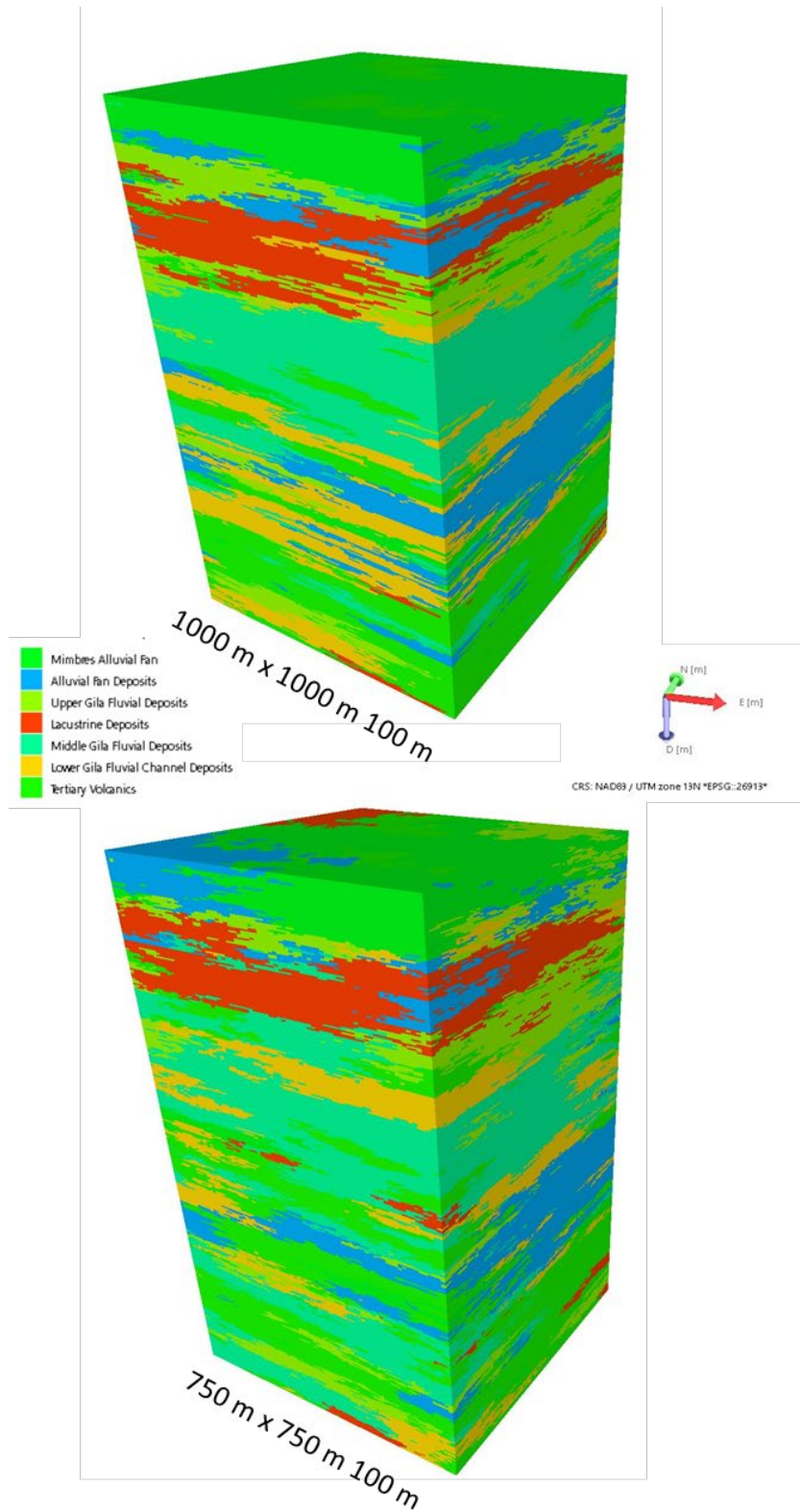
Figure 2-6. Three-dimensional perspectives of the two discontinuous facies models selected for computational meshing and modeling of flow and transport, clipped to the near field volume.

3. Physical Properties Modeling

3.1 Relative permeability estimates

To estimate relative permeability parameters the Buckles method (Buckles, 1965) was used to define residual saturations, which were then used with Brooks-Corey relative permeability curves (Brooks and Corey, 1966). The Buckles method assumes that porosity and residual saturation are hyperbolically related (Equation 3-1)

$$n * S_{rw} = C \qquad\qquad (3\text{-}1)$$

where n represents porosity, S_{rw} is the residual water saturation, and C is the Buckle's constant. Buckles proposed that C should fall between 0.02 to 0.1 for sandstone and 0.01 to 0.06 for intergranular carbonates. The larger the constant the more residual saturation is predicted. We applied different Buckle's constants to each lithofacies to take into account that the fine grained textures of the lacustrine and overbank deposits would retain more water than the coarser lithofacies. Table 3-1 presents the chosen Buckle's Constants as well as the calculated mean residual saturation for each lithofacies. The residual air saturation is assumed to be 0 throughout the model. In this manner the residual saturation and relative permeability curves vary heterogeneously throughout the model domain and account for expected differences between lithofacies.

Table 3-1 Buckle's constant and Residual Saturation

Lithofacies	JS Facies	Buckle's Constant	Mean Residual Saturation
Mimbres Alluvial Fan	1	0.02	0.06
Alluvial Fan Deposits	3	0.02	0.06
Upper Gila Fluvial Deposits	4	0.02	0.05
Lacustrine Deposits	5	0.1	0.22
Middle Gila Fluvial Deposits	6	0.02	0.07
Lower Gila Fluvial Channel Deposits	7	0.01	0.03
Lower Gila Fluvial Overbank Deposits	8	0.06	0.24
Tertiary volcanics (rhyolitic tuff)	9	0.02	0.1

3.2 Property modeling in JewelSuite™

Physical properties were assigned to the alluvial lithofacies and underlying bedrock based on values reported in the literature for similar rock types in the Mimbres and other alluvial basins (Kennedy et al., 2000; Phelps et al., 2010; Mariner et al 2018; Sevougian et al., 2019). For each lithofacies, the mean, standard deviation, minimum and maximum values for porosity and permeability are presented in Table 3-2. Permeability modeling in JS was performed using micro-darcy units, which were converted back to m^2 units for flow and transport simulations. For

geostatistical models, the sequential gaussian simulation (SGS) variogram method was used and a directional anisotropy was imposed in the horizontal plane, with a major axis of 015 degrees azimuth parallel to the basin margin and range-bounding normal faults. Horizontal variogram ranges were estimated based on degree of connectivity reported by Hawley et al. (2000). Permeability was conditioned on porosity with a 0.5 correlation. Property modeling was performed on four facies models (refer to Table 3-3), resulting in a total of eight property output files (four each of porosity and permeability).

For the tabular facies model, one set of hydrogeologic models (Model 1A) assigned constant porosity and permeability for each facies whereas the other set of models (Model 1B) distributed the properties geostatistically (Figure 3-1). The geostatistical model (1B) allows for varying degrees of heterogeneity within each unit, though lithofacies layering remains prominent throughout. In both the constant and heterogenous models for the tabular facies, the lacustrine layer (fourth unit from the top) is characterized by a low permeability zone of finite thickness (Figure 3-1). This unit would serve as a major barrier to vertical flow in the unsaturated zone due to its continuity across the volume.

Applying the same statistical parameters from Table 3-2 to the discontinuous facies models yield markedly different results from the tabular facies models. Porosity values are dispersed more widely throughout the volume rather than mostly confined to discrete intervals, and permeability within the lacustrine layer is not fully connected (Figure 3-2). The differences between the 1000 m range and the 750 m is rather subtle, but close inspection of the porosity models shows greater connectivity and stratigraphic definition for the 1000 m range (Model 2A).

Table 3-2. Values for porosity, permeability and variogram ranges used to model physical properties in JS.

Lithofacies	JS Facies	Porosity				Permeability (k)					Variogram Ranges		
		Mean	StanDev	Min	Max	Mean	log Mean	log StanDev	log Min	log Max	Major	Minor	Vertical
		-	-	-	-	m2	µd	µd	µd	µd	m	m	m
Mimbres Alluvial Fan	1	0.35	0.07	0.09	0.53	2.96E-12	6.48	6.18	4.48	8.48	90	30	15
Alluvial Fan Deposits	3	0.33	0.07	0.08	0.49	1.18E-12	6.08	5.78	4.08	8.08	90	30	15
Upper Gila Fluvial Deposits	4	0.38	0.04	0.19	0.49	3.55E-11	7.56	7.26	5.56	9.56	300	100	15
Lacustrine Deposits	5	0.45	0.05	0.23	0.59	1.18E-15	3.08	2.78	1.08	5.08	500	500	15
Middle Gila Fluvial Deposits	6	0.30	0.03	0.15	0.39	2.37E-11	7.38	7.08	5.38	9.38	300	100	15
Lower Gila Fluvial Channel Deposits	7	0.30	0.03	0.15	0.39	1.18E-11	7.08	6.78	5.08	9.08	300	100	15
Lower Gila Fluvial Overbank Deposits	8	0.25	0.03	0.13	0.33	5.92E-13	5.78	5.48	3.78	7.78	225	150	15
Tertiary volcanics (rhyolitic tuff)	9	0.21	0.02	0.15	0.25	1.78E-12	6.26	5.95	4.26	8.26	400	400	50

Table 3-3. The four suites of property models investigated in this study.

Model Type	Model Name	Facies Model	Property Model for porosity and permeability
Tabular	1A	Constant facies	Constant properties
	1B	Constant facies	Geostatistical properties (SGS, facies specific)
Discontinuous	2A	Geostatistical facies (SIS, 750m x 750m x 100m)	Geostatistical properties (SGS, facies specific)
	2B	Geostatistical facies (SIS, 1000m x 1000m x 100m)	Geostatistical properties (SGS, facies specific)
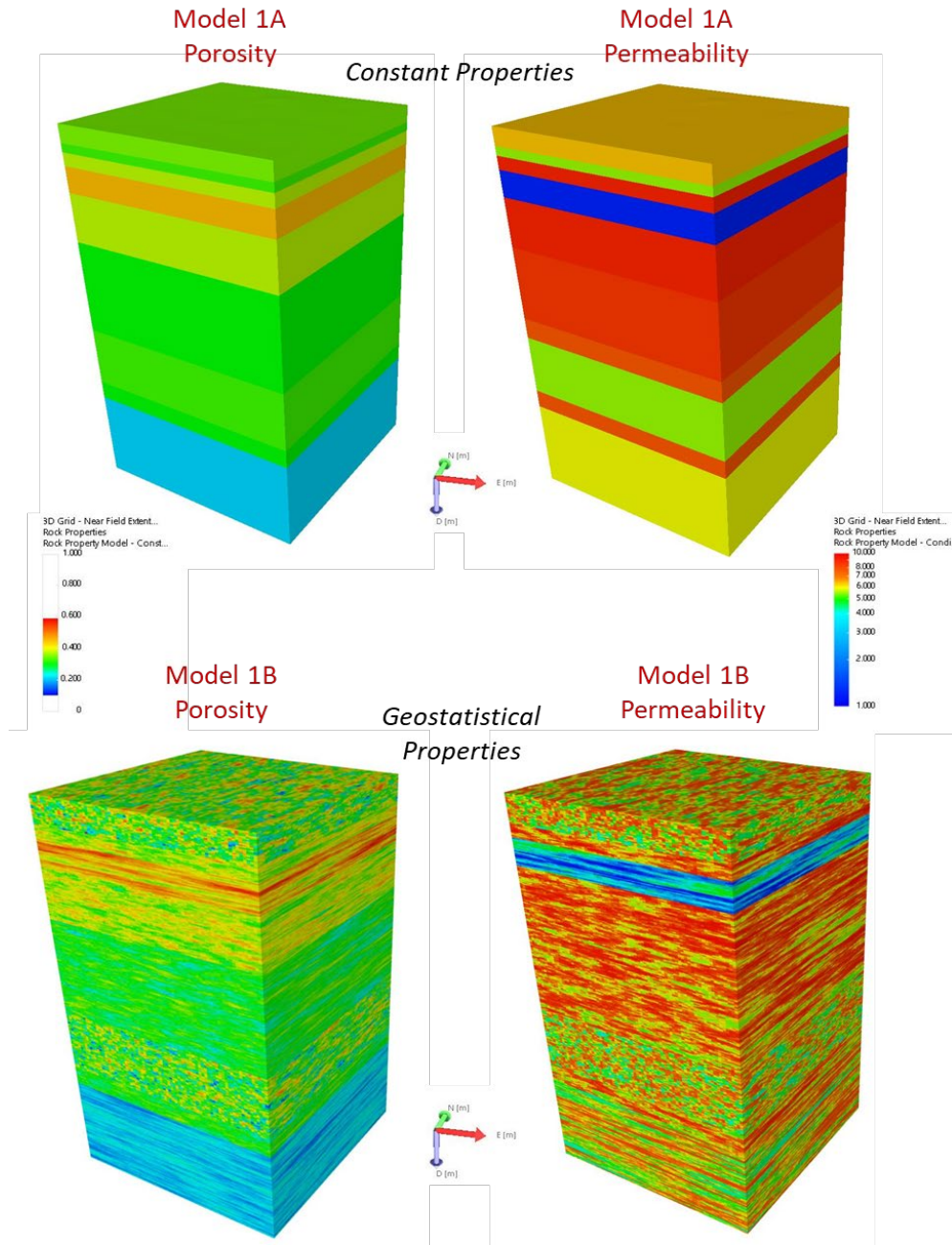
Figure 3-1. Porosity and permeability model results for tabular facies (Models 1A and 1B).
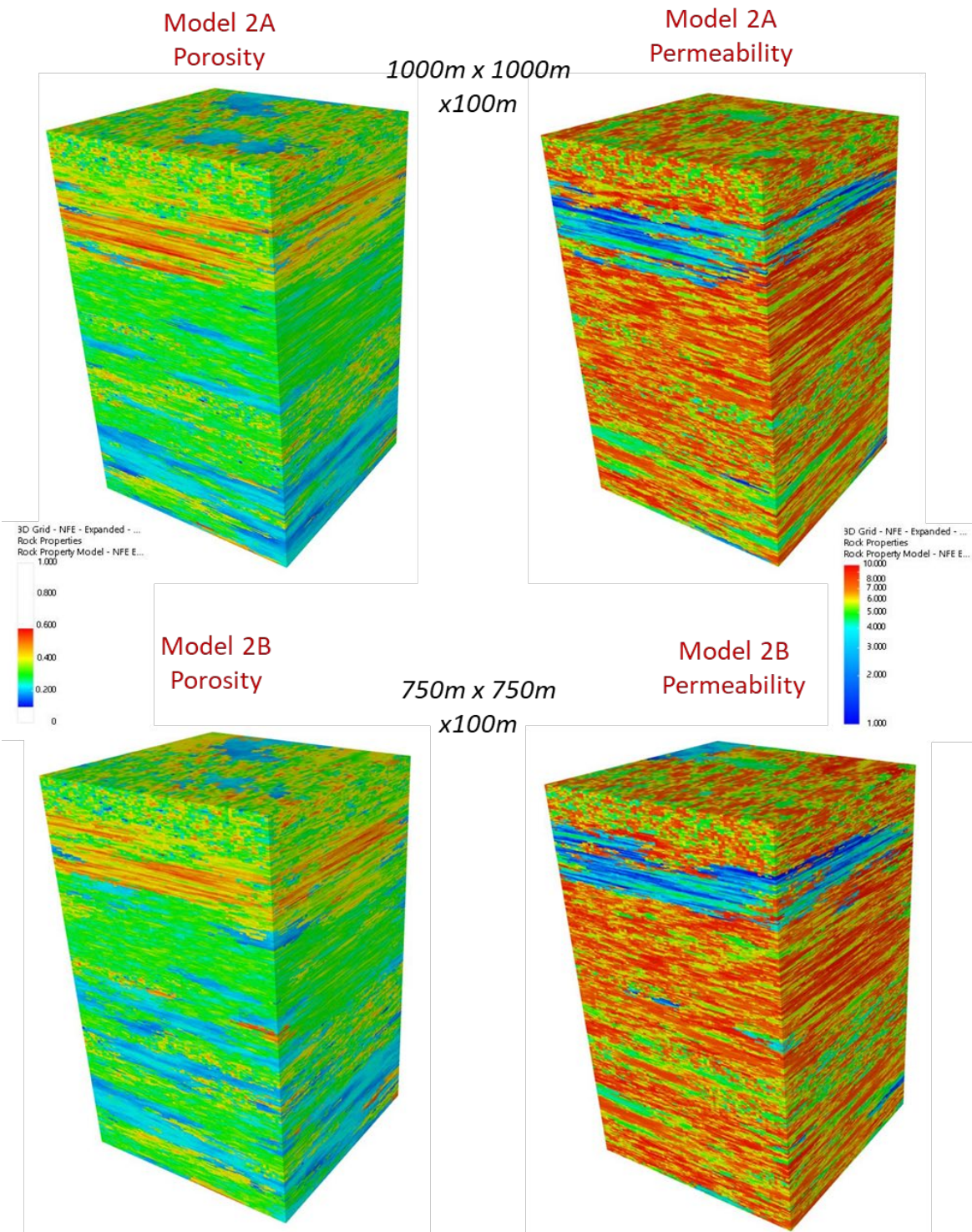
Figure 3-2. Porosity and permeability model results for discontinuous facies (Models 2A and 2B).

4. Computational Meshing

This work establishes a meshing workflow between JewelSuite™ and geologic modeling applications. Methods for this workflow were tested in FY19 and FY20 using an early version JS GFM and synthetic property data. This workflow converts information from the GFM into computational meshes which are later used in hydrogeologic models (Miller et al., 2007).

JS has well developed tools for defining geologic properties based on facies distribution including permeability and porosity. We start with a Tabular 1B model to test and evaluate methods developed in FY20. This method reads the properties calculated in JS and applies them to a computational mesh and writes files for simulations.

This year the workflow emphasized geostatistical models from JS applied to computational meshes for simulations. Two model areas were defined; a large box shaped domain within the extents of the JS basin model, and a fine resolution domain located entirely within the deepest alluvium with 1000 x 1000 meter sides and 1000 meters deep. This small area model is the work accomplished this year FY21.

The following are the steps we use for this work. The steps are iterative from building the JS model, to meshing, to the modeling simulations. Each step may reveal changes to be made at an earlier step so that all the next steps have to be done again. The necessity for the process being iterative also makes it important that as much of the workflow as possible be automated.

- Import GOCAD 3D geometry and materials exported from JS

- Examine and clip model areas into subsets for meshing

- Build small area mesh for PFLOTRAN and FEHM simulations

- For JS property models 1B, 2A, and 2B

  - Process and check JS property data

  - Upscale property data to computational mesh

  - Check and report upscale results

  - Write FEHM and PFLOTRAN simulation input files

The simulations are performed using PFLOTRAN (PFLOTRAN, 2020) and FEHM (FEHM, 2020) and are compared using the same boundary conditions and computational meshes. FEHM and PFLOTRAN have mesh requirements that ensure the accuracy of simulations used on the mesh. They use a two point flux approximation across control volume faces that are the Voronoi dual of a Delaunay tetrahedral mesh. Therefore we use meshing software that can create meshes to meet the Delaunay criteria, LaGriT (LaGriT, 2021).

LaGriT is an open source software developed at Los Alamos National Laboratory that provides a variety of meshing tools with capabilities specific to geologic applications and Voronoi control volume solvers. LaGriT is used to generate meshes with control volume discretization such that the underlying control volumes are Voronoi tessellations as required by FEHM and

PFLOTRAN. LaGriT also provides tools to write setup files that meet the simulation software requirements. Flow and transport simulation setup includes boundary conditions, initial conditions, properties such as the material distribution and geostatistical properties generated from JS.

The upscale command used by LaGriT for this work is described at
https://lanl.github.io/LaGriT/pages/docs/commands/UPSCALE.html.

For a set of high resolution data points and a computational mesh located in the same space, this command finds all points inside the volume of each mesh node. A single value is applied to each mesh node using a choice of averaging functions. For the facies integer values we use min and max. For the float type property values we use the geometric average where for each sink point, we calculate the geometric average of n values found for a mesh node. The value is calculated by $(x(1) * x(i)\ldots * x(n)) * *(1/n)$ where n is the number of data points found for a mesh node. We also use the sum function to check that every mesh node has at least one data point within its volume.

4.1   JewelSuite™ 3D GFM Export for Meshing

The first step in the meshing workflow is to import the JS GFM into files that can be used by LaGriT for creating a mesh and property files for the modeling applications.

We developed an interface between JS and LaGriT by adding a GOCAD TETRA reader to LaGriT software. The JS application can export a tessellated mesh that represents the bounding surface of each geologic volume. The exported mesh must be air-tight, i.e., cannot have gaps between volumes, and the volumes cannot intersect.

LaGriT is used to extract the outside boundary surfaces as well as the internal interfaces as represented by differing cell colors. For ZoneId, the surfaces representing a material can be extracted so there is one internal surface between ZoneId 1 and 2. Using CompartmentId the fault surface can be extracted by the surface between CompartmentId 1-2 and 3-4. The extracted surfaces are valid triangulations and used in the meshing process to build a computational mesh.
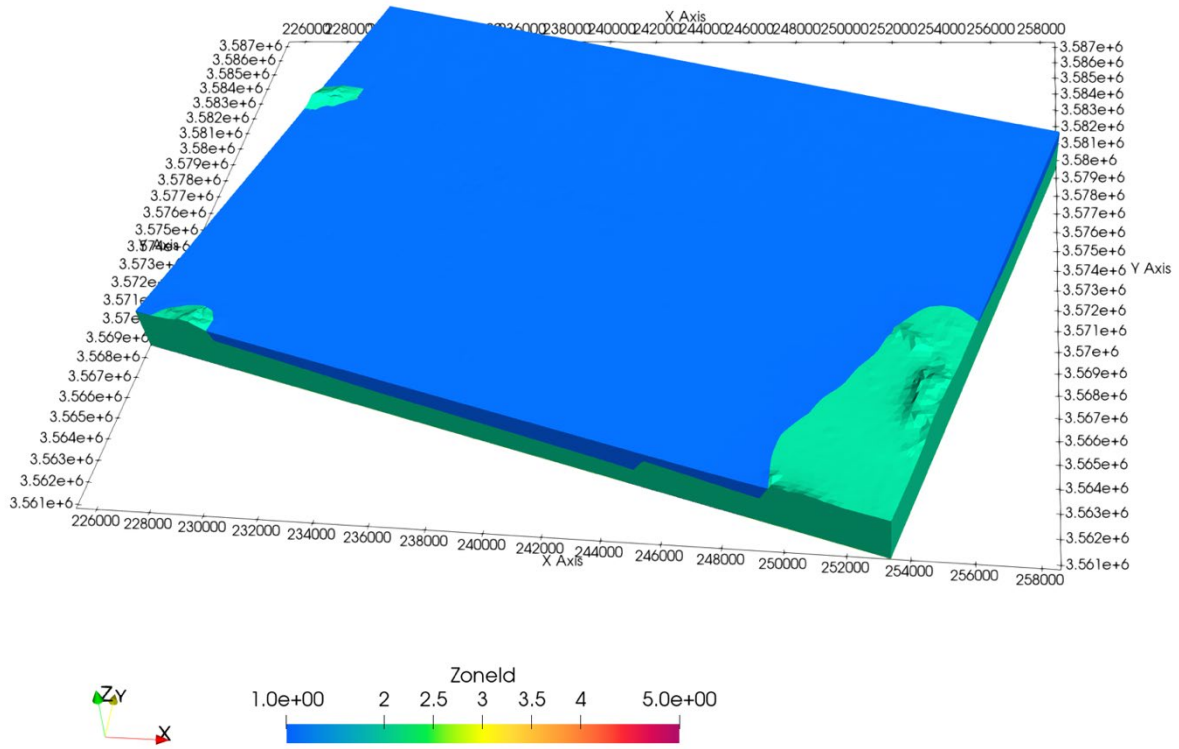
Figure 4-1. Exported JS GFM showing Zone ID material layers, alluvium (blue) and basement (green).
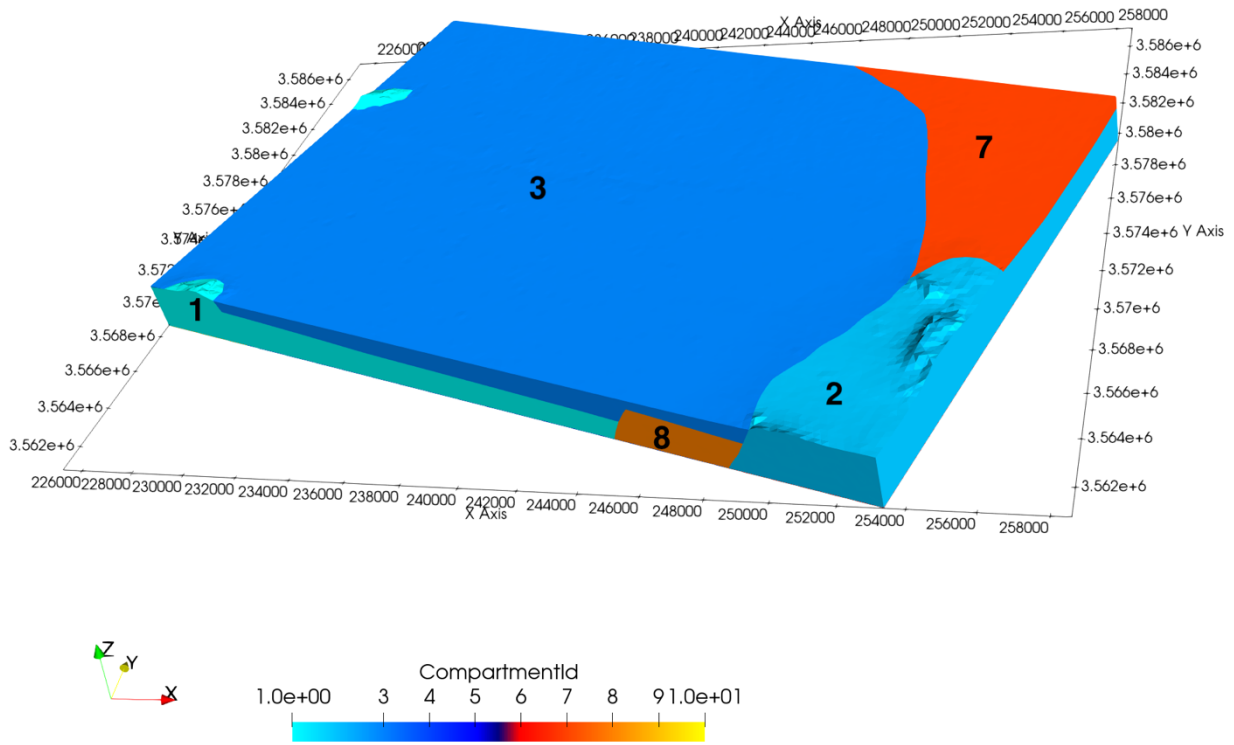
Figure 4-2. Exported JS GFM showing Compartment ID numbers which divide zones into pieces separated by faults.

Surfaces for the meshing workflow are extracted using Compartment ID, which includes the faults and alluvium surfaces. LaGriT extracts surfaces defining boundaries and material or compartment interfaces. For example, the eastern fault surface is the interface between Compartment ID combined blocks 7,2 and 3,8 in Figure 4-2 The alluvium bottom surface is the interface below Compartment ID 3,7. The resulting fault surfaces are shown in Figure 4-3 and the alluvium top and bottom surfaces in Figure 4-4 and **Error! Reference source not found.**.
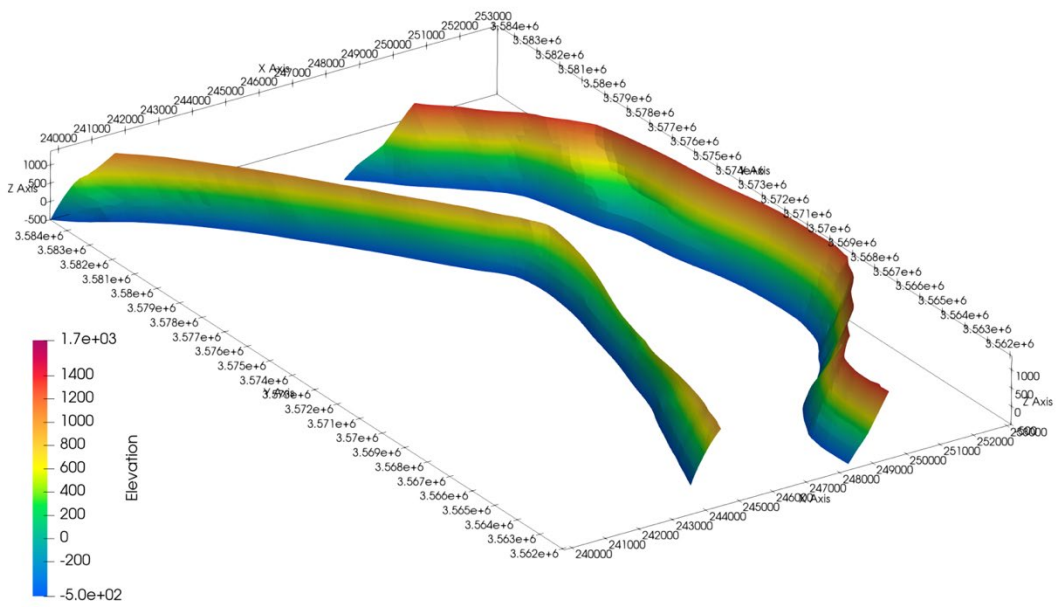
Figure 4-3. Fault surfaces extracted from JS GFM showing elevation (meters).
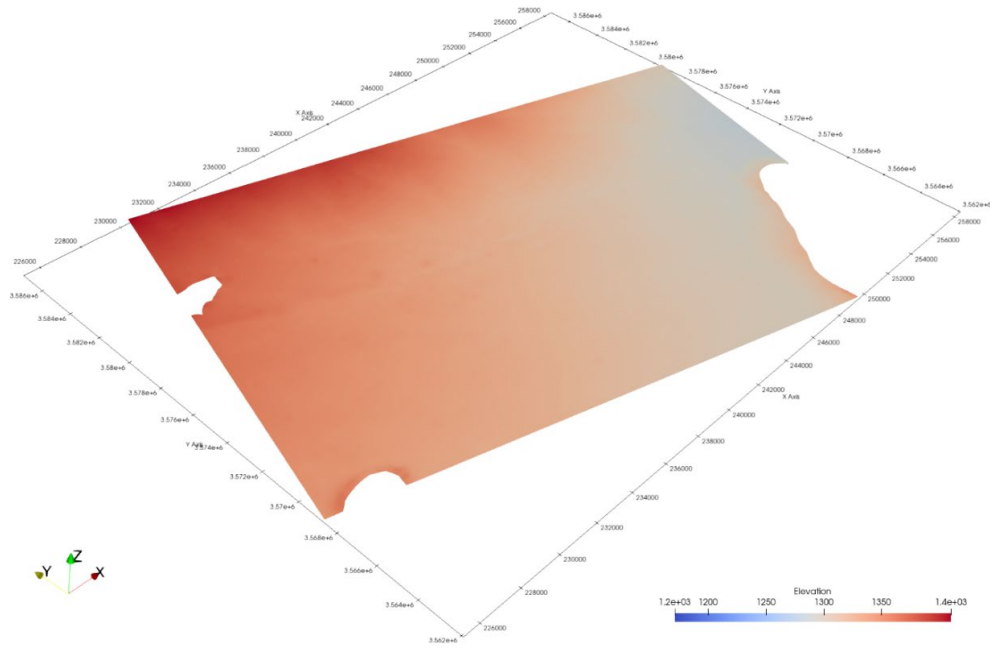
Figure 4-4. Alluvium top surface extracted from JS GFM showing elevation (meters).
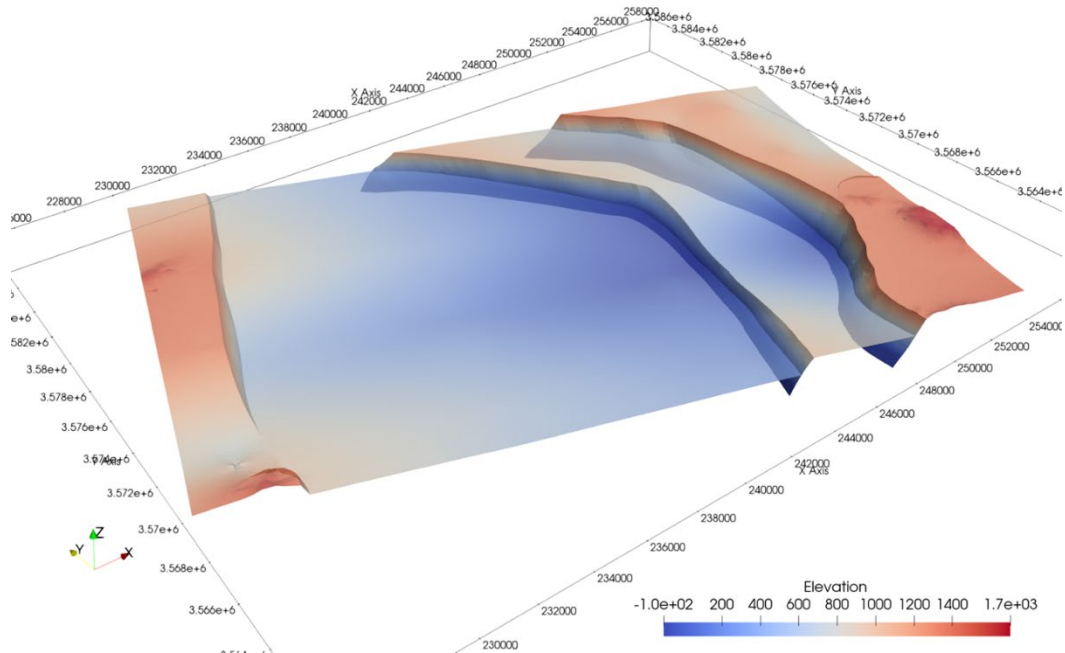
Figure 4-5. Alluvium bottom (transparent) and fault surfaces extracted from JS GFM showing elevation (meters).

The last step of processing for the extracted GFM is to move the JS diagonal coordinates to the X-aligned computational space. The surfaces are aligned along the X-Axis and the X,Y coordinates are translated to 0,0 for improved numerical accuracy (Figure 4-6). These surfaces are used in the meshing workflow to examine location and elevations for the mesh design and modeling plans.
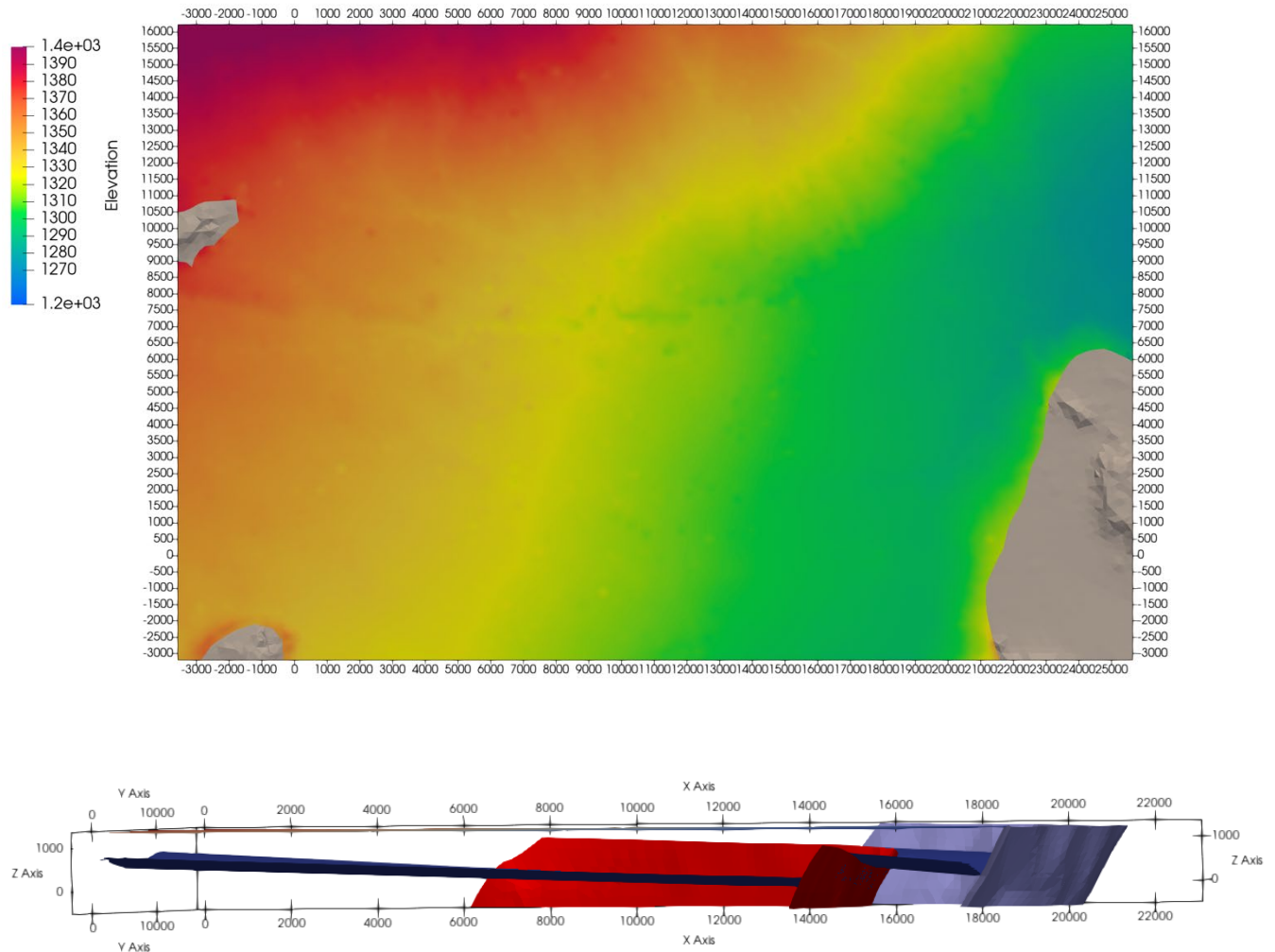
Figure 4-6. Extracted JS surfaces with top view (top image) showing elevations and outcrops on translated alluvium surface. Gray shading represents exposed bedrock. Bottom image shows side view alluvium surfaces and faults. Translated coordinates are X-Aligned with intermediate lower left corner positioned at 0,0. The Z coordinates are unchanged.

4.2   GFM Subset Models for Meshing

Intermediate and small subsets were determined by evaluating the JS GFM. The small subset is the near field 1x1 km model and the intermediate subset is the 20x10 km model. The intermediate subset was a box located within the full basin model and intersected by one fault. The small area model was located within the intermediate model and in the deepest (i.e.,

thickest) alluvium not intersected by a fault. The subsets are box shaped with small and larger intermediate domain (Figure 4-7).
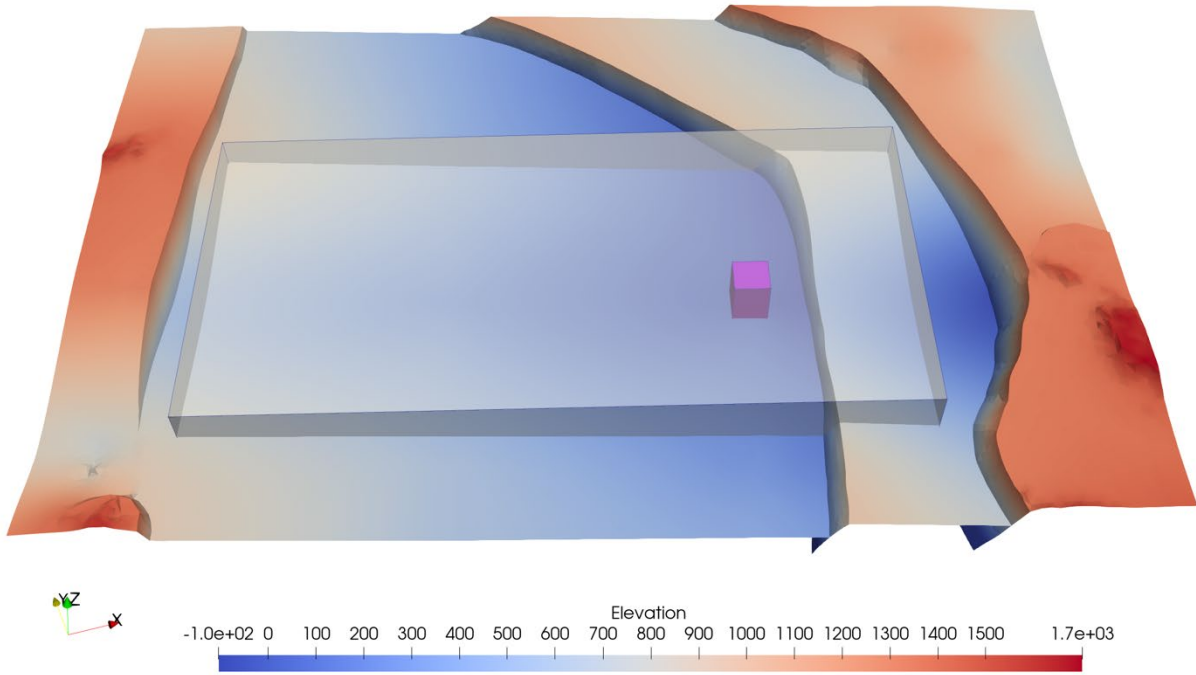
Figure 4-7. Intermediate area (transparent box) and small area (pink box) shown with full model alluvium bottom and faults (elevation meters).

The alluvium top and bottom surfaces exported from JS are used during the meshing process to evaluate the model domain for mesh design and then later for checking results from the property data. Figure 4-8 shows the alluvium intermediate subset relative to extracted fault surfaces. This shows that the intermediate domain intersects the central fault but is not far from the eastern fault.
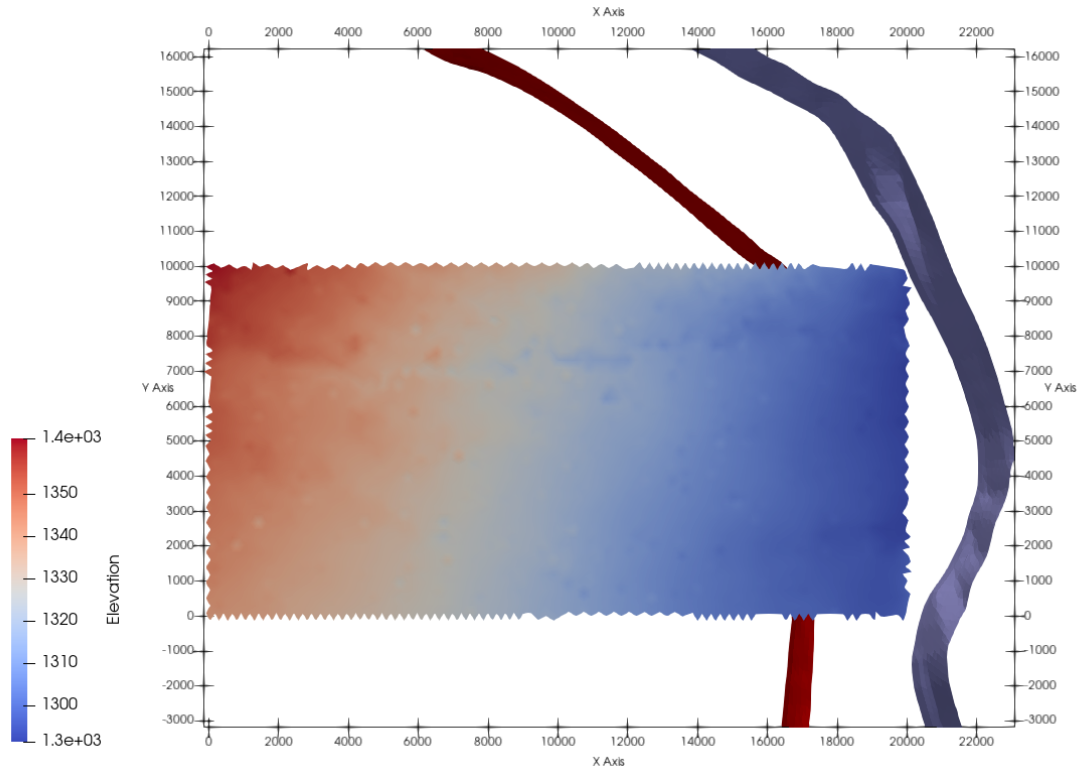
Figure 4-8. JS top alluvium surface clipped for the intermediate size area shown with fault surfaces.

As seen in Figure 4-9, the subset surfaces for the small area domain show that a 1000 meter deep model will be located fully inside the alluvium. We find the top alluvium surface has a change of elevation near 6 meters across the small area domain. This means that a mesh with vertical resolution of 10 meters can be represented with a flat top.
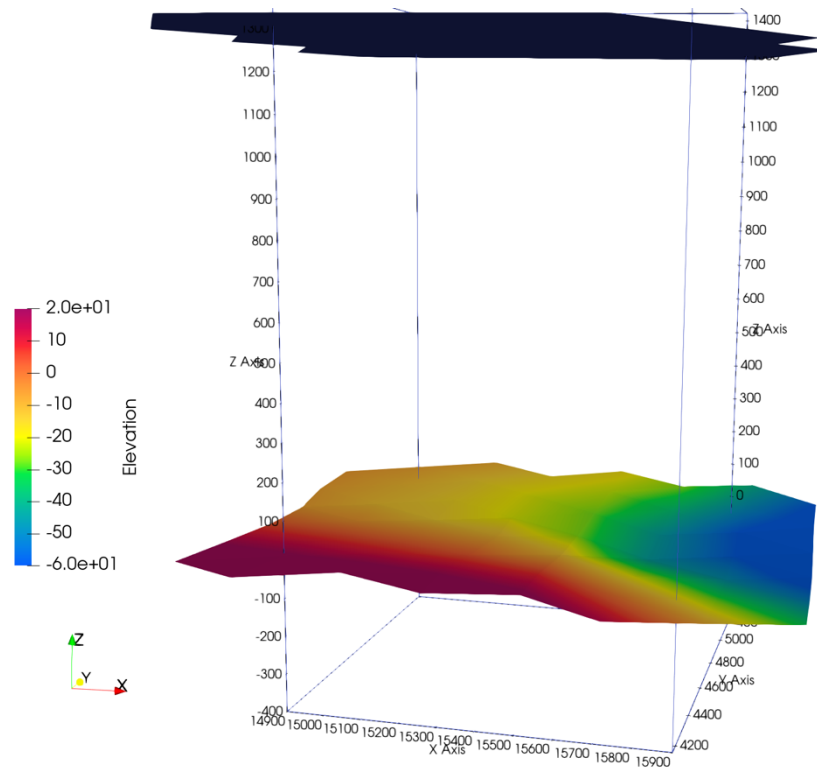
Figure 4-9. JS alluvium top and bottom surfaces clipped to the small area domain. The box outline shows full model vertical elevations between -60 to 1400 meters. For a 1000 meter deep model, the domain will be entirely in the alluvium.

4.3   Computational Mesh for Flow and Transport Simulations

The small area domain is chosen to develop a workflow for using JS properties for simulations. The same mesh is used to upscale all the JS Property models, including models 1B, 2A and 2B as described in Section 3.

There are various meshing methods used for geologic applications which include unstructured and structured mesh types, both with adaptive refinement to geological features. The unstructured approach allows for the creation of meshes that exactly conform to the geometric model, but requires some expertise in building the mesh such that it will also meet the Delaunay criteria.

We use a structured mesh which is the easiest to create. It is a rectangle domain with flat boundaries broken into cells of equal sizes in 3 directions. When this point distribution is connected into a tetrahedral mesh, it satisfies the Delaunay criteria. This method is also very useful for creating quick meshes for multiple simulations to explore possible mesh effects and help determine mesh resolution. The mesh resolution is usually tested by running a flow simulation using various computational meshes of differing resolutions.

The small area domain computational mesh has flat boundaries on all sides, including top and bottom. Flat boundaries avoid inaccuracies that can occur with more complex surfaces. Even though the GFM top surface (alluvium top) is not flat, the variation of elevation within the small area is less than the mesh resolution. Second, the topology of the model top in this area is not expected to be a driver for the physics used in these simulations. Therefore, this simplification will not affect simulations.

Various mesh resolutions were explored in FY20, with cell spacing from 10 meters to 100 meters in size. The spacing of 25 meters in the horizontal is adequate for flow and transport simulations. For these simulations we wanted to balance the needs of keeping the total node count within reason while ensuring a fine enough resolution to capture the facies distributions created by JS. Based on past experience in modeling geostatistical properties, the vertical resolution should not exceed 10 meters. Therefore the mesh resolution used for these models is 25 x 25 x 10 meters as shown in Figure 4-10.

We use a hexahedral mesh for the mesh construction and preparation for the modeling applications. The mesh nodes are connected into a tetrahedral mesh satisfying the Delaunay criteria for FEHM and PFLOTRAN simulations. The mesh nodes are the same for both meshes and the hexahedral meshes are used for most images to avoid the extra edges complicating the views. The following are the computational mesh statistics.

- Orthogonal computational mesh 1000 meters on each boundary

- Coarse resolution is 25x25x10 meter spacing

- Top is flat 1300 m, bottom is flat at 300 m elevation

- Located entirely within the alluvium

- number of nodes = 169781

- number of hexahedral elements = 160000

- connected into tetrahedral elements = 960000

- Rotated to align with the X axis for easier modeling setup

- Translated X and Y relative to intermediate model at 0,0 coordinate

- Min X,Y,Z corner is 14900, 4160, 300 m

- Max X,Y,Z corner is 15900, 5160, 1300 m
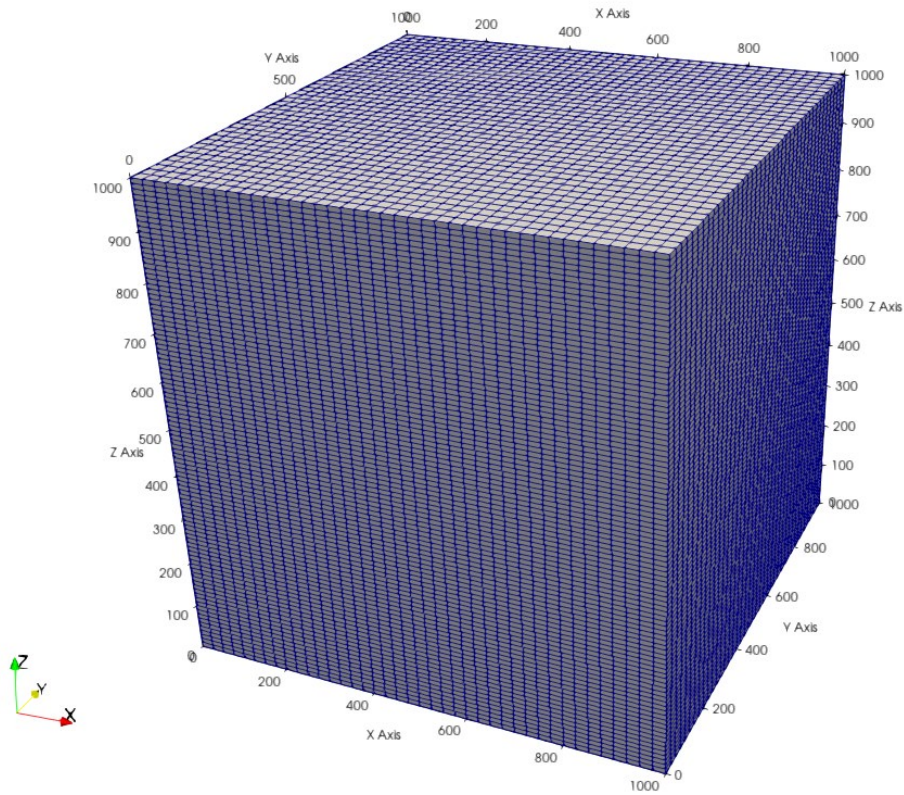
Figure 4-10. Small area computational hexahedral mesh with 1000 meter boundaries, 25 meter horizontal spacing, and 10 meter vertical spacing.

4.4 Meshing Workflow for JewelSuite™ Property Model Tabular 1B

This JS Property model has flat layers with constant facies values as represented in Figure 2-2 . These simple and flat layers allow for easier testing and evaluations of the workflow and results. This model is used to detail the workflow and describe evaluations and lessons learned from this simple property model. See Appendix A-1 for JS file formats used as input files for the meshing workflow.
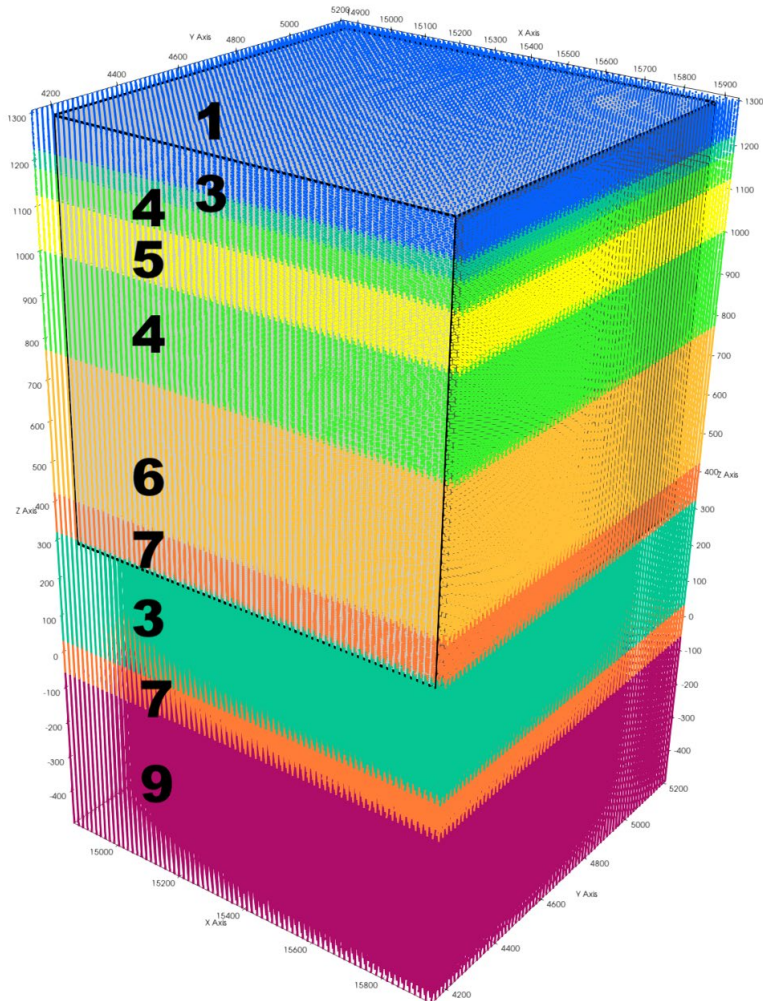
Layers with Facies ID

1 Mimbres alluvial fan
2 Minor Lacustrine deposits
3 Alluvial Fan deposits
4 Upper Gila fluvial
5 Main Lacustrine deposits
6 Middle Gila fluvial
7 Gila fluvial channel
8 Lower Gila fluvial overbank
9 Bedrock Volcanics

Figure 4-11. JS Tabular 1B Facies exported as data points and colored by ID 1-9. The JS property data are full model, black lines in image show position of the computational mesh relative to the data points. Facies 2 and 8 are not present in the near field model.

The following describe the steps to upscale JS property data to the computational mesh. The first step is the processing of the exported data from JS into point data for LaGriT. This includes translation of data to the mesh coordinate space and visualization to ensure data are correct. The LaGriT upscale command is used to define facies and properties from JS on the computational mesh.

4.4.1　Process the JS Property Data

This step includes reading the data file into LaGriT, checking the data values, and writing a subset of the data with respect to the computational mesh. The point data are translated to the same coordinate space as the mesh, followed by these steps:

- Check that data cover mesh extents

- Check that data are finer resolution than mesh

- Check data elevations with respect to mesh

- Check data values with respect to property model

The translation of data to the same space as the mesh is the same as used for the JS GFM. To ensure the same numbers are used for all the property models, the same LaGriT define file is used in all the runs:

```
# FY21 llcorner of intermediate area model
define old_x 229526.29119434830
define old_y 3570758.1006789361
define old_z 0.
trans/1,0,0/ old_x old_y 0. / 0. 0. 0.

define ROTDEG 15.5
rotateln/1,0,0/nocopy/0. 0. -5000./0. 0. 5000./ROTDEG

# small domain and coordinates
define Sxmin 14900.
define Sxmax 15900.
define Symin 4160.
define Symax 5160.
define Szmin 300.
define Szmax 1300.

# small plus 1 cell each direction
define SPxmin 14850.
define SPxmax 15950.
define SPymin 4110.
define SPymax 5210.
define SPzmin 290.
define SPzmax 1310.

finish
```

The data points must cover the entire mesh domain, sides, top and bottom. JS defines K-layers as horizontal layers with a thickness equal to the JS cell height. Care must be taken when creating

the K-layers in JS especially in relation to any surfaces used. The K-layers will be proportional between the surfaces and will therefore have elevations relative to those surfaces. In our first iteration, the K-layers were not flat, as they conformed to the top of the alluvial (ground) surface. This positioned some points too far from the flat topped mesh be used in the upscale averaging. Likewise, if the JS data do not extend slightly beyond the domain, some points may be too far from the mesh edge to be captured in the upscaling process.

4.4.2   Upscale Facies from Property Model Tabular 1B

Using LaGriT, property values are interpolated by using the upscale command. The upscale algorithm captures all source data points that are located inside each mesh node Voronoi volume. The point values in each volume are averaged or selected by a min-max criteria to assign a single value to the mesh node.

The facies data are integer values representing material distribution. Because these are integers, we do not use the averaging function to assign a value to the mesh nodes. Instead we use the min- and the max-values from each set of data. We examine the results visually and compare elevations to the JS data. For this data, selecting max value gives a result closest to the JS property model.

The upscaled facies properties have flat elevations as expected and are within the 10 meter spacing of the mesh (Figure 4-12). Once the facies property values are assigned, the other properties (e.g., porosity and permeability) can be upscaled.
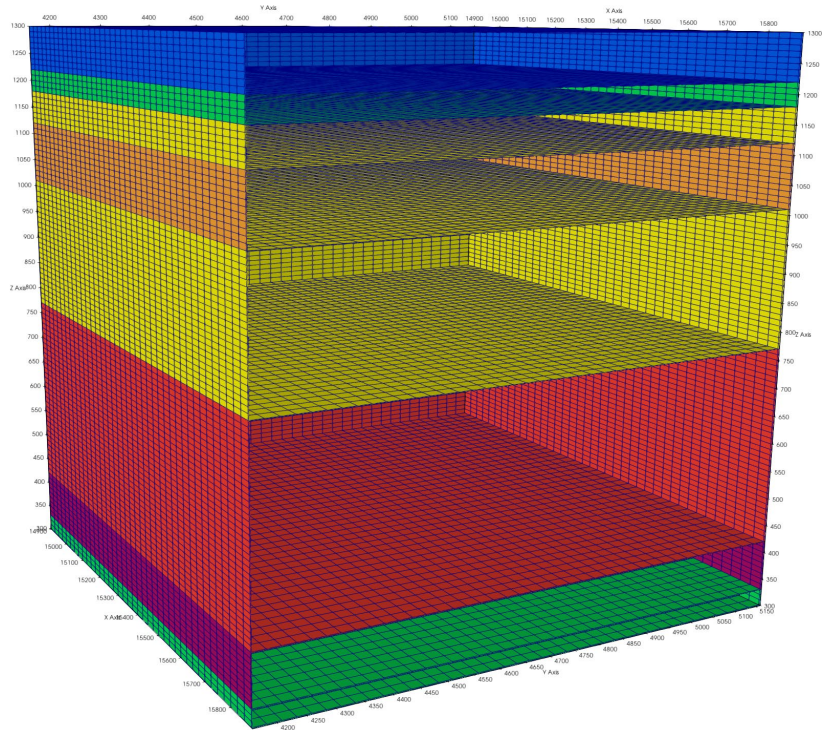
Figure 4-12. Upscaled Facies on computational mesh showing internal interfaces and layer elevations. The upscale function used for this mesh is max value. See Table 4-1 for Facies and elevations for each layer.

Table 4-1 Facies top elevations (m) for JS data and computational mesh

ID	Facies Name	Min-Value Mesh Elevation	Max-Value Mesh Elevation	JS Elevation
1	Mimbres Alluvial Fan	1300	1300	1322.54
3	Alluvial Fan Deposits	1210	1220	1219.07
4	Upper Gila Fluvial	1170	1180	1182.47
5	Main Lacustrine Deposits	1110	1120	1122.02
4	Upper Gila Fluvial	990	1000	999.45
6	Middle Gila Fluvial	760	770	771.87
7	Lower Gila Fluvial Channel	410	420	424.93
3	Alluvial Fan Deposits	310	320	323.08

4.4.3   Upscale Porosity from Property Model Tabular 1B

Once the facies properties are upscaled and confirmed on the mesh, we can upscale the porosity property. We use the geometric average for values upscaled to mesh nodes.

The result is acceptable within the vertical mesh resolution of 10 meters (Figure 4-13). LaGriT reports the min- and max-values of the property data and the mesh nodes (Table 4-2). The porosity values are within the min- and max-values of the JS data as expected for averaged data. The mesh images compare well to the JS image of this property data (Figure 3-1
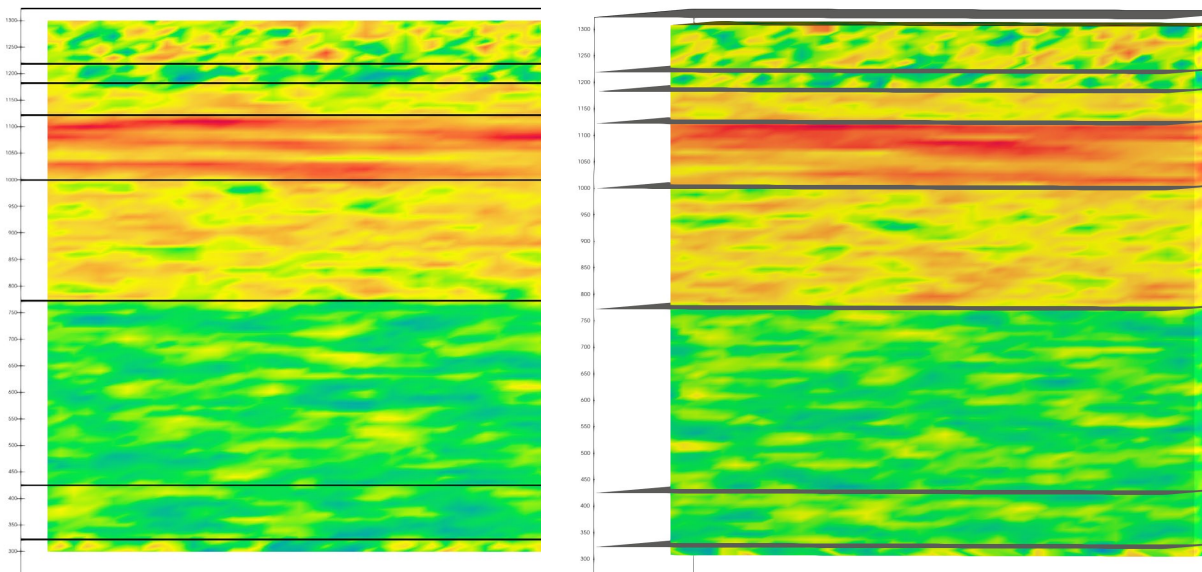
Figure 4-13. Computational mesh with upscaled porosity from property model Tabular 1B. The black lines outline the facies layers. Image shows X Axis Front South (left) and X Axis sliced halfway through at Y = 4660 (right)

Table 4-2 Porosity min- and max-values for property model Tabular 1B

	Min	Max	Difference
Mesh	1.42E-01	5.77E-01	4.35E-01
JS Data	8.17E-02	5.85E-01	5.03E-01

4.4.4   Upscale Permeability from Property Model Tabular 1B

The permeability properties for this model are based on conditioning the permeability to the porosity across the facies, as explained in Section 3. The result is acceptable within the mesh resolution of 25 meters horizontally and 10 meters vertically (Figure 4-14). LaGriT reports the min- and max-values of the property data and the mesh nodes. The permeability values are within the min- and max-values of the JS data as expected for averaged data (Table 4-3). The mesh images compare well to the JS images in Section **Error! Reference source not found.** (Figure 3-1).
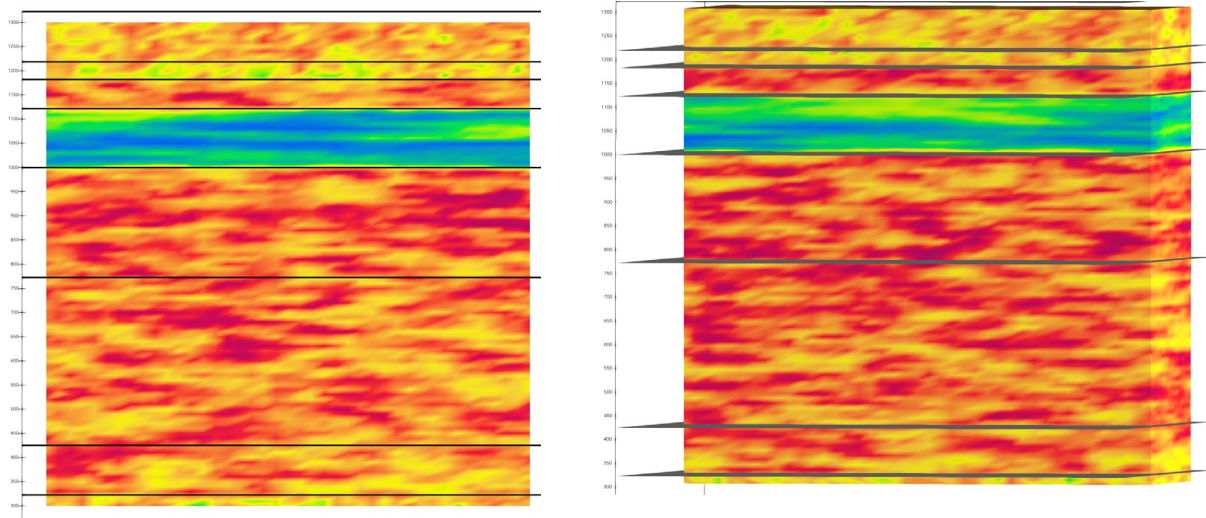
Figure 4-14. Computational mesh with upscaled conditioned permeability (m²) from property model Tabular 1B. The black lines outline the facies layers. Image shows X Axis Front South (left) and X Axis sliced halfway through at Y = 4660 (right).

Table 4-3 Conditioned permeability (m²) min- and max-values for property model Tabular 1B.

	Min	Max	Difference
Mesh	1.27E-17	3.58E-09	3.58E-09
JS Data	1.19E-17	3.58E-09	3.58E-09

4.4.5   Lessons Learned with Property Model Tabular 1B

Using the constant layers illuminated issues and solutions to resolve these issues. There are some simple checks that can be made in the early stages that avoid problems later. In general, it is recommended that the facies data be upscaled and evaluated first. The upscaled facies should be compared to JS numbers and images early on in the meshing process.

The following is a summary of lessons learned:

- Export JS data in a file with coordinates and property values for each data point. The file should include coordinates where the z-coordinate is elevation and not depth.

- Property data must have a finer resolution than the mesh. Using an upscaled sum function can count and confirm there is at least 1 data point inside each node volume.

- Property data should be equal or greater than the vertical and horizontal mesh extents.

- Be aware that the JS property values are spread proportionally from selected top and bottom surfaces and will reflect topology surface topology.

- Compare all mesh upscale properties to JS images and numbers.

4.5 JewelSuite^{TM} Property Models Discontinuous 2A and 2B

This model is more representative of heterogenous facies for simulations than the constant Tabular model. There are two discontinuous models: (1) Model 2A has 1000m major and minor horizontal range and vertical 100 m range, and (2) Model 2B has 750m major and minor horizontal range with a vertical 100 m range. This model conditions permeability (log μd) to porosity using a 0.5 correlation factor. The minimum, maximum, and standard deviation of properties is the same as the Tabular Property Model 1B (Table 4-3).

Visual inspection to determine accurate upscaling is harder for heterogeneous distributions, but some patterns have been identified to help check that results are correct. Note that facies in the 2A model are more continuous than the facies in the 2B model. These images compare correctly with the Figures in Section 2.
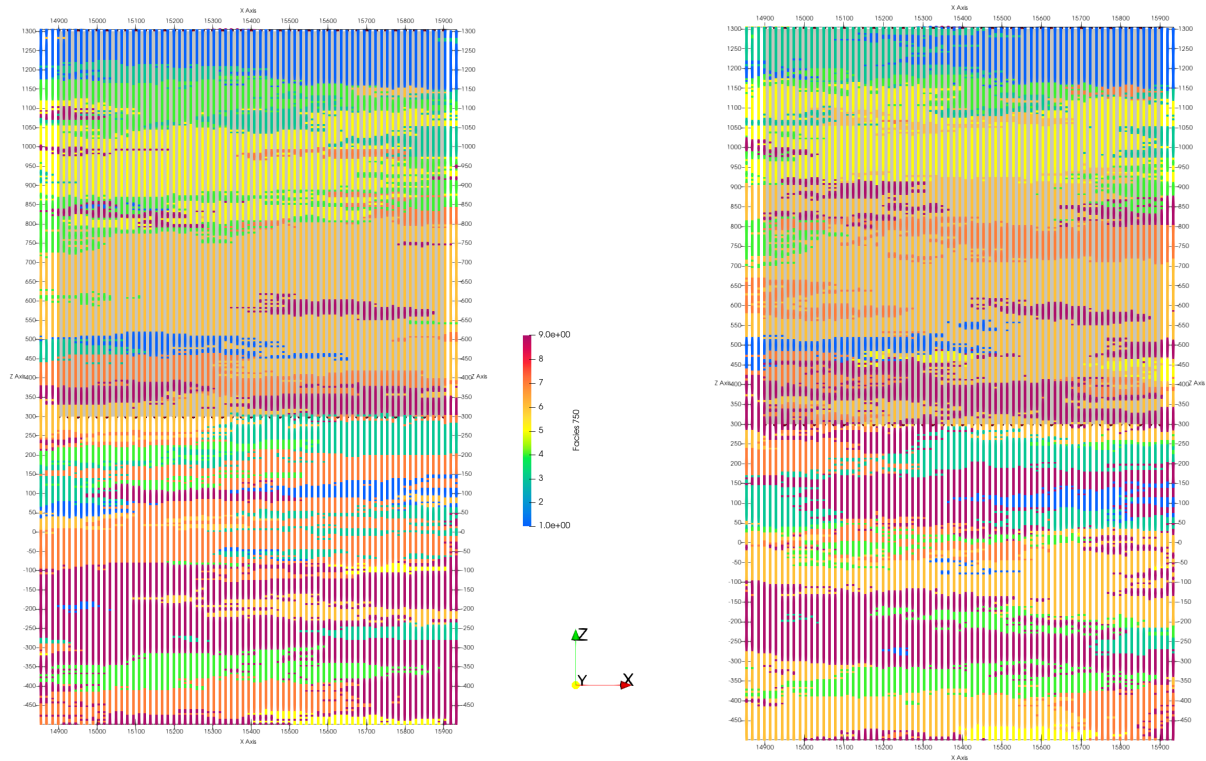
Figure 4-15. JS discontinuous property data for models 2A (left) and 2B (right). Domain for the computational mesh is shown as a gray shadow behind the point data.

4.5.1 Upscale Facies from Property Models Discontinuous 2A and 2B

The facies are upscaled to the computational mesh and checked visually with respect to the JS data. Though it is not as easy as checking flat layers of Tabular 1B, visual inspection and node counts for each facies can be used to evaluate the results. The expected visual patterns are correct relative to the coarser mesh resolution of 25 x 25 x 10 meters. See images for each facies ID with respect to mesh facies in Figure 4-16 and Table 4-4.
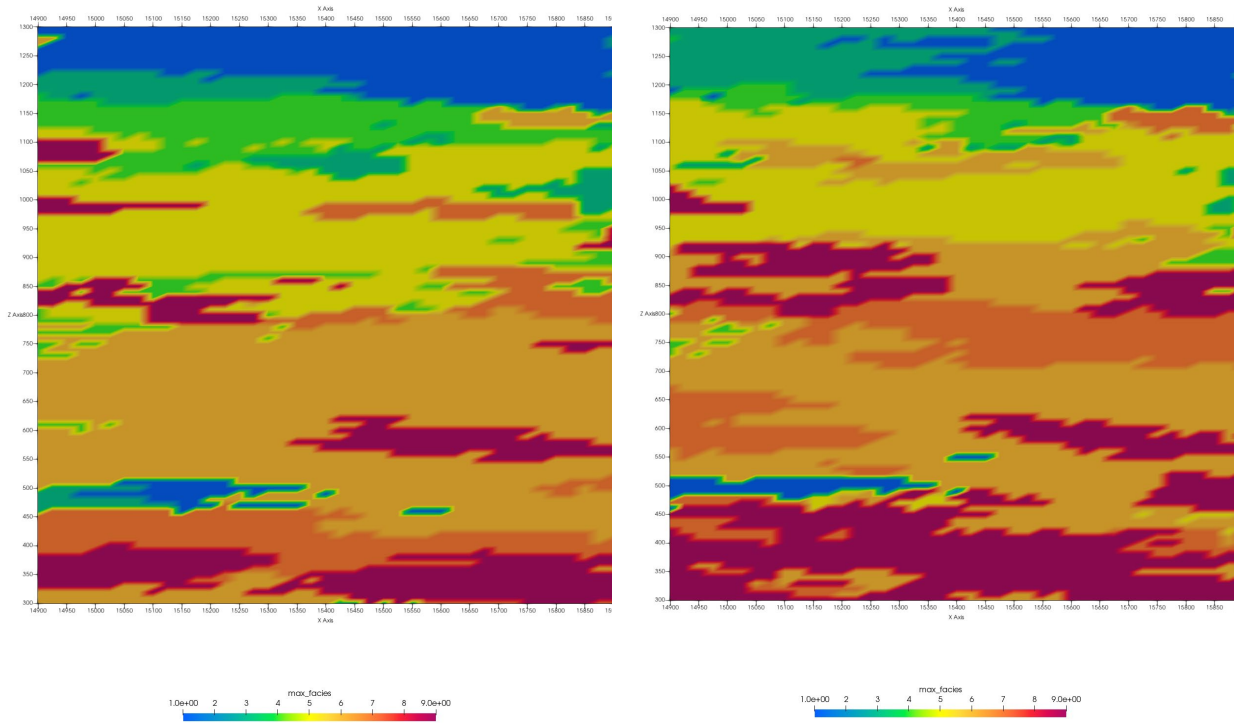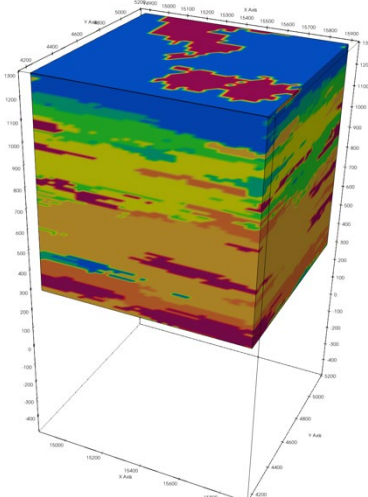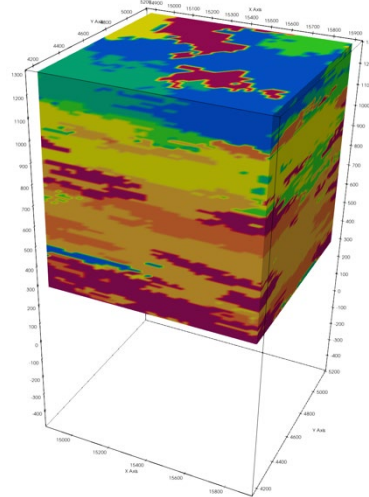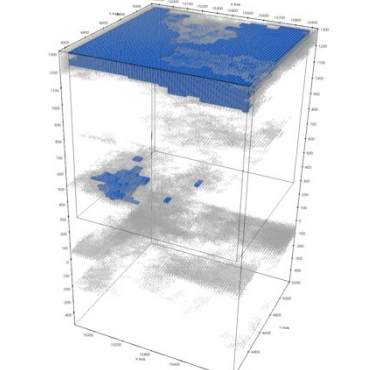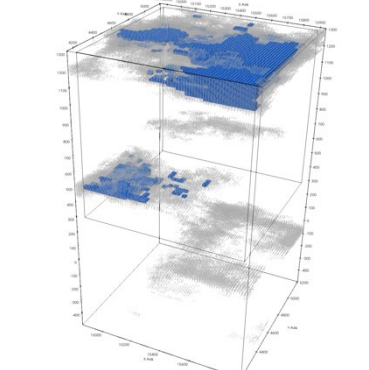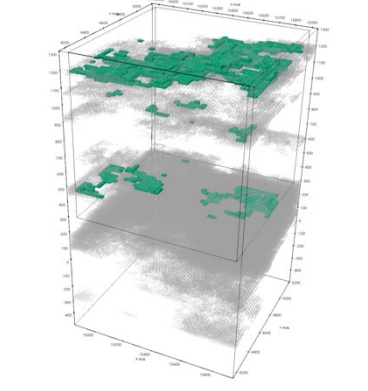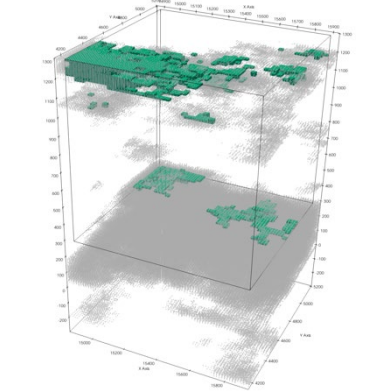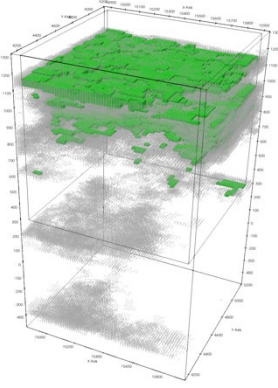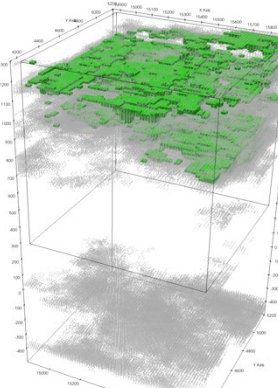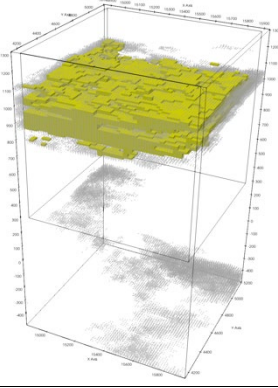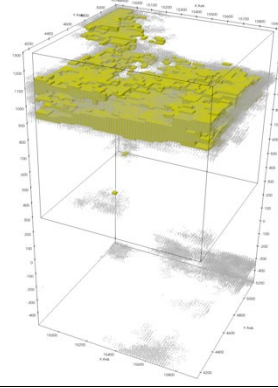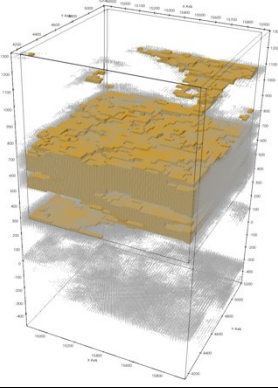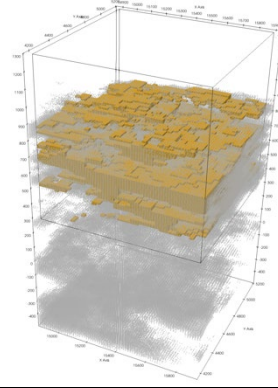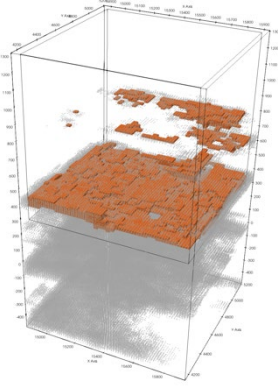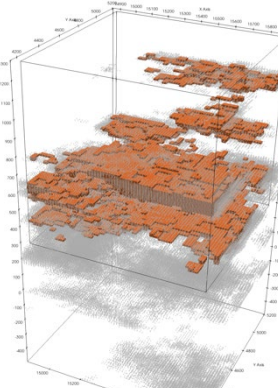
Figure 4-16. Computational mesh with upscaled facies for models 2A (left) and 2B (right). View is x-axis front face of mesh.

Table 4-4 shows images of both the JS facies full vertical data points (in gray) and the computational mesh volumes colored by their upscaled values 1-9. These type of images are very helpful in checking that the upscale routine has worked, and how well the mesh resolution is capturing the finer resolution JS data. These images also show the distribution of each facies relative to the selected mesh domain (small box outline). This can help determine if a mesh should extend deeper to capture more facies if important for the simulations. For this mesh, the facies representing the main lacustrine deposits (ID 5) are more continuous with less spreading for model 2A than 2B as described in Section 2.3. As a result of upscale averaging on a coarser mesh, some of the thin facies extents are not captured. For these models, the results are acceptable.

Table 4-4 JS data and mesh facies images for distributed property models

Facies ID and Name	Facies for Model 2A	Facies for Model 2B
1 – 9 All		
1 Mimbres alluvial fan		
3 Alluvial Fan deposits		

4 Upper Gila fluvial		
5 Main Lacustrine deposits		
6 Middle Gila fluvial		
7 Lower Gila fluvial channel		

9 Bedrock Volcanics		

LaGriT is used to report the number of nodes for each of the facies. This gives the relative quantity of the facies for each of the models as a further check for correctness. These numbers correspond to the expected extents in visual inspections. For example, in Table 4-5 we see the largest facies extents are 6 and 4.

Table 4-5 Facies mesh node count and percent for models 2A and 2B

	Nodes Counts 2A	Nodes Counts 2B	Fractional Node Count 2A	Fractional Node Count 2B
1	16220	10898	0.0955	0.0641
3	7464	7987	0.0439	0.047
4	34154	31076	0.2011	0.183
5	22070	22215	0.1299	0.1308
6	58554	51769	0.3448	0.3049
7	17813	26892	0.1049	0.1583
9	13506	18944	0.0795	0.1115

4.5.2 Upscale porosity and permeability from property models discontinuous 2A and 2B

The properties from both models are upscaled to the computational mesh and checked visually with the JS Data (see Section 2). The expected patterns are correct relative to the mesh resolution. The porosity images in Figure 4-17 compare favorably to those in Figure 3-2. The permeability images in Figure 4-18 compare favorably to those in Figure 3-2 and also show the relationship to porosity from which it was conditioned.

LaGriT is used to report the min- and max-values for both the data and the mesh. The resulting mesh-averaged values are within the range of the JS property data. The porosity values are given in Table 4-6, the permeability values are given in Table 4-7.
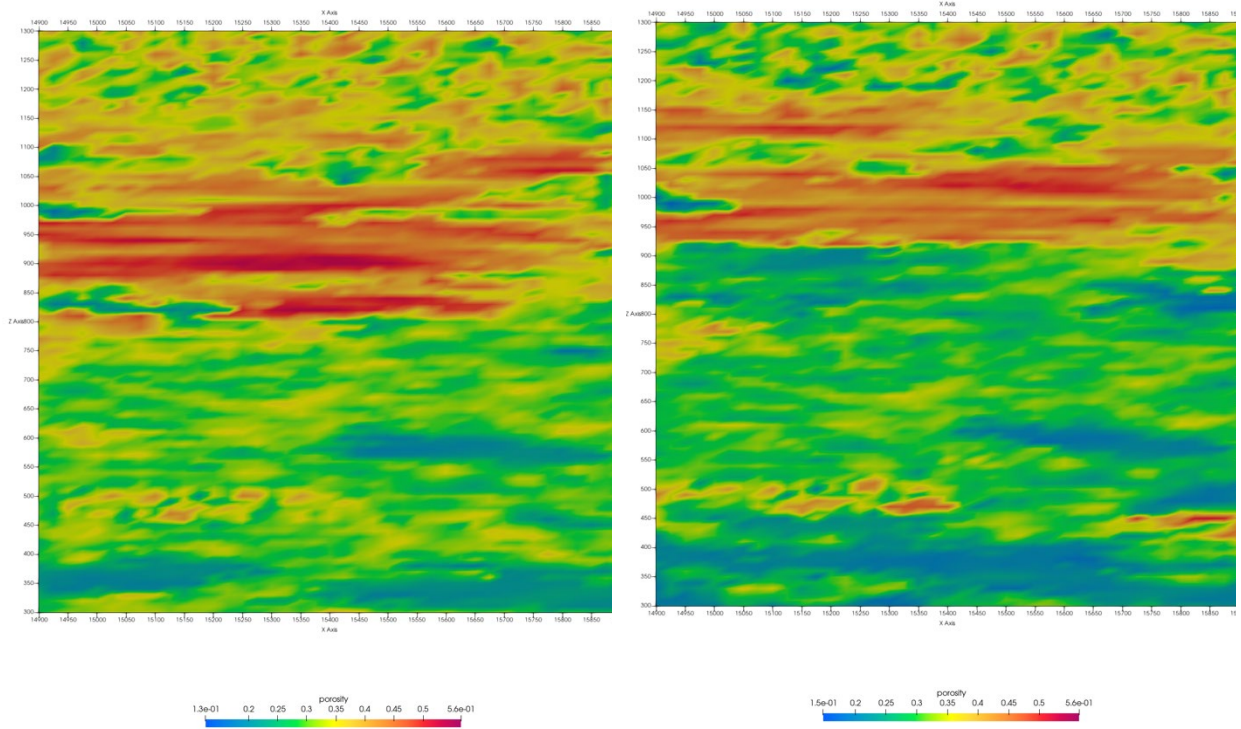
Figure 4-17. Computational mesh with upscaled porosity for models 2A(left) and 2B (right). View is x-axis front face of mesh.
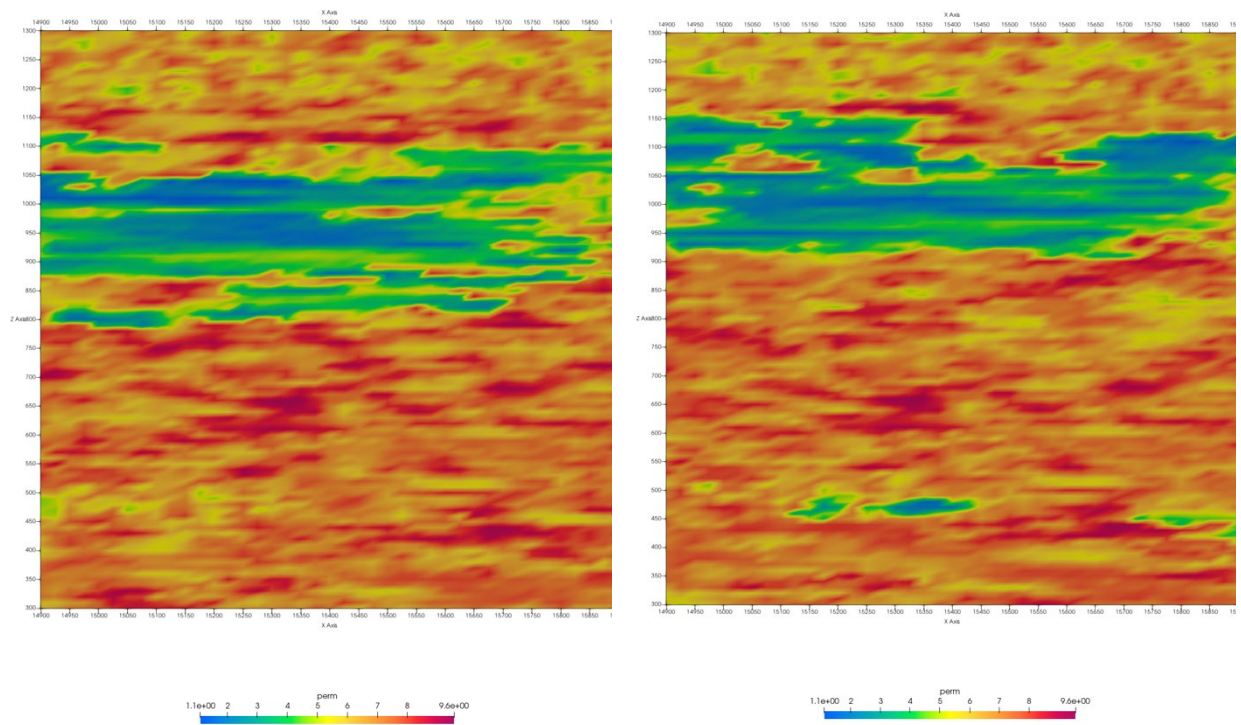
Figure 4-18. Computational mesh with upscaled permeability (log μd) for models 2A (left) and 2B (right). View is x-axis front face of mesh.

Table 4-6 Porosity min- and max-values for property models 2A and 2B

	Min	Max	Difference
Mesh 2A	1.25E-01	5.65E-01	4.40E-01
JS 2A	8.93E-02	5.84E-01	4.95E-01
Mesh 2B	1.47E-01	5.65E-01	4.18E-01
JS 2B	8.24E-02	5.85E-01	5.02E-01

Table 4-7 Permeability (log μd) min- and max-values for property models 2A and 2B

	Min	Max	Difference
Mesh 2A	1.09E+00	9.56E+00	8.47E+00
JS 2A	1.08E+00	9.56E+00	8.48E+00
Mesh 2B	1.10E+00	9.56E+00	8.46E+00
JS 2B	1.08E+00	9.56E+00	8.48E+00

4.6   Setup Files for Flow and Transport Simulations

Once the mesh is created, the computational mesh is formatted and flow and transport simulation input files are written for use in the simulation software. Input files were written for both FEHM and PFLOTRAN which require the same mesh information but have different file formats. These include the geometric coefficients for the Voronoi volumes, zone lists that can be used to identify mesh nodes of various materials, and zone lists for mesh nodes on the boundaries. The upscaled model properties are written to a mesh file for visualization and as a tabular ASCII file with properties for each node number. The same computational mesh and associated files are used for all version of the property models. The same mesh files are repeated in each model directory for convenience. LaGriT output reports mesh statistics these are written to the README file for each model see Appendix A-2.

The following model setup files were written for the computational mesh:

Mesh 1000 x 1000 x 1000 meters
Mesh with spacing 25x25x10 meters
number of nodes = 169781
number of hex elements = 160000
number of tet elements = 960000

Position relative to x-aligned intermediate mesh
Translate 0. 0. 0. to llcorner this mesh 14900. 4160. 300.
Z elevation 300m to 1300m (flat top alluvium)

hex0.inp   AVS format hexahedral mesh (nodes for tet mesh)

```
tet0.inp                        AVS format tetrahedral mesh file
tet0.fehmn                      FEHM format tetrahedral mesh file
```

The project directories are:

```
/project/meshing/GEO_Integration/JewelSuite/GFM_to_ModelsV2/area_small/
drwxrwxr-x 3 tamiller   Jul 28 10:11 mesh_25x25x10m
drwxrwxrwx 2 eguiltinan Aug 11 15:36 properties_aug2021
drwxrwxr-x 5 tamiller   Sep 21 18:13 mesh_25x25x10m_aug2021
drwxrwxrwx 2 eguiltinan Sep  8 17:02 properties_sept_2021
drwxrwxr-x 4 tamiller   Sep  9 16:16 mesh_25x25x10m_i750
drwxrwxr-x 4 tamiller   Sep  9 16:16 mesh_25x25x10m_i1000
```

5.   Flow and Transport Simulations

5.1   Simulation Initialization

Flow and transport simulations are carried out using the porous medium flow simulator FEHM (Finite Element Heat and Mass transfer code; Zyvoloski et al., 2015; https://fehm.lanl.gov). To conduct each simulation, the FEHM mesh created by LaGrit and a list of porosity and permeability values for each node were provided (Section 4). In general, FEHM simulations are created with an input file which contain a series of "macros" which specify the various parameters of a simulation. To specify parameters which vary across every node of the domain (i.e. heterogeneous porosity, permeability, and relative permeability parameters) python scripts were used to develop separate files which include lists of parameters at every node for the "perm", "rock", "rlp" macros (Appendix A-3). These files are referred to within the main control file for reading in the heterogeneous parameter distributions developed in JS and LaGriT. Figure 5-1 shows the heterogeneous permeability field and a slice through the center of the model.
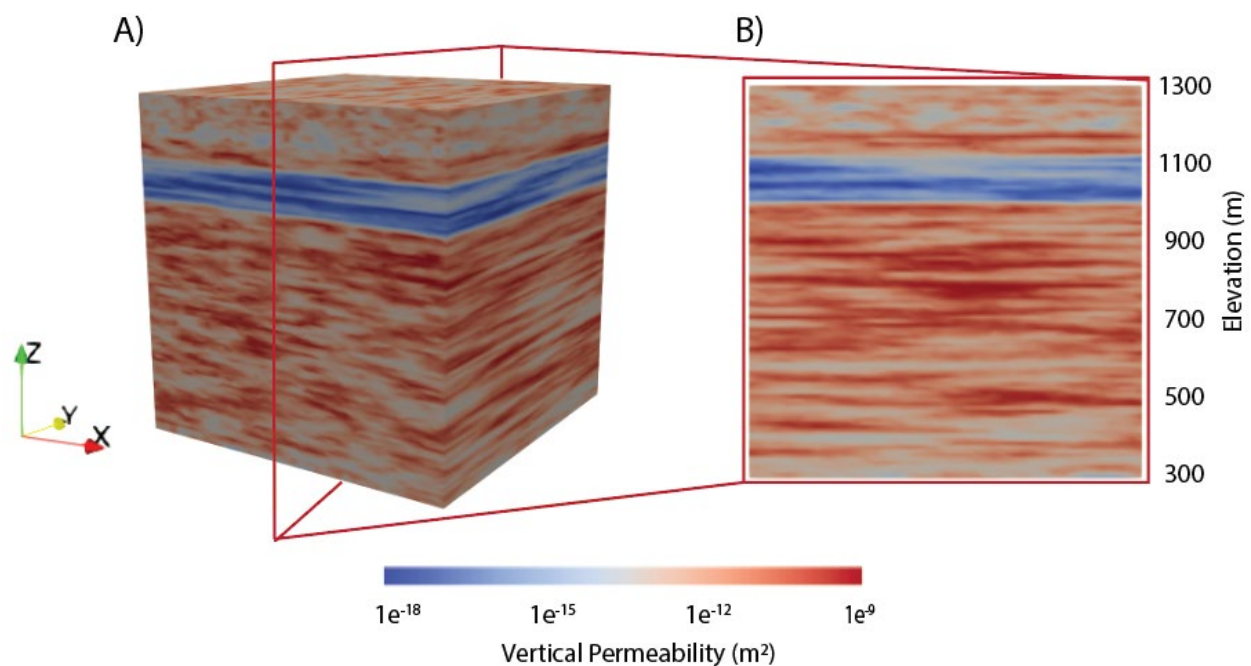
Figure 5-1. A) Vertical permeability within the FEHM model. B) A slice through the center of the model.

For each of the four hydrogeologic models (1A, 1B, 2A, 2B) an initial simulation was conducted to develop steady state saturation and pressure distributions. These simulations include recharge from the top of the domain at 1 mm/year and a flowing water table with a gradient of 2.9 m/km which is the approximate gradient in the Mimbres Basin (Gross et al., 2020). Because the vertical resolution of the mesh is 10 m and the horizontal length of our domain is 1 km a saturation boundary condition would be limited to a groundwater gradient of 10 m/km (one side of the domain saturated 1 node above the other side). To correct this, water pressure boundary

conditions were implemented on each side of the domain. On one side of the domain the water pressure is equivalent to an 802.9 m column of water and on the other it is 800 m. The end result is a flat water table saturated at an elevation of 800 m (500 m depth below the ground surface) across the domain but flowing due to an imposed pressure gradient equivalent to 2.9 m/km. With the recharge and groundwater gradient boundary conditions implemented, each of the four hydrogeologic models were simulated to 100,000 years. At this point the water input and water output of the domain were equal for each model, a condition called 'steady state'.. The development of a steady state saturation distribution for model 1B is shown in Figure 5-2. Beginning with appropriate initial conditions is critical to accurately simulating the transport of a radionuclide release.
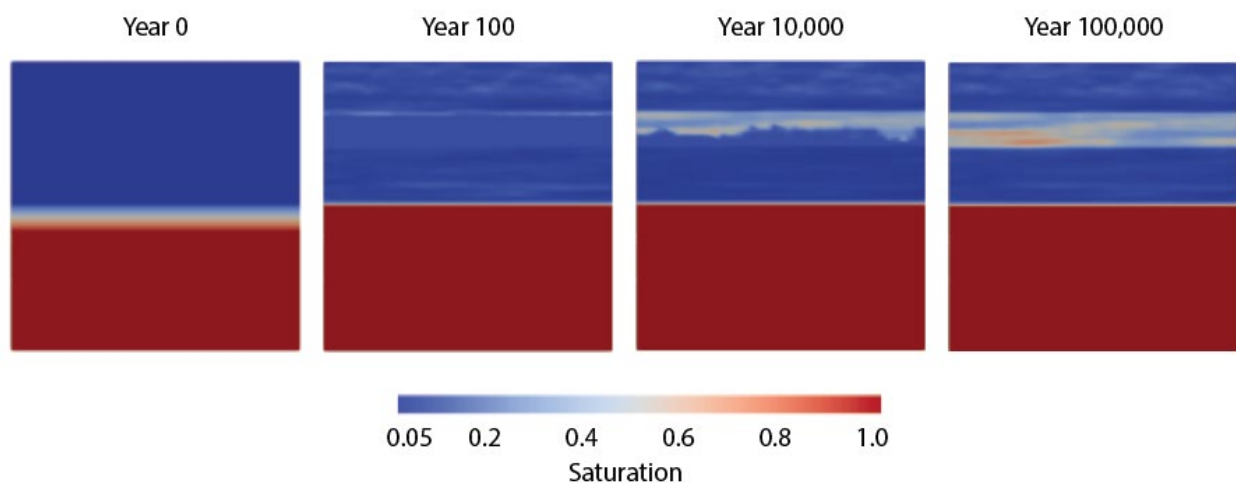
Figure 5-2. Steady-state saturation development through a cross section in the middle of model 1B. Water enters the top through recharge and the left side through groundwater flow. Water exits the right side of the domain below the water table. At year 100,000 the water input into the domain is equal to the water leaving, indicating steady state has been reached. The lacustrine layer, which has higher residual saturations, is clearly evident in the unsaturated zone.

5.2   Transport Simulations

The steady-state pressure and saturation distributions were used to initialize transport simulations. We define a 100x100x10 m box centered in the domain at a depth from 140-150 m below the surface (Figure 5-3). This box represents the bottom of the repository and is considered the "release zone" for our simulations. The depth of the release zone places it above the lacustrine facies which we anticipate to significantly inhibit the transport of radionuclides. We begin the simulations by initializing the release zone with a mass of 1,000 kg (1 metric ton) of Uranium-235 (^{235}U). This is approximately equivalent to 4,255 mols of ^{235}U. ^{235}U is a typical component of reactor waste and is present in over 500 reactors worldwide (Bussod et al., 2020). A uniform adsorption ratio of 8.7 L/kg rock was applied to the entire domain. This adsorption ratio is derived from ^{235}U batch sorption experiments previously conducted by LANL on

alluvium from the Negev desert in Israel (Bussod et al., 2020). Mechanical diffusion and dispersion of ^{235}U is set to zero leaving only numerical dispersion, which is on the order of half the vertical mesh spacing, or 5 m. The half-life of ^{235}U is several hundred million years and so radioactive decay is ignored in our simulations. The 1,000 kg release is not meant to represent the size of a particular release, which would be dependent on the storage capacity of a repository, but is instead meant to represent a unit of measure easily scalable depending on the amount of radionuclides contained within a particular repository.
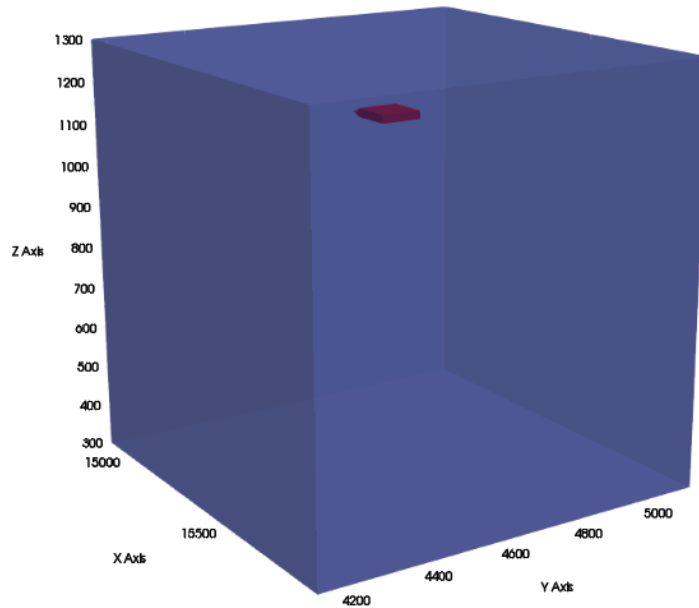
Figure 5-3. 3D representation of the ^{235}U "release zone" (red) within the larger model domain (translucent blue).

Figure 5-4 depicts the movement of ^{235}U in a cross section through the center of model 1B. The tracer initially moves very slowly through the unsaturated portion of the model. Upon reaching the water table, at approximately 10,000 years, the ^{235}U is quickly carried out of the domain. By 40,000 years little ^{235}U remains and by 100,000 years it is almost completely removed.
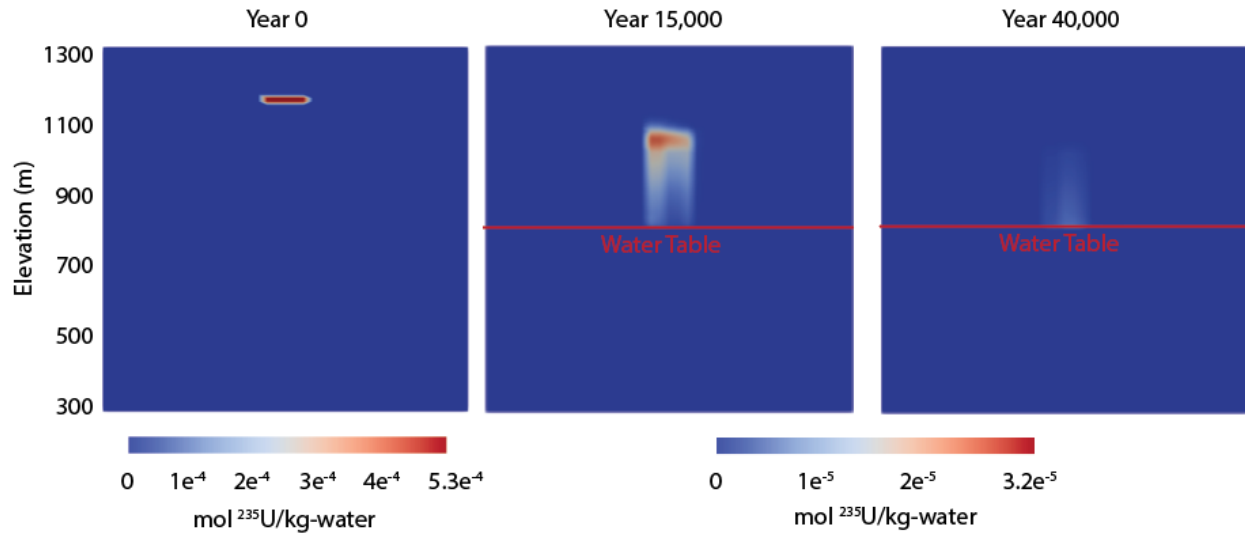
Figure 5-4. ^{235}U progress during simulation of model 1B. The tracer begins at the repository (left) and moves slowly downward through the unsaturated zone until reaching the water table (middle). Upon reaching the water table the ^{235}U is quickly removed from the domain (right).

The average recharge within the Mimbres basin is very low at approximately 0.6 mm/year (Finch et al., 2008). This rate was selected as our base recharge rate. To include the potential for increased recharge due to future climate change we also simulated recharge rates of 1mm and 2mm/year. Together with the four hydrogeologic models and three recharge scenarios we completed twelve radionuclide transport simulations. To investigate the rate at which a 1,000 kg release of ^{235}U may reach a human source we assume that upon leaving the 1 km model domain the ^{235}U becomes accessible to a drinking water well. Figure 5-5 through Figure 5-8 display the results of the four models in terms of rate of ^{235}U leaving the domain as well as the total ^{235}U which has escaped.
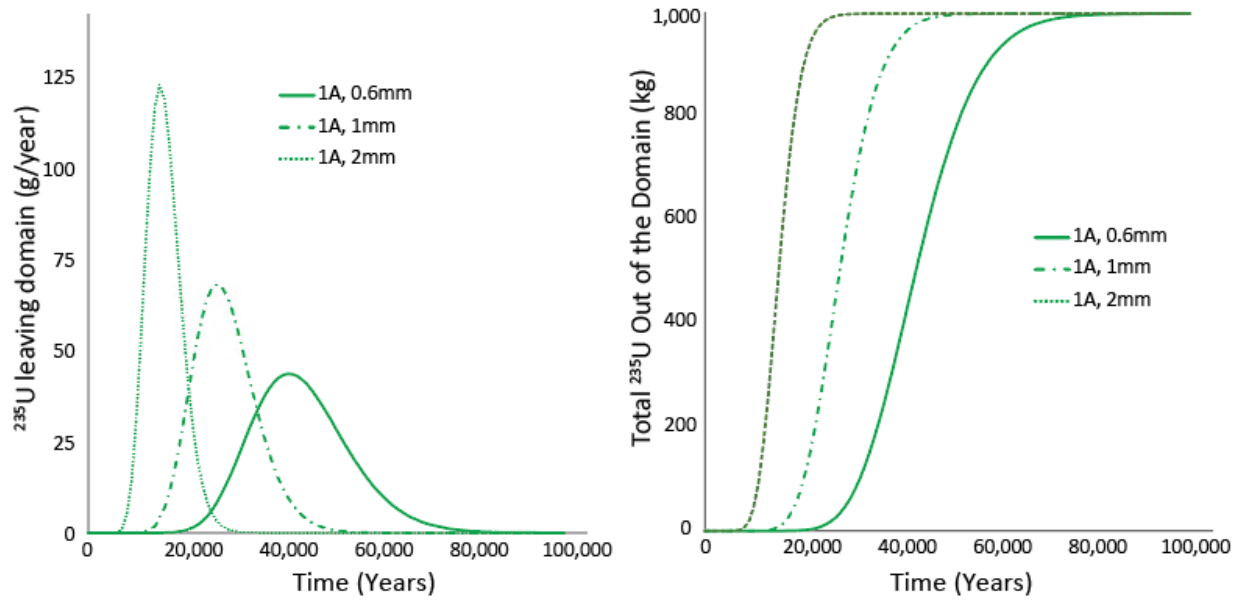
Figure 5-5. Rate of [235]U leaving the model domain for Model 1A (left) and total [235]U which has left the domain for Model 1A (right). The three recharge scenarios are plotted: 2 mm/year (solid line), 1 mm/year (dashed-dot), and 0.6 mm/year (dotted).
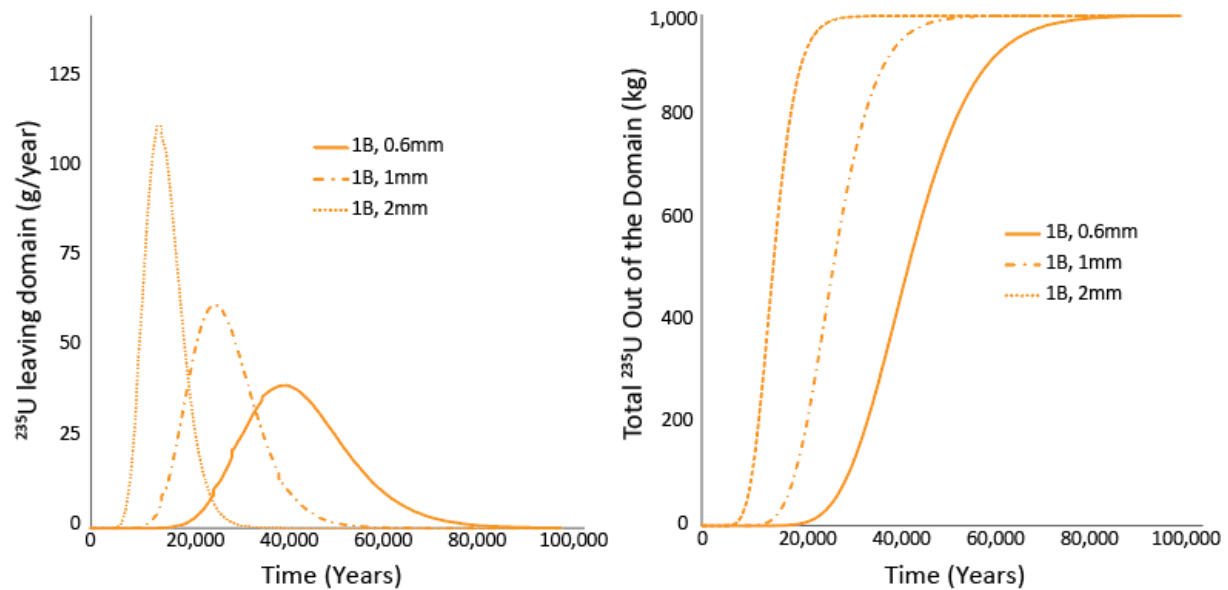
Figure 5-6. Rate of [235]U leaving the model domain for Model 1B (left) and total [235]U which has left the domain for Model 1B (right). The three recharge scenarios are plotted: 2 mm/year (solid line), 1 mm/year (dashed-dot), and 0.6 mm/year (dotted).

63
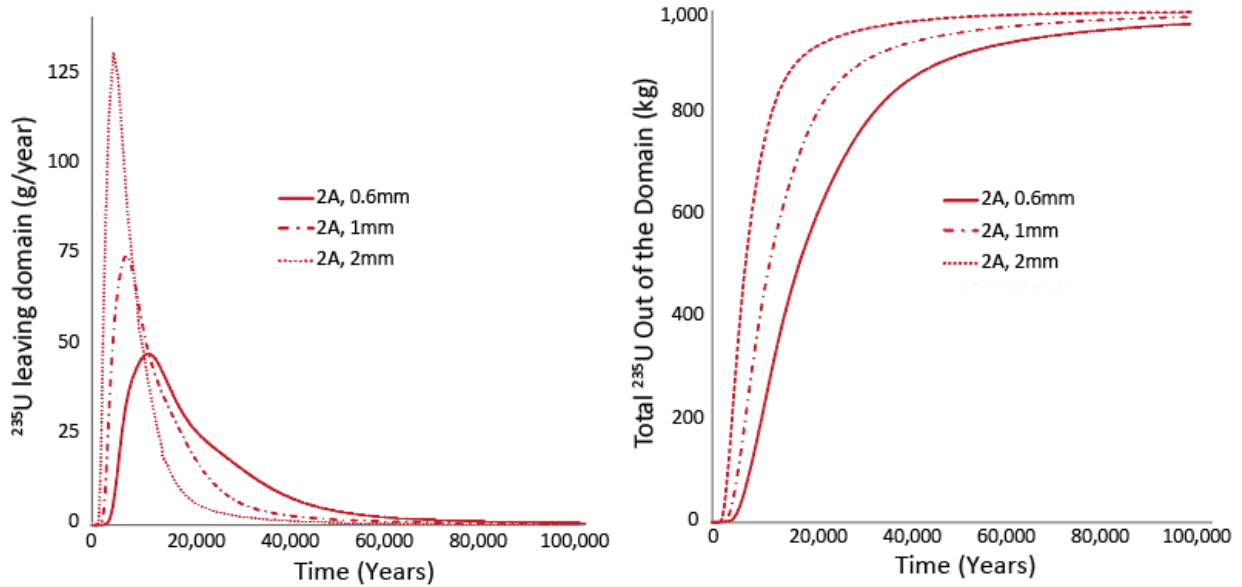
Figure 5-7. Rate of ^{235}U leaving the model domain for Model 2A (left) and total ^{235}U which has left the domain for Model 2A (right). The three recharge scenarios are plotted: 2 mm/year (solid line), 1 mm/year (dashed-dot), and 0.6 mm/year (dotted).
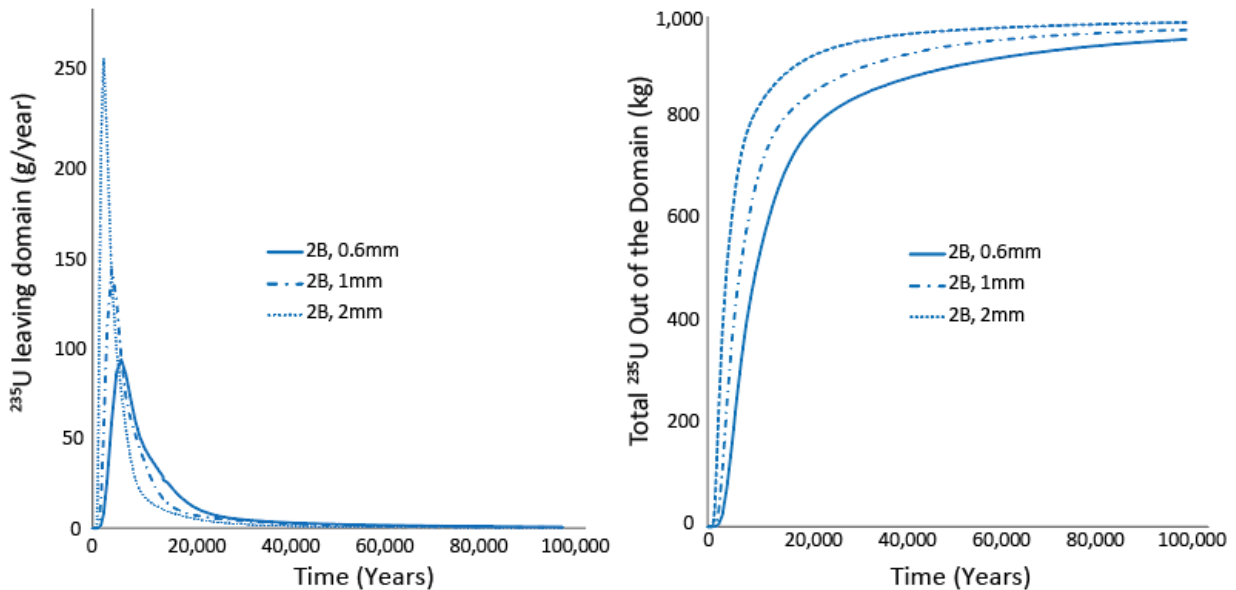
Figure 5-8. Rate of ^{235}U leaving the model domain for Model 2B (left) and total ^{235}U which has left the domain for Model 2B (right). The three recharge scenarios are plotted: 2 mm/year (solid line), 1 mm/year (dashed-dot), and 0.6 mm/year (dotted).

6. Discussion

6.1 Effect of Heterogeneity on Transport Simulations

In this study we investigate the effect of lithofacies heterogeneity (continuity and thickness of lithofacies) and property heterogeneity (constant vs heterogeneous porosity and permeability) on the transport of ^{235}U beneath a hypothetical nuclear waste repository. The results of the transport simulations of ^{235}U highlight the importance of including lithofacies heterogeneity into alluvial basin modeling. We define the breakthrough of ^{235}U as the point at which 10% of the initial mass has left the modeling domain. This ranges from 1,200 years (model 2B with 2 mm/year recharge) to 32,000 years (model 1A with 0.6 mm/year, Table 6-1). The largest difference between two models with the same recharge is 27,500 years. This occurred during the 0.6 mm/year recharge scenario in model 2B (4,500 years) and model 1A (32,000 years). In general, our simulations show that increasing heterogeneity decreases the containment of ^{235}U. The increased heterogeneity provides more conductive pathways for radionuclide transport and the initial breakthrough is controlled by the fastest pathway across the domain.

Table 6-1 Time until 10, 50, and 90% breakthrough (in thousands of years) for each model and each recharge scenario (0.6, 1, 2 mm/year).

Breakthrough	1A			1B			2A			2B		
	0.6	1	2	0.6	1	2	0.6	1	2	0.6	1	2
10%	32	20.5	11	30.7	19	11	7.8	5.4	3.3	4.5	3	1.2
50%	43	28	15	43	27	15	17.9	11.8	7.1	10	7	4.1
90%	58	37	20	60	38	21	47.8	31	17.5	50	32	18

Perhaps the most enlightening aspect of this work is the increased sensitivity to lithofacies heterogeneity over simple property heterogeneity. The plots of breakthrough in Figure 6-1 show each of the breakthrough curves for all the simulations. Figure 6-1b shows model 2A which is the model with heterogeneous lithofacies based on variograms with a 1,000 m horizontal range. Figure 6-1c shows that model 1A and model 1B (the tabular models with and without property heterogeneity) behave very similar despite very different porosity and permeability distributions. However, Figure 6-1d shows that there is a 30,000 year gap between model 1B and model 2A (tabular lithofacies vs discontinuous lithofacies). The sensitivity to lithofacies heterogeneity is likely because the lacustrine layer strongly influences the travel time of the ^{235}U. The property differences between the lacustrine lithofacies and the other lithofacies surrounding it are greater than the property differences within the lacustrine lithofacies. Therefore, our results are more sensitive to lithofacies heterogeneity than property heterogeneity. In addition, our simulations are likely highly sensitive to the lithofacies realization as some realizations of the same geostatistical lithofacies model have a more continuous and thick lacustrine lithofacies directly beneath the repository than others.

Besides the heterogeneity's impact on breakthrough time it also controls the overall transport of ^{235}U. Increased heterogeneity provides quick pathways which decreases breakthrough time but it also creates very slow pathways. This causes a long tail in the ^{235}U response. Figure 6-2 shows

the total ^{235}U which has left the domain for all models. Models 2A and 2B show the quickest rise in removed ^{235}U but also have very long tales and are still approaching the 1,000 kg initial mass when the simulations end at 100,000 years. In contrast, the tabular models Figure 6-2c have sharp breakthroughs and all ^{235}U is removed before the end of the simulation.

While our models demonstrate the importance of including lithofacies heterogeneity and the chosen property values for each lithofacies we also had to make broad assumptions about the location of lithofacies and magnitude of property values and their variation. This creates the wide differences in our results. In reality, a nuclear waste repository sited in a deep alluvial basin would also allow for significant characterization of the lithologic variability and lithofacies properties. Installing wells, collecting core, and employing modern geophysical tools would dramatically constrain these models and provide a high level of confidence in radionuclide transport simulations.
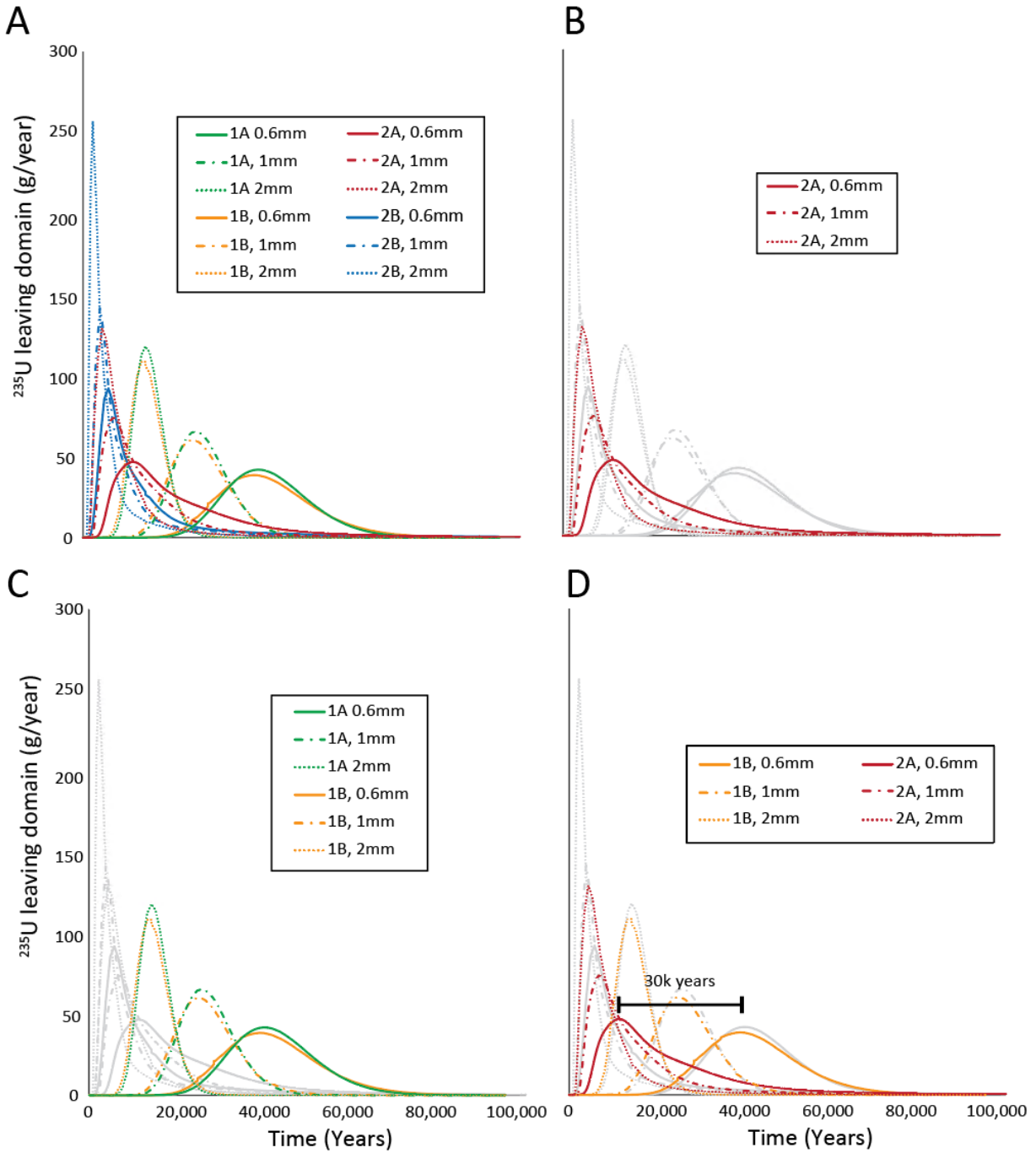
Figure 6-1. (A) Rate of ^{235}U leaving the model domain for all models. (B) Model 2A, considered the most realistic. (C) A comparison of the two tabular models. (D) Models 1B and 2A, demonstrating the effect of lithofacies heterogeneity.
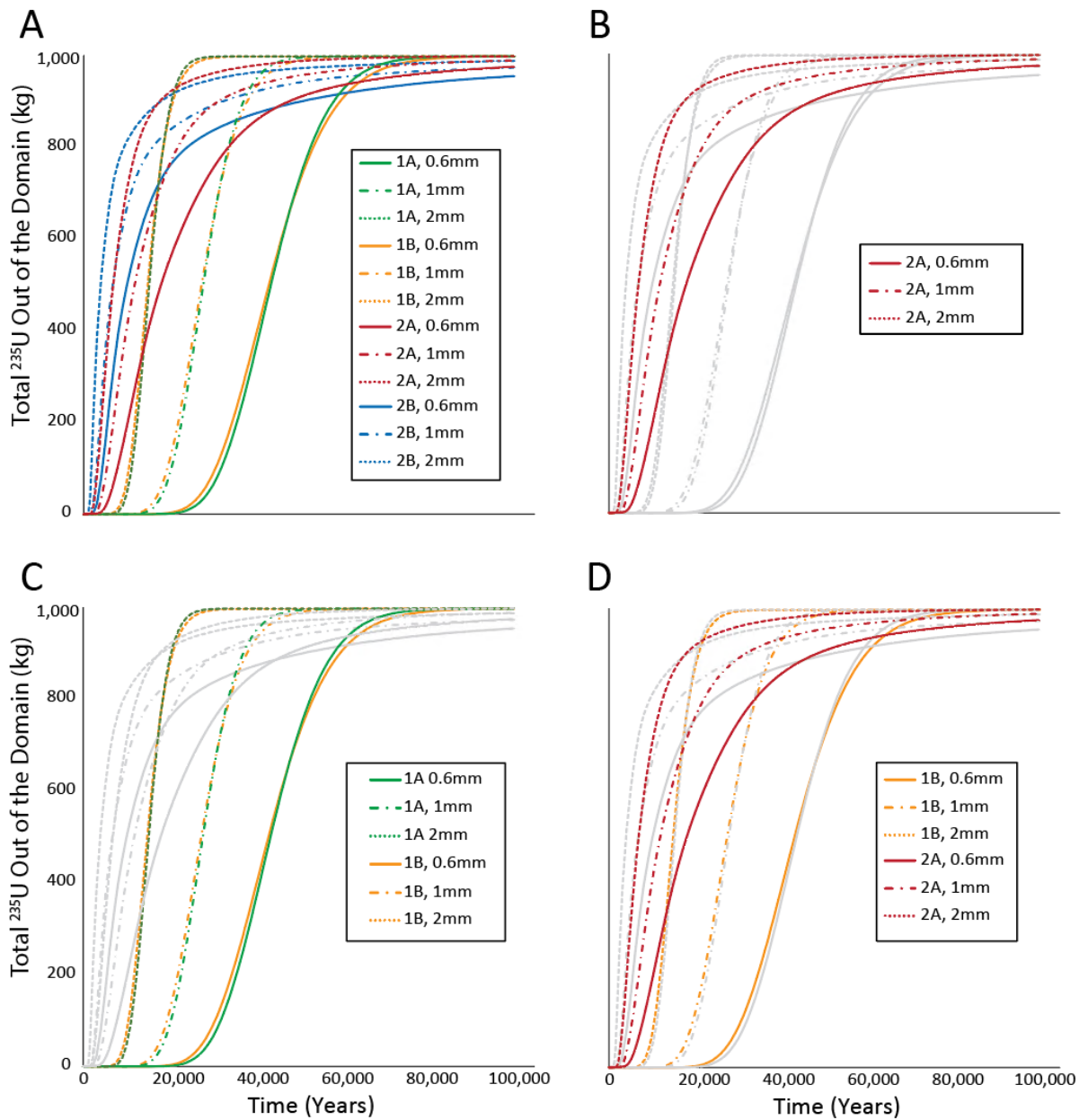
Figure 6-2. (A) Total [235]U leaving the model domain for all models. (B) Model 2A, considered the most realistic. (C) A comparison of the two tabular models. (D) Models 1B and 2A, demonstrating the effect of lithofacies heterogeneity.

6.2 Computational Meshing

JS allows us to build a GFM that includes geology and property models based on data and expert knowledge. This represents an idealization of the basin we want to use within the flow and

transport simulations. But the accuracy of this representation is dependent on the computational mesh used as input for simulations. How closely the mesh represents the GFM and its properties depends on the mesh size and design.

There is usually a trade-off between the accuracy of the GFM and property models, and a mesh that fits the constraints imposed by the modeling application goals. These are the main considerations for building a computational mesh:

- mesh computation size (node count under 200,000 preferred for fast runs)

- mesh domain size (small area to capture small details with high resolution) or large for regional simulations (where small features are not important contributions to simulations)

- mesh resolution with spacing determined by cell size (more resolution means more mesh cells and associated nodes)

- mesh type such as structured or unstructured (conforming to surfaces or stair-step boundaries)

- domain shape (flat boundaries preferred but sometimes need one or more boundaries to conform to ground or other surfaces)

- modeling application criteria (hexahedral or tetrahedral or general polyhedral, orthogonal orientation, Delaunay connectivity etc.)

The sufficiency of a computational mesh to represent the JS property models and GFM is investigated by running flow simulations using meshes of varying resolutions and design. Visual inspection checks that material or property features such as thin layers or distributed facies are adequately represented. Simulation results from different meshes can show improved results or no difference. To establish a good workflow we knew we would need multiple iterations between JS, meshing, and the simulations. This required the total number of mesh nodes to be small for faster runs. The 10 meter vertical mesh used this year is as coarse as possible yet still adequate to capture geostatistical properties when upscaled.

The meshing workflow established for meshing and upscaled properties from JS worked well and has been streamlined to be more efficient. This enabled the exploration of more JS property models for simulations but we did not have time to vary the mesh resolution. Experience has shown that vertical resolutions 1 – 3 meters are best for a domain of this size and should be used to explore simulations that may have been affected by the coarse mesh and averaged JS properties.

The intermediate size model was not attempted this year. This larger area will include both the alluvium and bedrock, as well as a major boundary fault. Using experiences from this year's small area domain will help build the larger model. The main issue for meshing will be the mesh design and resolution. The mesh will not be able to have the convenience of a flat top like the small area mesh, but rather it should conform to the alluvium surfaces. The difficulty in creating a computational mesh that meets the modeling criteria will take more time and effort.

Methods of creating a mesh include using a structured mesh with fine resolution, or a coarser mesh that uses octree refinement to increase resolution in user specified regions of interest. Experience has shown that a structured mesh can provide accurate solutions so long as there is adequate resolution to represent the geometry of the geologic layers. Particular constraints for accuracy and numerical stability are imposed by the modeling application. This is very important because depending on the mesh, you can get a stable but inaccurate solution to the physics (Zyvoloski and Vesselinov, 2006). The design is chosen with consideration of the physics to be modeled, mesh size restrictions versus mesh resolution needed for model features, and the mesh and model information needed by the model application.

The structured mesh can be used with octree refinement to add features such as wells and a repository. As long as refinement is internal, the mesh will satisfy the Delaunay criteria. If there is time and interest, the structured mesh can be stretched vertically to conform to one of the alluvium surfaces. This may form undesirable coupling coefficients but may still be adequate for flow solutions, although it may create problems for particle tracking or pumping scenarios.

Meshing the entire basin would likely require a very large number of cells with highly-refined spacing to be used for flow and transport calculations. A mesh with enough resolution will likely require running PFLOTRAN in parallel mode on several million nodes. The Sandia developed meshing software, VoroCrust (https://vorocrust.sandia.gov), can be used to create a Voronoi mesh that conforms to the alluvium surfaces and that will meet the modeling criteria of a Delaunay mesh. Controls for spacing and the distribution of volumes in the mesh would need to be explored. At this time VoroCrust cannot handle a terminating fault, but future work may enable this capability.

6.3   Characterizing Heterogeneity with 3D Geocellular Models

Facies and property modeling in JewelSuite^{TM} or similar software provides considerable insight into the characterization of alluvial sediments. When combined with computational meshing (LaGriT) and flow and transport applications (e.g., FEHM, PFLOTRAN), the resulting workflow can generate models of radionuclide transport for different scenarios of heterogeneity (Figure 6-3). Preliminary models of UZ repositories consider horizontal tabular units of alluvial stratigraphy (Mariner et al., 2018; Sevougian et al., 2019). However, modeling results from this year's study, even when incorporating heterogeneous physical properties, suggest that tabular facies (Models 1A and 1B) may overestimate time to breakthrough when compared to more complex facies distributions (Figure 6-1 and Figure 6-2).

The main takeaway from our FY21 work is that heterogeneity inherent to alluvial lithofacies may significantly impact the flow and transport of radionuclides originating from a UZ-hosted repository. Therefore, characterizing the heterogeneity of facies and physical properties, and exploring their impact on flow behavior, should be a necessary component of the geologic disposal safety assessment (GDSA) for the generic alluvial basin repository. Results from FY21 will help constrain the modeling parameters and define the important questions to address in future evaluations of unsaturated zone heterogeneities. As examples, one can vary the thickness and interfingering geometry of lacustrine sediments, explore different geostatistical methods and

variogram ranges, and validate the upscaling of physical properties from the wellbore scale to computational grid cell dimensions.
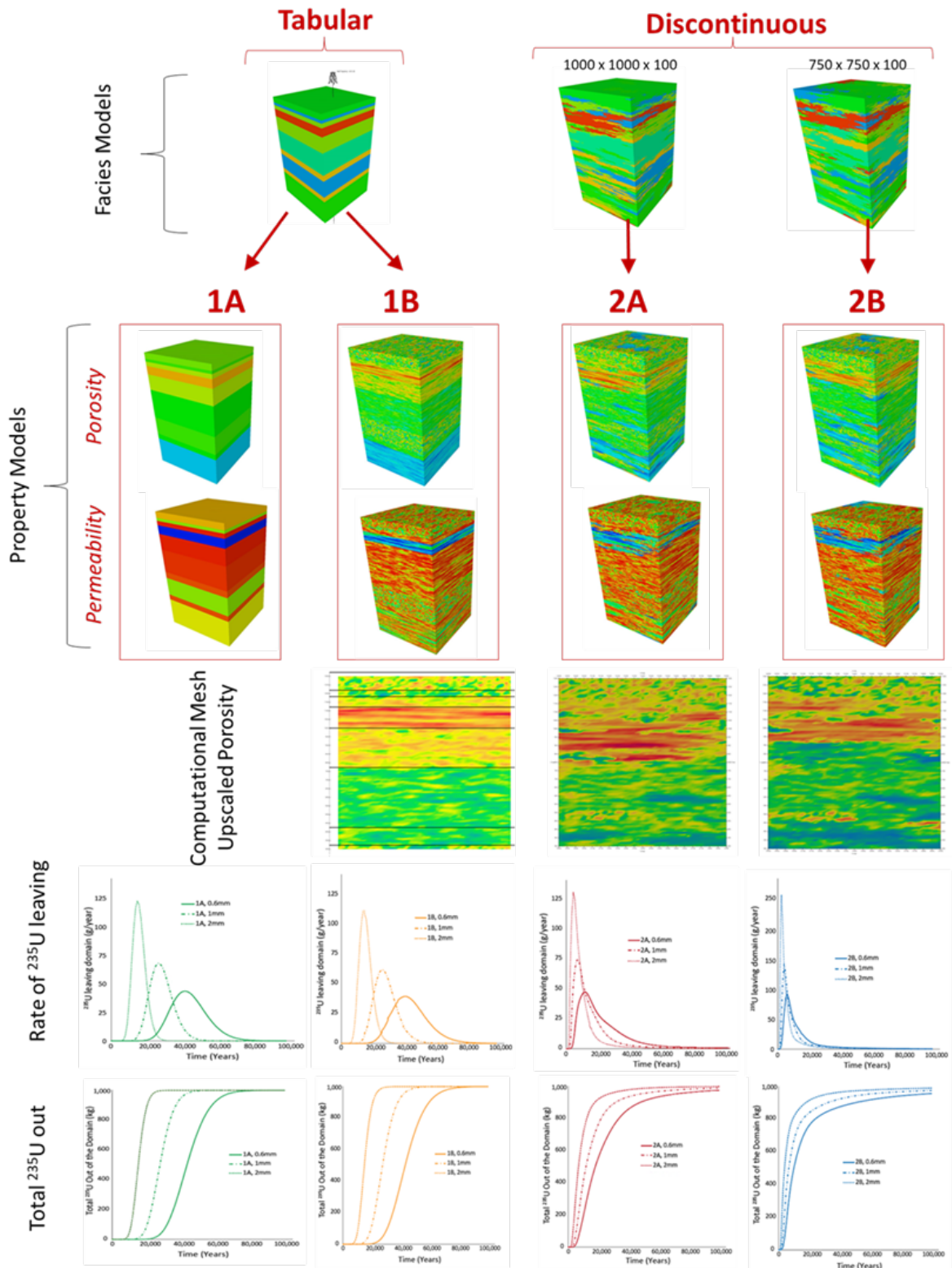
Figure 6-3. Summary of models and workflow explored in FY21 for the near-field volume.

7. Conclusions and Future Work

This FY21 we successfully developed a process whereby we could develop statistically appropriate lithofacies and properties models, incorporate them into Voronoi meshes, and conduct flow and transport simulations on them. Our analysis revealed a strong sensitivity to the geostatistical representation of the lithofacies. This result underpins the importance of this work and the necessity for constraining the geostatistical model parameters through the incorporation of new datasets. Work during FY21 uncovered geophysical logs from two deep boreholes in the Mimbres Basin. One log is within the near field extent and the other is close by. Timing and budgetary concerns prevented the analysis of these logs but during FY22 the incorporation of the data from these logs will be a top priority. This data should significantly reduce the uncertainty in our geostatistical modeling.

While the work during FY21 was able to elucidate some meaningful insights into the effect of lithologic heterogeneity a more complete sensitivity analysis is important. It is possible that our simulations are highly sensitive to our model realizations. To investigate this we plan to automate our process from geostatistical modeling, to mesh generation, to flow and transport simulation. Prior to the methodologies developed during this FY a streamlined and automated process was not possible. With the expertise developed during last FY we believe we will be able to generate geostatistical models and develop meshing inputs and conduct flow and transport simulations all through a seamless automated process which will allow many more realizations and a true sensitivity analysis to the model realizations as well as other flow and transport parameters.

In this work we treated recharge as a constant 0.6, 1, and 2 mm/year rate. Increasing the recharge rate was meant to incorporate the possibility of a wetter environment due to climate change. Future work could include simulations with higher recharge rates, and time varying recharge to take into effect the periodic nature of recharge and that climate change could increase over time. In addition, the current work sets a prescribed water pressure gradient which did not allow the water table to rise. Future work could be performed to implement a free water table which may rise or lower depending on recharge. Changing the water table depth will affect the rate that ^{235}U is removed from the system.

In FY21 we focused on the near field model. Future work could be performed to expand on this to the regional scale. This work would incorporate regional facies and allow for nested flow models where larger scale simulations could supply the boundary conditions to the smaller area. This could be used to develop a water table that reacts in a realistic way to changing recharge rates.

Our model results emphasize the importance of lacustrine sediments in delaying the transport of radionuclides from a repository within an alluvial basin. A thick, continuous layer of lacustrine deposits, often found in basin depocenters, is most desirable for hosting a repository due to its low permeabilities (several orders of magnitude lower than other alluvial sediments). Therefore, quantifying the distribution, thickness, petrophysical properties and heterogeneity of lacustrine sediments is a necessary step in evaluating the suitability of an alluvial basin to host a nuclear waste repository. Geostatistical modeling within a subsurface modeling application (i.e., geologic framework construction) is ideally suited for this task.

8.   Acknowledgements

9. References

Anderson, T. W., 1995. Summary of the Southwest Alluvial Basins, Regional Aquifer-System Analysis, south-central Arizona and parts of adjacent states. U.S. Geological Survey Professional Paper 1406-A. 44 p. https://pubs.er.usgs.gov/publication/pp1406A

Baker Hughes, 2020, JewelSuite[TM] 10 Subsurface Modeling User Manual, Delft, The Netherlands, 2324 p.

Brooks, R. H., & Corey, A. T. (1966). Properties of porous media affecting fluid flow. *Journal of the irrigation and drainage division*, *92*(2), 61-88.

Buckles, R. (1965). Correlating and averaging connate water saturation data. *Journal of Canadian Petroleum Technology, 4*(01), 42-52.

Bussod,G., P.H. Stauffer, H. Boukhalfa, M. Dangelmayr, S. Kuluris, N. HayesRich, T.A. Miller, G. Woldegabriel, R. Rosenzweig, R. Calvo, N. Balaban ,O. Klein-Ben David, A. Dody (2020), 2017-2020 Final Report NNSA-IAEC Science Area 5 Enviornmental ISR, *Los Alamos National Laboratory* LAUR-20-28271

FEHM (2020), https://fehm.lanl.gov/, last accessed July 23, 2020.

Finch, S.T. Jr., McCoy, A. and Melis, E., 2008, Geologic controls on ground-water flow in the Mimbres Basin, southwestern New Mexico in Geology of the Gila Wilderness-Silver City area, New Mexico Geological Society Guidebook, 59th Field Conference, p. 1889-198.

Gross, M., Bussod, G., Gable, C.W., Kelley, R., Lavadie-Bulnes, A., Milazzo, D., Miller, E., Miller, T.A., Roback, R., Stauffer, P.H., Swanson, E. and Perry, F., 2019, Progress report on the development of a geologic framework model capability to support GDSA, Prepared for the U.S. Department of Energy Spent Fuel and Waste Disposition, LA-UR-19-27943.

Gross, M., Miller, E., Milazzo, D., Miller, T.A., Lavadie-Bulnes, A., Swanson, E., Hayes-Rich, N., Roback, R., Stauffer, P.H., LaForce, T. and Ebeida, M.S., 2020, Geologic framework models for the alluvial basin reference case, Prepared for the U.S. Department of Energy Spent Fuel and Waste Disposition, LA-UR-20-25594.

Hanson, R.T., McLean, J.S. and Miller, R.S., 1994, Hydrogeologic framework and preliminary simulation of ground-water flow in the Mimbres Basin, southwestern New Mexico: U.S. Geological Survey Water-Resources Investigations Report 94-4011, 118 p.

Hawley, J.W., Hibbs, B.J., Kennedy, J.F., Creel, B.J., Remmenga, M.D., Johnson, M., Lee, M.M. and Dinterman, P., 2000, Trans-International Boundary aquifers in southwestern New Mexico: New Mexico Water Resources Research Institute, New Mexico State University, prepared for U.S. Environmental Protection Agency, Region 6, and International Boundary and Water Commission; Technical Completion Report-Interagency Contract X-996350-01-3, 126 p.

Kennedy, J.F., Hawley, J.W. and Johnson, M.M., 2000, The hydrogeologic framework of basin-fill aquifers and associated ground-water-flow systems in southwestern New Mexico – an overview, in New Mexico Geologic Society Guidebook, 51st Field Conference, p. 235-244.

Kwicklis, E.M., A.V. Wolfsberg, P.H. Stauffer, M.A. Walvoord, and M.J. Sully. 2006. Multiphase, multicomponent parameter estimation for liquid and vapor fluxes in deep arid systems using hydrologic data and natural environmental tracers. Vadose Zone J. 5:934– 950. doi:10.2136/vzj2006.0021

Los Alamos Grid Toolbox, LaGriT, Los Alamos National Laboratory, (https://LaGriT.lanl.gov), 2020.

Mariner, P.E., Stein, E.R., Sevougian, S.D., Cunningham, L.J., Frederick, J.M., Hammond, G.E., Lowry, T.S., Jordan, S., and Basurto, E. 2018. Advances in Geologic Disposal Safety Assessment and an Unsaturated Alluvium Reference Case. SFWD-SFWST-2018-000509, SAND2018-11858 R.

2007 Miller, T.A., V. V. Vessilinov, P.H. Stauffer, K. H. Birdsell, and C. W. Gable, Integration of geologic frameworks in meshing and setup of computational hydrogeologic models, Pajarito Plateau, New Mexico, *New Mexico Geological Society Guide Book, 58th Field Conference*, Geology of the Jemez Mountains Region III.

PFLOTRAN (2020), https://www.pflotran.org/, last accessed July 23, 2020.

Perry, F.V., Swanson, E., Milazzo, D.M., Bussod, G.Y.A. and Kelley, R.E., 2018. Regional geologic evaluations for disposal of HLW and SNF: alluvial basins of the Basin and Range Province. SFWD-SFWST-2018-000512. U.S. Department of Energy, Used Fuel Disposition Campaign, Los Alamos Unlimited Release LA-UR-18-28909, 46p.

Phelps, G.A., Boucher, A. and Halford, K.J., 2010, A refined characterization of the alluvial geology of Yucca Flat and its effect on bulk hydraulic conductivity: U.S. Geological Survey Open-File Report 2010-1307, 33p.

Rawling, G., 2021, Evaluation of water-level trends using spatiotemporal kriging in the Mimbres Basin, southwest New Mexico: New Mexico Bureau of Geology and Mineral Resources Open-File Report 616, 46 p.

Sevougian, S.D., Stein, E.R., LaForce, T., Perry, F.V., Lowry, T.S., Cunningham, L.J., Nole, M., Haukwa, C.B., Chang, K.W., and Mariner, P.E., 2019, GDSA Repository Systems Analysis Progress Report. M2SF-19SN010304051 SAND2019-5189 R.

Shepherd, M., 2009, Geostatistical methods, in M. Shepherd, Oil field production geology: AAPG Memoir 91, p. 159-174.

Sun, A.Y., Ritzi, R.W. and Sims, D.W., 2008, Characterization and modeling of spatial variability in a complex alluvial aquifer: implications on solute transport: Water Resources Research, v. 44, W04402. doi:10.1029/2007WR006119.

Sweetkind, D.S., 2017, Three-dimensional hydrogeologic framework model of the Rio Grande transboundary region of New Mexico and Texas, USA, and northern Chihuahua, Mexico: U.S. Geological Survey Scientific Investigations Report 2017-5060.

Zyvoloski, G.A., B.A. Robinson, Z.V. Dash, S. Kelkar, H.S. Viswanathan, R. J. Pawar, P. H. Stauffer, T. A. Miller, S. Chu, 2015. Software Users Manual (UM) for the FEHM Application Version 3.1 - 3.X, Los Alamos National Laboratory document LA-UR-12-24493.

Appendix

A-1 JewelSuite^{TM} File Formats for Meshing

JewelSuite has various options to export information. The following formats were determined to contain the information needed for the meshing workflow.

The GOCAD file format from JewelSuite can write user defined vertex and cell properties, it also has some default properties available through menu selection. By convention we ignore all user defined properties but we require the JewelSuite cell properties ZoneID and CompartmentID. The GOCAD TETRA mesh file has the following important elements that are used by LaGriT in the meshing workflow. Note the vertex property NodeId is included here as it is often included by default. This property is ignored in the LaGriT workflow.

```
GOCAD TSolid 1 = 3D volume filled tetrahedral mesh

AXIS_NAME "X" "Y" "Z" = x, y, z axis represented
AXIS_UNIT "m" "m" "m" = coordinates in meters

ZPOSITIVE Depth = positive downward distance from 0 (otherwise this is ELEVATION)

PROPERTIES NodeId = node attributes if they exist, these can be ignored

PROPERTY_CLASS_HEADER NodeId{ = node attribute range of values, can be ignored
low_clip:1
high_clip:4
}

TETRA_PROPERTIES CompartmentId  ZoneId = cell attributes for compartments and zones

TETRA_PROPERTY_CLASS_HEADER CompartmentId{ = range of CompartmentId from 1 to max
low_clip:1
high_clip:3
}
}
TETRA_PROPERTY_CLASS_HEADER ZoneId{ = range of ZoneId from 1 to max
low_clip:1
high_clip:2
}

VRTX or PVRTX = id, xyz location of element vertices (nodes) followed by attribute values for that point
TETRA = element connectivity of 4 vertices followed by attribute values for that element
```

JewelSuite has well developed tools for defining geologic properties such as permeability and porosity. We developed a method to read the properties calculated in JewelSuite and then apply them to the computational mesh as a mesh attribute that can be used by simulations. Using LaGriT, these property values can be interpolated on to a computational mesh by using the upscale command. This algorithm captures all geostat data points located inside a mesh Voronoi volume. Preferably each volume will contain and number of data points. The data points for a volume may have a range of property values. To assign a single value on the mesh, these point values are averaged or selected by a min max criteria.

JewelSuite can export property data file in tabular form with rows of each point x, y, z (elevation), property values. The "#" character is added to each line of the header so LaGriT knows to skip the non data header lines.

```
# 3D Grid 1  (9, 198, 15)  Start Depth 1
# 4
# X  Unit m
# Y  Unit m
# Z  Unit m
# Distance  Template Distance  Unit m
238731.719422316 3571423.93279472 -422.930961234996 6719.94291785036
238779.900945972 3571410.57087416 -423.15766431377  6670.28112964709
238828.082468495 3571397.2089556  -423.386984220641 6620.62472790031
```

A-2   Mesh Statistics for Property Models

LaGriT reports mesh statistics and values, these are copied into the README.txt file for each of the models and included here.

A-2.1 README for Tabular 1B

GDSA Basin Model small mesh with August 2021
Version 2 with nearly flat layers
/project/meshing/GEO_Integration/JewelSuite/GFM_to_ModelsV2/area_small/mesh_25x25x10m_aug2021

V2 August 2021 JewelSuite Conceptual Model for geostat properties
Well F3-19 Elevations above SL(m)

../properties_aug2021/
tamiller sft 100475832 Aug 5 10:23 ../properties_aug2021/Facies_unix.dat
tamiller sft 130621331 Aug 5 10:24 ../properties_aug2021/Porosity_unix.dat
tamiller sft 136314754 Aug 5 10:10 ../properties_aug2021/Conditioned_Perm_m2_unix.dat
tamiller sft 136313864 Aug 5 10:25 ../properties_aug2021/Unconditioned_Perm_m2_unix.dat

Mesh 1000 x 1000 x 1000 meters
Mesh with spacing 25x25x10 meters
number of nodes = 169781
number of hex elements = 160000
number of tet elements = 960000

Position relative to x-aligned intermediate mesh
Translate 0. 0. 0. to llcorner this mesh 14900. 4160. 300.
Z elevation 300m to 1300m (flat top alluvium)

Outside Boundary Nodes:
 THE PSET TOP_NODES   HAS 1681 POINTS
 THE PSET BOT_NODES   HAS 1681 POINTS
 THE PSET LEFT_NODES HAS 4141 POINTS
 THE PSET FRONT_NODES HAS 4141 POINTS
 THE PSET RIGHT_NODES HAS 4141 POINTS
 THE PSET BACK_NODES HAS 4141 POINTS

Facies upscaled and actual top elevations:

	min_facies	max_facies	actual
1	1300	1300	1322.54
3a	1210	1220	1219.07
4a	1170	1180	1182.47
5	1110	1120	1122.02
4b	990	1000	999.45
6	760	770	771.87
7	410	420	424.93
3b	310	320	323.08

Material zones are assigned from upscale attribute max_facies
(ID 3 and 4 have repeated layers, same number. (no a or b designation):

Minimum material ID value =   1
Maximum material ID value =   7
Total possible materials =   7
Material   1 has   13448 nodes. #nodes/nnodes is 0.792079195380E-01
No nodes found in material =   2
Material   3 has   10086 nodes. #nodes/nnodes is 0.594059415162E-01
Material   4 has   47068 nodes. #nodes/nnodes is 0.277227729559
Material   5 has   21853 nodes. #nodes/nnodes is 0.128712877631
Material   6 has   58835 nodes. #nodes/nnodes is 0.346534639597
Material   7 has   18491 nodes. #nodes/nnodes is 0.108910888433

Min Max Mesh Node Attributes from upscle mesh:

ATTRIBUTE   MIN   MAX   DIFFERENCE   LENGTH
 xic   1.490000000E+04 1.590000000E+04 1.000000000E+03   169781
 yic   4.160000000E+03 5.160000000E+03 1.000000000E+03   169781
 zic   3.000000000E+02 1.300000000E+03 1.000000000E+03   169781

 min_facies   1.000000000E+00 7.000000000E+00 6.000000000E+00   169781
 max_facies   1.000000000E+00 7.000000000E+00 6.000000000E+00   169781
 porosity   1.416079707E-01 5.768461207E-01 4.352381500E-01   169781
 perm_m2   1.273824808E-17 3.581685353E-09 3.581685340E-09   169781
 uperm_m2   1.273338756E-17 3.539985104E-09 3.539985091E-09   169781
 near_facies   1   7   6   169781

Compare to JewelSuite:

Cropped data set:

ATTRIBUTE NAME   MIN   MAX   DIFFERENCE   LENGTH
 xic   1.485348968E+04 1.593348968E+04 1.080000003E+03 1066873
 yic   4.143942164E+03 5.208942291E+03 1.065000127E+03 1066873
 zic   2.934904644E+02 1.304635409E+03 1.011144944E+03 1066873

 pordat   8.174379947E-02 5.849446335E-01 5.032008340E-01 1066873
 perdat   1.186932600E-17 3.583527122E-09 3.583527111E-09 1066873
 uperdat   1.191992178E-17 3.583269939E-09 3.583269927E-09 1066873
 facdat   1.000000000E+00 7.000000000E+00 6.000000000E+00 1066873
 elev   2.934904644E+02 1.304635409E+03 1.011144944E+03 1066873

Outside Boundary Nodes:
 THE PSET TOP_NODES   HAS 1681 POINTS
 THE PSET BOT_NODES   HAS 1681 POINTS
 THE PSET LEFT_NODES HAS 4141 POINTS
 THE PSET FRONT_NODES HAS 4141 POINTS
 THE PSET RIGHT_NODES HAS 4141 POINTS
 THE PSET BACK_NODES HAS 4141 POINTS

*** Construct and Compress Sparse Matrix:3D ***
  *** Compress Area Coefficient Values ***
SparseMatrix initialize epsilon to 1.000000e-08
SparseMatrix using Epsilon 1.000000e-08

AMatbld3d_stor: *****Zero Negative Coefficients ******
AMatbld3d_stor: Number of 'zero' (< compress_eps) coefs   0
AMatbld3d_stor: npoints =   169781 ncoefs =   1168541
AMatbld3d_stor: Number of unique coefs =   7
AMatbld3d_stor: Maximum num. connections to a node =   7
PFLOTRAN total CELL nodes =   169781
AMatbld3d_stor: Volume min =   7.8125000E+02
AMatbld3d_stor: Volume max =   6.2500000E+03
AMatbld3d_stor: Total Volume: 1.0000000E+09
AMatbld3d_stor: abs(Aij/xij) min =   0.0000000E+00
AMatbld3d_stor: abs(Aij/xij) max =   6.2500000E+01
AMatbld3d_stor: (Aij/xij) max =   0.0000000E+00
AMatbld3d_stor: (Aij/xij) min = -6.2500000E+01
PFLOTRAN will filter zero coefs.
PFLOTRAN coefficient from matbld Aij/Xij max =   0.0000000E+00
PFLOTRAN filter = epsilon * abs(max Aij/Xij) : 1.0000000E-12 0.0000000E+00
PFLOTRAN coefficients: epsilon for zero filter =   1.0000000E-12
  -count nconn   499380
  -count nzero   0

PFLOTRAN total matbld matrix coefficients   =   1168541
PFLOTRAN matrix i>j (written)   =   499380
PFLOTRAN matrix i<=j (not written)   =   669161
PFLOTRAN zero coefs < epsilon (not written) =   0

PFLOTRAN total CONNECTIONS written   =   499380
PFLOTRAN coefficient Aij min   =   6.2500000E+01
PFLOTRAN coefficient Aij max   =   6.2500000E+02
AMatbld3d_stor Matrix coefficient values stored as scalar area/distance

*** SPARSE COEFFICIENT MATRIX for PFLOTRAN SUCCESSFUL ***
3D Matrix Coefficient file written with name tet0.uge

A-2.2 README for Discontinuous Model 2A

GDSA Basin Model small mesh Sep 2021 for ISO 1000
Version 2 had flat layers Version 3 ISO 1000 is variable throughout mesh
This directory contains V3 mesh files for ISO 1000
/project/meshing/GEO_Integration/JewelSuite/GFM_to_ModelsV2/area_small/mesh_25x25x10m_i1000

V3 Sep 2021 JewelSuite Conceptual Model for geostat properties
There are 2 models, ISO 750 and 1000 extent with heterogenous facies.
Model ISO 1000 has 1000m major and minor horizontal range, vertical 100m.
Model ISO 750 has 750m major and minor horizontal range, vertical 100m.
The permeability is conditioned to the porosity using a 0.5 correlation factor.
The units of the permeability are in log µd.
The min, max, and and standard deviation of the properties is unchanged from V2.

Data files:
/project/meshing/GEO_Integration/JewelSuite/GFM_to_ModelsV2/area_small/properties_sept_2021
Facies_Iso_1000.dat: ASCII text
Facies_Iso_750.dat: ASCII text
Iso_1000_Perm_log_ud.dat: ASCII text
Iso_1000_Poro.dat: ASCII text

Iso_750_Perm_log_ud.dat: ASCII text
Iso_750_Poro.dat: ASCII text

1 Mimbres alluvial fan
2 Minor Lacustrine deposits
3 Alluvial Fan deposits
4 Upper Gila fluvial
5 Main Lacustrine deposits
6 Middle Gila fluvial
7 Lower Gila fluvial channel
8 Lower Gila fluvial overbank
9 Bedrock Volcanics

CROPPED DATA ISO 1000 data min max difference
facies   1.000000000E+00 9.000000000E+00 8.000000000E+00
por   8.927918200E-02 5.841295830E-01 4.948504010E-01
perm   1.080059223E+00 9.559987286E+00 8.479928063E+00

MESH UPSCALE for ISO 1000 min max difference
facies   1.000000000E+00 9.000000000E+00 8.000000000E+00
porosity   1.252311969E-01 5.649452037E-01 4.397140069E-01
perm   1.086279510E+00 9.556997189E+00 8.470717679E+00

FACIES Material Zones ISO 1000:
Material zones are assigned from upscale attribute max_facies

ISO 1000:
Minimum material ID value =   1
Maximum material ID value =   9
No Material 2, 8
Material 1 has   16220 nodes. #nodes/nnodes is   0.955348387361E-01
Material 3 has   7464 nodes. #nodes/nnodes is   0.439625158906E-01
Material 4 has   34154 nodes. #nodes/nnodes is   0.201165035367
Material 5 has   22070 nodes. #nodes/nnodes is   0.129990994930
Material 6 has   58554 nodes. #nodes/nnodes is   0.344879567623
Material 7 has   17813 nodes. #nodes/nnodes is   0.104917511344
Material 9 has   13506 nodes. #nodes/nnodes is   0.795495361090E-01

ISO 750 included for comparison:
Minimum material ID value =   1
Maximum material ID value =   9
No Material 2, 8
Material 1 has   10898 nodes. #nodes/nnodes is   0.641885697842E-01
Material 3 has   7987 nodes. #nodes/nnodes is   0.470429547131E-01
Material 4 has   31076 nodes. #nodes/nnodes is   0.183035790920
Material 5 has   22215 nodes. #nodes/nnodes is   0.130845025182
Material 6 has   51769 nodes. #nodes/nnodes is   0.304916322231
Material 7 has   26892 nodes. #nodes/nnodes is   0.158392280340
Material 9 has   18944 nodes. #nodes/nnodes is   0.111579030752

MINMAX by Facies Zone ID:

porosity MIN   MAX   DIFFERENCE
 1   1.486581229E-01 5.178173364E-01 3.691592135E-01
 3   1.252311969E-01 4.827098111E-01 3.574786142E-01

```
4    1.970974878E-01  4.806965318E-01 2.835990441E-01
5    2.004681544E-01  5.649452037E-01 3.644770494E-01
6    1.894576229E-01  4.951164590E-01 3.056588360E-01
7    1.813667272E-01  4.746860013E-01 2.933192741E-01
9    1.601345861E-01  4.997760508E-01 3.396414647E-01


perm   MIN          MAX          DIFFERENCE
1    4.484179288E+00  8.473111531E+00 3.988932242E+00
3    4.112358905E+00  8.114644199E+00 4.002285294E+00
4    4.654746868E+00  9.556997189E+00 4.902250321E+00
5    1.086279510E+00  8.602981602E+00 7.516702092E+00
6    1.550682572E+00  9.384323701E+00 7.833641129E+00
7    1.650215480E+00  9.175472706E+00 7.525257226E+00
9    2.230176056E+00  9.008563013E+00 6.778386956E+00
```

Mesh 1000 x 1000 x 1000 meters
Mesh with spacing 25x25x10 meters
number of nodes = 169781
number of hex elements = 160000
number of tet elements = 960000

Position relative to x-aligned intermediate mesh
Translate 0. 0. 0. to llcorner this mesh 14900. 4160. 300.
Z elevation 300m to 1300m (flat top alluvium)

MESH COORDINATES min max difference
xic 1.490000000E+04 1.590000000E+04 1.000000000E+03
yic 4.160000000E+03 5.160000000E+03 1.000000000E+03
zic 3.000000000E+02 1.300000000E+03 1.000000000E+03

Outside Boundary Nodes:
 THE PSET TOP_NODES   HAS 1681 POINTS
 THE PSET BOT_NODES   HAS 1681 POINTS
 THE PSET LEFT_NODES HAS 4141 POINTS
 THE PSET FRONT_NODES HAS 4141 POINTS
 THE PSET RIGHT_NODES HAS 4141 POINTS
 THE PSET BACK_NODES HAS 4141 POINTS

*** Construct and Compress Sparse Matrix:3D ***
  *** Compress Area Coefficient Values ***
SparseMatrix initialize epsilon to 1.000000e-08
SparseMatrix using Epsilon 1.000000e-08
AMatbld3d_stor: *****Zero Negative Coefficients ******
AMatbld3d_stor: Number of 'zero' (< compress_eps) coefs   0
AMatbld3d_stor: npoints =   169781 ncoefs =   1168541
AMatbld3d_stor: Number of unique coefs =   7
AMatbld3d_stor: Maximum num. connections to a node =   7
PFLOTRAN total CELL nodes =   169781
AMatbld3d_stor: Volume min =   7.8125000E+02
AMatbld3d_stor: Volume max =   6.2500000E+03
AMatbld3d_stor: Total Volume: 1.0000000E+09
AMatbld3d_stor: abs(Aij/xij) min =   0.0000000E+00
AMatbld3d_stor: abs(Aij/xij) max =   6.2500000E+01
AMatbld3d_stor: (Aij/xij) max =   0.0000000E+00

AMatbld3d_stor: (Aij/xij) min = -6.2500000E+01
PFLOTRAN will filter zero coefs.
PFLOTRAN coefficient from matbld Aij/Xij max = 0.0000000E+00
PFLOTRAN filter = epsilon * abs(max Aij/Xij) : 1.0000000E-12 0.0000000E+00
PFLOTRAN coefficients: epsilon for zero filter = 1.0000000E-12
  -count nconn   499380
  -count nzero   0

PFLOTRAN total matbld matrix coefficients   =   1168541
PFLOTRAN matrix i>j (written)   =   499380
PFLOTRAN matrix i<=j (not written)   =   669161
PFLOTRAN zero coefs < epsilon (not written) =   0

PFLOTRAN total CONNECTIONS written   =   499380
PFLOTRAN coefficient Aij min   = 6.2500000E+01
PFLOTRAN coefficient Aij max   = 6.2500000E+02
AMatbld3d_stor Matrix coefficient values stored as scalar area/distance

*** SPARSE COEFFICIENT MATRIX for PFLOTRAN SUCCESSFUL ***
3D Matrix Coefficient file written with name tet0.uge

A-2.3 README for Discontinuous Model 2B

GDSA Basin Model small mesh Sep 2021 for ISO 750
Version 2 had flat layers Version 3 ISO 750 is variable throughout mesh
This directory contains V3 mesh files for ISO 750
/project/meshing/GEO_Integration/JewelSuite/GFM_to_ModelsV2/area_small/mesh_25x25x10m_i750

V3 Sep 2021 JewelSuite Conceptual Model for geostat properties
There are 2 models, ISO 750 and 1000 extent with heterogenous facies.
Model ISO 1000 has 1000m major and minor horizontal range, vertical 100m.
Model ISO 750 has 750m major and minor horizontal range, vertical 100m.
The permeability is conditioned to the porosity using a 0.5 correlation factor.
The units of the permeability are in log µd.
The min, max, and and standard deviation of the properties is unchanged from V2.

Data files:
/project/meshing/GEO_Integration/JewelSuite/GFM_to_ModelsV2/area_small/properties_sept_2021
Facies_Iso_1000.dat: ASCII text
Facies_Iso_750.dat: ASCII text
Iso_1000_Perm_log_ud.dat: ASCII text
Iso_1000_Poro.dat: ASCII text
Iso_750_Perm_log_ud.dat: ASCII text
Iso_750_Poro.dat: ASCII text

1 Mimbres alluvial fan
2 Minor Lacustrine deposits
3 Alluvial Fan deposits
4 Upper Gila fluvial
5 Main Lacustrine deposits
6 Middle Gila fluvial
7 Lower Gila fluvial channel
8 Lower Gila fluvial overbank
9 Bedrock Volcanics

JewelSuite CROPPED DATA ISO 750 data min max difference
facies   1.000000000E+00 9.000000000E+00 8.000000000E+00
por   8.236579832E-02 5.846879138E-01 5.023221155E-01
perm   1.081348322E+00 9.559998046E+00 8.478649724E+00

MESH UPSCALE for ISO 750 min max difference
facies   1.000000000E+00 9.000000000E+00 8.000000000E+00
porosity 1.467142125E-01 5.645251088E-01 4.178108963E-01
perm   1.097981549E+00 9.557071938E+00 8.459090389E+00

FACIES Material Zones ISO 750:
Material zones are assigned from upscale attribute max_facies

ISO 750:
Minimum material ID value =   1
Maximum material ID value =   9
No Material 2, 8
Material 1 has   10898 nodes. #nodes/nnodes is   0.641885697842E-01
Material 3 has   7987 nodes. #nodes/nnodes is   0.470429547131E-01
Material 4 has   31076 nodes. #nodes/nnodes is   0.183035790920
Material 5 has   22215 nodes. #nodes/nnodes is   0.130845025182
Material 6 has   51769 nodes. #nodes/nnodes is   0.304916322231
Material 7 has   26892 nodes. #nodes/nnodes is   0.158392280340
Material 9 has   18944 nodes. #nodes/nnodes is   0.111579030752

ISO 1000 included for comparison:
Minimum material ID value =   1
Maximum material ID value =   9
No Material 2, 8
Material 1 has   16220 nodes. #nodes/nnodes is   0.955348387361E-01
Material 3 has   7464 nodes. #nodes/nnodes is   0.439625158906E-01
Material 4 has   34154 nodes. #nodes/nnodes is   0.201165035367
Material 5 has   22070 nodes. #nodes/nnodes is   0.129990994930
Material 6 has   58554 nodes. #nodes/nnodes is   0.344879567623
Material 7 has   17813 nodes. #nodes/nnodes is   0.104917511344
Material 9 has   13506 nodes. #nodes/nnodes is   0.795495361090E-01

MINMAX by Facies Zone ID:

porosity	MIN	MAX	DIFFERENCE
1	1.486581229E-01	5.153267641E-01	3.666686412E-01
3	1.491742772E-01	4.723110898E-01	3.231368127E-01
4	1.467142125E-01	4.733555200E-01	3.266413075E-01
5	2.151921319E-01	5.645251088E-01	3.493329769E-01
6	1.960097906E-01	4.744673902E-01	2.784575996E-01
7	1.835676967E-01	4.714237269E-01	2.878560301E-01
9	1.607965324E-01	4.524741325E-01	2.916776001E-01

perm	MIN	MAX	DIFFERENCE
1	4.498218365E+00	8.473370478E+00	3.975152113E+00
3	4.097591983E+00	8.228669758E+00	4.131077775E+00
4	4.720863882E+00	9.557071938E+00	4.836208056E+00
5	1.097981549E+00	8.949681586E+00	7.851700037E+00
6	1.749826800E+00	9.379609224E+00	7.629782424E+00

```
7     1.683031496E+00  9.262708728E+00  7.579677231E+00
9     1.667095535E+00  9.094650567E+00  7.427555033E+00


Mesh 1000 x 1000 x 1000 meters
Mesh with spacing 25x25x10 meters
number of nodes = 169781
number of hex elements = 160000
number of tet elements = 960000

Position relative to x-aligned intermediate mesh
Translate 0. 0. 0. to llcorner this mesh 14900. 4160. 300.
Z elevation 300m to 1300m (flat top alluvium)

MESH COORDINATES min max difference
xic  1.490000000E+04  1.590000000E+04  1.000000000E+03
yic  4.160000000E+03  5.160000000E+03  1.000000000E+03
zic  3.000000000E+02  1.300000000E+03  1.000000000E+03

Outside Boundary Nodes:
 THE PSET  TOP_NODES   HAS  1681 POINTS
 THE PSET  BOT_NODES   HAS  1681 POINTS
 THE PSET  LEFT_NODES  HAS  4141 POINTS
 THE PSET  FRONT_NODES HAS  4141 POINTS
 THE PSET  RIGHT_NODES HAS  4141 POINTS
 THE PSET  BACK_NODES  HAS  4141 POINTS


*** Construct and Compress Sparse Matrix:3D ***
  *** Compress Area Coefficient Values ***
SparseMatrix initialize epsilon to 1.000000e-08
SparseMatrix using Epsilon 1.000000e-08
AMatbld3d_stor: *****Zero Negative Coefficients ******
AMatbld3d_stor: Number of 'zero' (< compress_eps) coefs        0
AMatbld3d_stor: npoints =   169781  ncoefs =    1168541
AMatbld3d_stor: Number of unique coefs =        7
AMatbld3d_stor: Maximum num. connections to a node =        7
PFLOTRAN total CELL nodes =      169781
AMatbld3d_stor: Volume min =   7.8125000E+02
AMatbld3d_stor: Volume max =   6.2500000E+03
AMatbld3d_stor: Total Volume:   1.0000000E+09
AMatbld3d_stor: abs(Aij/xij) min =   0.0000000E+00
AMatbld3d_stor: abs(Aij/xij) max =   6.2500000E+01
AMatbld3d_stor: (Aij/xij) max =   0.0000000E+00
AMatbld3d_stor: (Aij/xij) min =  -6.2500000E+01
PFLOTRAN will filter zero coefs.
PFLOTRAN coefficient from matbld Aij/Xij  max =   0.0000000E+00
PFLOTRAN filter = epsilon * abs(max Aij/Xij) :  1.0000000E-12  0.0000000E+00
PFLOTRAN coefficients: epsilon for zero filter =   1.0000000E-12
  -count nconn          499380
  -count nzero               0

PFLOTRAN total matbld matrix coefficients  =   1168541
PFLOTRAN matrix  i>j (written)          =    499380
PFLOTRAN matrix  i<=j (not written)       =    669161
PFLOTRAN zero coefs < epsilon (not written) =        0
```

PFLOTRAN total CONNECTIONS written   =   499380
PFLOTRAN coefficient Aij min   = 6.2500000E+01
PFLOTRAN coefficient Aij max   = 6.2500000E+02
AMatbld3d_stor Matrix coefficient values stored as scalar area/distance

*** SPARSE COEFFICIENT MATRIX for PFLOTRAN SUCCESSFUL ***
3D Matrix Coefficient file written with name tet0.uge

A-3   Python Script for Developing FEHM Macros

```python
#This script converts a list of nodes with porosity and permeability
#to FEHM macros (rock, perm, and rlp).  It applies the Buckle's method
#to estimate residual saturation as a function of permeability.
#This script was developed for the GDSA Alluvium modeling task which
#applies heterogeneous porosity and permeability fields developed in
#Jewelsuite and LaGriT

import numpy as np

data = np.loadtxt('mesh_upscale_properties.dat')
data[:,0] = data[:,0].astype(int)
size= data.shape
print(size)
one = np.ones(size[0]).astype(int)
one = one.transpose()

#Rock Macro
rock = np.zeros((size[0],6))
rock[:,0]= data[:,0]
rock[:,1]= data[:,0]
rock[:,2]= one
rock[:,3]= one*1000
rock[:,4]= one*1000
rock[:,5]= data[:,5]
np.savetxt ('rock.dat',rock, fmt=['%i', '%i', '%i', '%e', '%e', '%e'])

#Perm Macro
#Anisotropic perm.  0.5 everywhere but 0.1 in the lacustrine
#perms are converted from log micro darcy to m2
perm = np.zeros((size[0],6))
perm[:,0]= data[:,0]
perm[:,1]= data[:,0]
perm[:,2]= one

for x in range(size[0]):
        perm[x,3]=(10**data[x,6])*(10**-6)*9.869233*(10**(-13))
        perm[x,5]=(10**data[x,6])*(10**-6)*9.869233*(10**(-13))
        if data[x,4] == 5:  #we base the anisotropy off the "max facie"
                perm[x,4]=(10**data[x,6])*(10**-6)*9.869233*(10**(-13))*0.1
        else:
                perm[x,4]=(10**data[x,6])*(10**-6)*9.869233*(10**(-13))*0.5
np.savetxt ('perm.dat',perm, fmt=['%i', '%i', '%i', '%e', '%e', '%e'])

#RLP Macro
#See FY21 GDSA alluvium report for discussion of chosen Buckle's Constant
#rlp_1.dat and rlp_2.dat are combined before import into FEHM.
#Facies 0, and 2 aren't represented in the model
rlp = np.zeros((size[0],5))
Buckles = np.zeros(10)
Buckles[0] = 0.0
Buckles[1] = 0.02
Buckles[2] = 0.0
Buckles[3] = 0.02
Buckles[4] = 0.02
```

```python
Buckles[5] = 0.1
Buckles[6] = 0.02
Buckles[7] = 0.01
Buckles[8] = 0.06
Buckles[9] = 0.02
print (Buckles[:])
for x in range(size[0]):
        rlp[x,0]= 2.0
        rlp[x,1]= Buckles[data[x,4].astype(int)]/data[x,5]
        rlp[x,2]= 0.0000001  #residual saturation of air
        rlp[x,3]= 0.1
        rlp[x,4]= 0.9
np.savetxt ('rlp_1.dat',rlp, fmt=['%i', '%e', '%i', '%f', '%f'])

rlp = np.zeros((size[0],4))
for x in range(size[0]):
        rlp[x,0]= data[x,0]
        rlp[x,1]= data[x,0]
        rlp[x,2]= 1.0
        rlp[x,3]= data[x,0]

np.savetxt ('rlp_2.dat',rlp, fmt=['%i', '%i', '%i', '%i'])
```